THE
PHYSICAL REVIEW
A Journal of Experimental and Theoretical Physics
VOL. 44, NO. 9 NOVEMBER 1, 1933 SECOND SERIES

Experimental Study of the Widths and Shapes of the $K\alpha$ X-Ray Doublet from Ca (20) to Ni (28)

LYMAN G. PARRATT, *University of Chicago*
(Received July 21, 1933)

The rocking curves of the $K\alpha$ x-ray doublet of elements Ca (20) to Ni (28) have been recorded with a vacuum double-crystal spectrometer, and measurements of the full widths at half maximum intensity, relative intensities, asymmetry and degree of resolution have been made. Resolution of the observed overlapping curves into the two component lines α_1 and α_2 has been attempted. The relative intensity of the doublet lines α_1 to α_2, if defined in terms of the double-crystal spectrometer as the ratio of areas under the component curves, is 2 to 1 for all elements studied within an estimated error of ± 2 percent. The asymmetry of the lines is found to increase from Ca to Fe, then to decrease with increasing atomic number. The values of the full widths, uncorrected for divergence and for the finite resolving power of the crystals, of the component lines, in X.U., follow:

	Ca	Ti	Va	Cr	Mn	Fe	Ni
$K\alpha_1$	1.60	1.22	1.15	1.08	1.10	1.02	0.72
$K\alpha_2$	1.54	1.43	1.35	1.30	1.22	1.12	0.88

The ratio of peak intensities is observed to vary from element to element in such a way as to compensate for the variations in line widths so that the ratio of component areas remains constant.

INTRODUCTION

THIS paper is a report of measurements of the contour of the $K\alpha$ x-ray doublet of elements Ca (20) to Ni (28) with a vacuum double-crystal spectrometer. Since the pioneer work of Ehrenberg and Mark and of Davis and Purks in the application of the high resolving power and dispersion of the two-crystal spectrometer, many investigators have reported experiments similar to these on x-ray lines of wave-lengths suitable to work with an open air instrument. Allison[1] of this laboratory very recently reported an experimental study of widths of the $K\alpha$ doublet from Fe (26) to Ag (47), and the present work with the vacuum spectrometer was undertaken to extend this series of measurements in the long wave-length region.

The calcite crystals employed in this research have been previously studied[2] in the parallel position (zero dispersion) throughout a wide range of wave-lengths, 1.54 to 5A, and have been found to present no evidence of mosaic structure in the crystal lattice. With these crystals, practically perfect, the rocking curves obtained in the (1, +1) position should yield valuable information about the natural shapes or the intrinsic inhomogeneity of wave-length contained in the x-ray "lines." Especially is this true in the study of K lines from elements of low atomic number because (1) the lines are broader in this region (in angular units but narrower in energy units) allowing greater relative accuracy in their measurement, and (2) rudimentary ideas as to what factors determine line widths and shapes

[1] Allison, Phys. Rev. **44**, 63 (1933).

[2] Parratt, Phys. Rev. **41**, 561 (1932).

seem to indicate that the region of low atomic number is more fertile for this type of research.[3]

Discussion of Apparatus

Details of the design and construction of the vacuum double-crystal spectrometer with which these rocking curves were observed have been presented in an earlier paper by the author.[4] No alterations have been made in the instrument, with one minor exception: The window of the ionization chamber has been increased in width from 3 mm to 5 mm to eliminate any chance that it would not be sufficiently wide to accommodate the full x-ray beam. A lead shield placed between the crystals reduces the base line to 1.7 percent for Ca and to 3 percent for Fe, of the maximum ordinate of the α_1 line. All curves were taken with the x-ray tube operating at 15 kilovolts and from 3 to 10 milliamperes. The maximum horizontal and vertical divergences of any ray, with respect to the central ray, in the beam before reaching the first crystal are approximately 8.7×10^{-3} and 1×10^{-2} radians respectively.

Distortions in Observed Rocking Curves

(1) Due to divergence

Allison discusses[1] the effect of slit width and height on the (1, +1) rocking curves and arrives at the conclusion that, if the spectral range covered by the rocking curve is not too wide, the divergence of the beam incident on the first crystal has negligible effect on the rocking curve observed from the second crystal. Just how wide this range may safely be is not exactly known and the divergence with the relatively large spectral ranges covered in recording the present lines of long wave-length may have a slight effect on the observed curves.

(2) Due to moving second crystal only

Other possible perturbations on wide rocking curves due to the fact that measurements are taken by moving the second crystal only, leaving the slits and first crystal fixed in position, have been discussed by DuMond and Hoyt.[5] First, the portion of the beam being reflected into the ionization chamber progressively moves across the face of the crystals in the process of recording a rocking curve and it is known that the reflecting properties of a crystal are not uniform over its face. Second, the portion of the beam whose intensity is being observed is emitted from but a fraction, a vertical section (due to the action of the slits), of the focal spot, and this section gradually changes in position, sweeping slightly across the focal spot, in the course of a rocking curve. This introduces difficulties because the intensity emitted from the focal spot is not uniform over its area. However, Allison[1] eliminated the question of the effect of these two perturbations on the curves for cobalt by rotating both crystals simultaneously, after the manner of DuMond and Hoyt.[5] The spectral width at half maximum intensity of Co $K\alpha_2$ is 0.95 X.U. and for this range the perturbations seem to have no appreciable effect. The maximum line width covered in the present report is that of Ca $K\alpha_1$, 1.68 X.U. Several rocking curves were taken of Ca $K\alpha_1$ with the focal spot, slits and first crystal set at various positions, at the peak of α_1, then at 300 seconds of arc (3.67 X.U.) on either side of the peak. The differences in the observed widths of α_1 were approximately twice as large as the experimental error, which is estimated as about 2 percent. However, measurements on all the curves except those of calcium are felt to be free (within the experimental error in recording electrometer readings) of disturbances of the type mentioned above.

(3) Due to finite size of focal spot

In measuring wide lines by rotating the second crystal only it is imperative that the focal spot be rather broad and as uniform in emission as possible. The face of the target was cut at 45° to the long axis to aid in attaining this objective. Then the shape of the focussing cup and filament-target distance were varied until a broad, fairly uniform focal spot was obtained. The x-ray tube is constructed with a sylphon and screw arrange-

[3] From the results of work now in progress (Parratt, Bull. Am. Phys. Soc. **8**, 26 (1933) Abs. No. 74) on the differences in the shape of the doublet lines as obtained from pure and alloy targets, there seems to be evidence to believe that the valence or outer electrons are in a large part responsible for the shape of the x-ray curve. If this be true, the region of long wave-lengths should prove especially rich for contour work due to the stronger couplings between the inner and outer electrons.

[4] Parratt, Phys. Rev. **41**, 553 (1932).

[5] DuMond and Hoyt, Phys. Rev. **36**, 1702 (1930).

ment in the target end[4] which allows slow horizontal motion of the target with respect to the rest of the tube and slits while the tube is in operation. The breadth and uniformity of the spot is conveniently measured as follows: With the slits and crystals set on the peak of an α_1 line, the intensity of the beam reaching the ionization chamber is observed as a function of the position of the target. If this curve is wide and flat the focal spot is broad and uniform. When the width of each slit is 2 mm, the widths used in all the work reported here, this curve of intensity *vs.* position of target is quite flat-topped over an angular range[6] of about 600 seconds of arc (more than twice the separation between α_1 and α_2) with an approximately 3 percent decrease at a distance of 800 seconds of arc from the optimum position of the target. Of course, moving the target alters the characteristics of the focal spot also, so that this method does not allow a true picture of the emitted intensity, but the relatively slight variations of $\frac{1}{4}$ to $\frac{1}{2}$ mm in the distance of 15 mm should not be very serious.

Because of the overlapping of the rocking curves of the two α-lines, curves of both lines were taken in a single "run." A preliminary curve of the type described in the previous paragraph, with the slits and crystals set on the angle midway between the peaks of the doublet, afforded an accurate determination of the optimum position for the focal spot, midway in the spectral range to be covered. The target was so placed prior to the recording of each rocking curve.

Base line readings were taken at distances of 500 and 600 seconds of arc removed from the peaks and a 3 percent correction due to the finite size and characteristics of the focal spot has been made on these readings. Errors in electrometer readings are of this order of magnitude and this 3 percent correction is probably superfluous.

(4) Due to the crystals

Distortions, of a type asymmetrical as well as symmetrical, due to the action of the two crystals as diffraction gratings may be present in the observed rocking curves. But for this distortion, though perhaps small, inherent in all two-crystal instruments, no satisfactory method of correction has been developed, and for this reason interpretations of the particular line contours reported in this paper and in similar research cannot be completely divorced from the type of instrument with which they are observed.

In order to make certain that the reflecting properties of the crystals had not changed and that the spectrometer had remained in proper adjustment, curves of calcium and titanium, the first to be studied, were repeated, and were the last to be recorded. Agreement was within the experimental error.

Preparation of Targets

The targets were of pure elements and made up in individual buttons of more or less uniform size that could be soft-soldered to the water-cooled target-carriage of the tube. The calcium button was made as follows: In a $\frac{1}{2}$ inch nickel rod, a flat-bottomed hole was drilled $\frac{5}{16}$ inch in diameter to a depth of about $1\frac{1}{4}$ inches. Bits of pure Ca, having a minimum amount of oxide on their surfaces, were pressed in the hole and hermetically sealed with melted borax to prevent further oxidation. The unit was then heated with an oxygen flame to a temperature slightly above the melting point of calcium. The liquid Ca fused with the sides and bottom of the nickel cup which, when cooled, was turned down to the desired size on the lathe and soldered to the target-carriage. The melting points of titanium and vanadium are sufficiently high that good thermal contact to the copper base of the target is not necessary. A piece of pure Ti was placed in a pool of liquid silver-solder to supply mechanical

[6] As previously mentioned, the portion of the beam whose intensity is being observed in the course of recording a rocking curve is emitted from but a fraction, a vertical section, of the focal spot and this effective section gradually sweeps across the focal spot as the second crystal is turned. The importance of the size and uniformity of the focal spot is that the intensity emitted throughout the spectral range including the α-lines be constant so that rocking curves of these lines will not be distorted by irregularities in the focal spot. Consequently, it is convenient to express in angular measure the linear distance that the focal spot can be moved without appreciably disturbing the intensity of the beam passing through the slits. This angular range, in radians, is obtained by dividing the linear distance of the target-motion by the distance from the focal spot to the first crystal.

TABLE I. *Measurements of rocking curves of the Kα x-ray doublet.*

Obs. = Observed curve (without corrections for overlapping).
Comp. = Component curve (corrected for overlapping).

Element	Ratio of peak intensities α_1/α_2 Obs.	Comp.	Ratio of areas under comp. curves α_1/α_2	Overlapping factor	Index to asymmetry Comp. α_1	α_2	Separation $\alpha_1 \rightarrow \alpha_2$ Obs. $\Delta\theta$	X.U.	Seigbahn X.U.
20 Ca	1.83	1.93	2.00	0.50	1.15	1.13	266″	3.26	3.26
22 Ti	2.19	2.31	1.98	0.34	1.15	1.10	281″	3.68	3.64
23 Va	2.22	2.35	1.99	0.32	1.25	1.15	287″	3.84	3.78
24 Cr	2.26	2.38	2.00	0.27	1.30	1.25	285″	3.88	3.88
25 Mn	2.15	2.24	2.00	0.22	1.60	1.35	288″	3.97	3.98
26 Fe	2.07	2.16	1.97	0.18	1.65	1.40	286″	3.98	3.95
28 Ni	2.30	2.35	1.92	0.09	1.35	1.35	278″	3.93	3.85

support when cooled and a free surface of Ti was obtained by grinding on an emery wheel. Va was treated in the same manner as Ti. Pure manganese is wet by low-melting-point silver-solder with borax as a flux, and, if care is taken to prevent sudden and uneven cooling, the Mn will not fracture. The samples of Ti, Va, Cr, Mn and Fe were prepared by an aluminothermic reduction from their oxides, thus assuring a purity within a few tenths of one percent.

RESULTS

Fig. 1 is a reproduction of six of the rocking curves. The curves are drawn through the experimental points and no points deviated from the curve by more than the width of the lines drawn. The dotted line in each case is an attempt to resolve the observed contour into the two components α_1 and α_2. This resolution will be discussed later. Measurements of these curves are given in Tables I and II. The data listed in these tables are the averages of at least three individual curves, usually more than five. In all of these curves the second crystal only was rotated and from long to shorter wave-lengths. After the completion of each curve the peak intensity of α_2 was checked and the curve discarded if the intensity had changed more than 4 percent. Most of them checked within 2 percent. An insufficient number of trials was taken to give a probable error, but an index to the degree of experimental consistency may be obtained from the following: The maximum deviation from the average of the width measurements is about 2 percent, and of the ratio of peak intensities about 4 percent, considering all the curves, except those for Ni, not discarded on the basis of the above criterion. The nickel curves were taken when the temperature in laboratory was just 100°F and the vacuum grease between the bearings[4] of axis *B* was suspected of gradually changing in thickness. This may have caused slight lateral distortions in the angular readings but would not disturb the peak intensities. Consequently the width measurements on the Ni curves may be less reliable than the other data.

ASYMMETRY AND RESOLUTION

From Fig. 1 it is observed that both α_1 and α_2 are asymmetrical about a line drawn through the maximum ordinate. To serve as an index of the asymmetry Allison has introduced[1] the ratio of that part of the full width at half maximum on the long wave-length side of the maximum ordinate to that part of the width on the short wave-length side. Values of these indices from the resolved component lines α_1 and α_2 are given in Table I. Both the Ca and Ti lines are but slightly asymmetrical, the asymmetry increasing to Fe then decreasing. For $K\alpha$ lines from elements of atomic number greater than Cu (29) the index of asymmetry rapidly decreases to unity.[1]

The fact that these curves are asymmetrical may lead one to suspect the existence of unresolved component lines[7] in addition to the α_1 and α_2 lines. However, considering the relatively large widths and the fact that the curves are quite smooth as observed with an instrument of very high resolving power, a preferable inter-

[7] Bearden and Shaw, Bull. Am. Phys. Soc. **8**, 15 (1933) Abs. No. 50.

pretation is that these asymmetrical curves actually represent the true experimental contour of the two α-lines.[8]

The method of resolving the observed curve into components is one of trial and error. Several attempts on each curve are made and the one giving the "most reasonable" component curves is decided upon. There is really not a very large difference between any "reasonable" components that can be drawn, and these differences except for calcium are close to the experimental error in recording the observed curve.

In Table I are listed values of the "overlapping factor," a term which is introduced by Allison[1] to indicate the reciprocal of the degree of resolution of the two overlapping lines. This term is defined as the ratio of the minimum ordinate between the peaks of the rocking curve of α_1 and α_2 to the maximum ordinate of α_1, all multiplied by the ratio of intensity of α_1 to α_2, which, for these K lines, is taken as 2 to 1.

Relative Intensities

The term relative intensity of two x-ray lines has been defined experimentally as the ratio of the peaks or maximum intensities of the two lines as measured with a single-crystal spectrometer. Some confusion has arisen as to the meaning of the term when applied to rocking curves obtained with a double-crystal spectrometer. In Table I is listed the ratio of peak intensities of α_1 to α_2. These values for the component lines vary with atomic number from 1.93 for Ca to 2.38 for Cr. The ratio of the areas under the component curves is also given (Table I) and is seen to be constant, 2 to 1, within experimental error. The Burger-Dorgelo "summation rules" predict the relative intensity of α_1 to α_2 as 2 to 1, constant for all elements, which also agrees with experimental work on the $K\alpha$ doublet with the single-crystal spectrometer.[9] The present work can be interpreted in either of two ways: (1) as determining the meaning of the term relative intensity as referring to the area under the component curves measured with a double-crystal spectrometer, or (2) on the assumption that the area ratio should be 2 to 1, as justifying the particular resolution into components employed in the analysis for the above data and as giving evidence for the accuracy of the data.

Widths

Fig. 2 presents graphically the data given in the last column of Table II. The points for Cu, Zn and Ge are taken from Allison's data.[1] It should be pointed out that the peculiar variations in width shown by this graph are well outside of the experimental error. The widths of both α_1 and α_2 vary, but also the ratio of peak intensities changes in such a compensating manner that the ratio of areas, as mentioned above, remains constant.

The series of elements here reported overlap the series studied by Allison.[1] The values of the widths of Fe $K\alpha_1$ and α_2 observed by Allison are 1.00 and 1.06 X.U., respectively with an estimated error of ± 10 percent, and the widths in Table II of this paper are 1.02 and 1.18 X.U. with an estimated error of ± 2 percent. Allison's values of the widths of the Ni lines are 0.64 and 0.82 X.U. with an error estimated as ± 5 per cent, and the present measurements give 0.72 and 0.91 X.U. for $K\alpha_1$ and α_2, respectively with an error of perhaps ± 5 percent.

This disagreement may possibly be explained as experimental. However, it should be investigated further. Three different types of targets were used in the present experiments: First,

[8] The rocking curve to be expected from the theory of x-ray reflection from a single calcite crystal is not symmetrical (reference 2, page 565), and if two such crystals are used in any anti-parallel position the rocking curve of the doubly-reflected monochromatic radiation would also be asymmetrical (reference 1). Of course, the theoretical rocking curve is derived on the assumption of monochromatic radiation incident on the first crystal and the width of this curve is rather narrow compared with the width of the observed curve. At any rate, it should follow that even though the x-ray line be symmetrical in its inhomogeneity of wave-length as emitted from the target, the rocking curve as observed with the double-crystal spectrometer would be expected to be somewhat asymmetrical. However, considering that symmetrical rocking curves are observed for $K\alpha$ radiation from elements of higher atomic numbers, say Mo (42) or Ag (47), in which the widths of the (1, −1) curves are a greater fraction of the (1, +1) curves, one might conclude that the effect of the crystals in producing asymmetry is small, and that the asymmetry of the $K\alpha$ lines reported in this paper are to a large extent characteristic of the radiation as it emerges from the target.

[9] Williams, Phys. Rev. **44**, 146 (1933).

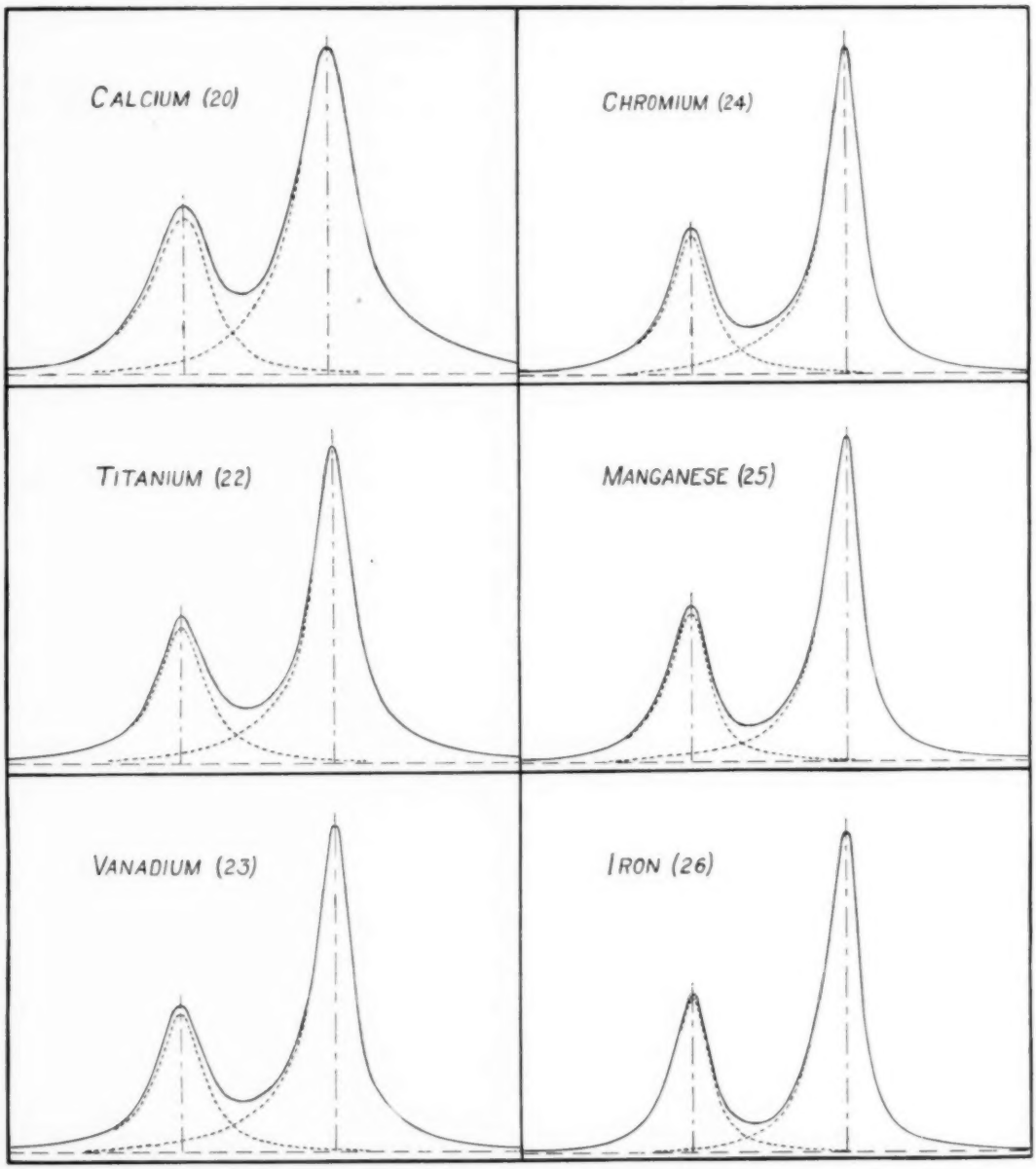

FIG. 1. Rocking curves of the $K\alpha$ x-ray doublet.

cold-rolled steel, second, pure Fe produced alumino-thermically and quickly chilled in water so that the crystal size would be microscopic, and, third, a single crystal of Fe produced by maintaining the temperature just a few degrees below the melting point of Fe for a period of 1000 hours, then cooling very slowly. The first two types of targets gave identical rocking curves but the single crystal of Fe gave widths of 1.06 and 1.23 X.U. for $K\alpha_1$ and α_2, respectively. This difference in the rocking curves, apparently due to the different heat treatments of the targets, is felt to be greater than experimental error, but warrants further study.[10] The samples of both Fe and Ni used in the present measure-

[10] The values of the widths of the Fe $K\alpha$ lines given in Table II and included in Fig. 2 are taken from the rocking curves with the first and second types of Fe targets. Perhaps the widths measured from the single-crystal of Fe should be taken as those characteristic of pure iron.

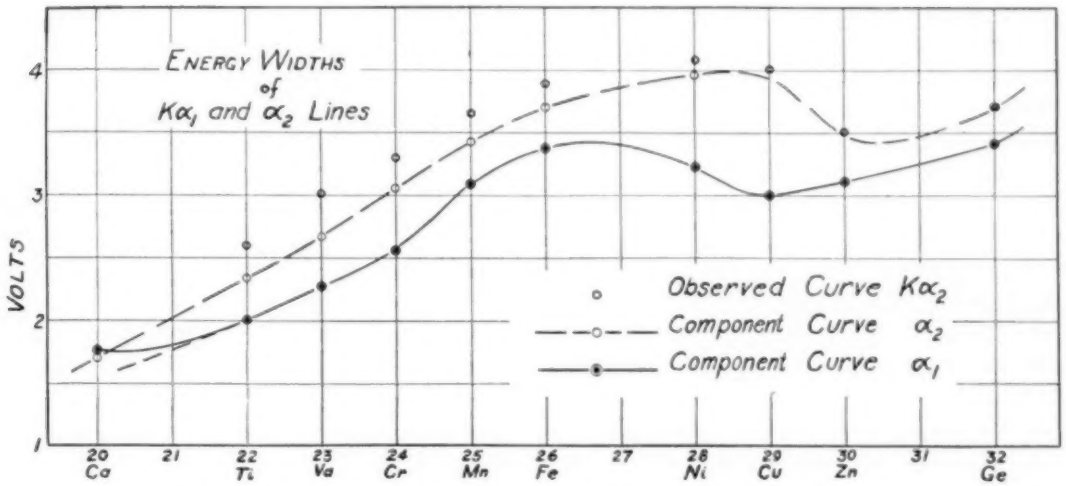

FIG. 2. Full widths (in volts) at half maximum intensity of the $K\alpha_1$ and $K\alpha_2$ x-ray lines. The values for Cu, Zn and Ge are taken from Allison's data (reference 1).

TABLE II. *Full widths at half maximum intensity of $K\alpha_1$ and $K\alpha_2$ x-ray lines.*

Obs. = Observed curve (without corrections for overlapping).
Comp. = Component curve (corrected for overlapping).

Line	Wave-length Angstroms	Widths					
		Seconds of arc		X. Units		$\Delta\nu/R$	Δv volts
		Obs.	Comp.	Obs.	Comp.	Comp.	Comp.
20 Ca $K\alpha_1$	3.352	137	131	1.68	1.60	0.130	1.76
$K\alpha_2$		—	126	—	1.54	0.125	1.69
22 Ti $K\alpha_1$	2.743	94.5	93.5	1.24	1.22	0.148	2.00
$K\alpha_2$		121	109	1.58	1.43	0.172	2.33
23 Va $K\alpha_1$	2.498	86	85.5	1.15	1.15	0.167	2.26
$K\alpha_2$		114	101	1.53	1.35	0.197	2.67
24 Cr $K\alpha_1$	2.285	80	79.5	1.09	1.08	0.188	2.55
$K\alpha_2$		103	95	1.40	1.30	0.225	3.05
25 Mn $K\alpha_1$	2.098	80	80	1.10	1.10	0.228	3.09
$K\alpha_2$		95	89	1.31	1.22	0.253	3.43
26 Fe $K\alpha_1$	1.932	73.5	73.5	1.02	1.02	0.249	3.37
$K\alpha_2$		85	80.5	1.18	1.12	0.273	3.70
28 Ni $K\alpha_1$	1.655	50.5	50.5	0.72	0.72	0.238	3.23
$K\alpha_2$		64	62	0.91	0.88	0.293	3.96

ments were different from those in Allison's experiments.

In Table I is included the observed separation in X.U. of the maximum ordinates of α_1 and α_2, and, for comparison, the values given by Siegbahn. In general the agreement is very good. This may be considered as a check on the regularity of motion of the second crystal and the calibration of the drum from which the differences in angular positions are read.

To convert the observed line width into terms of the natural or intrinsic width of the x-ray line as it emerges from the target, two corrections, in addition to the overlapping, are to be considered. First is the effect of the divergence of the beam incident on the first crystal which effect has been assumed to be of little importance. Second is the correction for the contributions to the width due to the finite resolving power of the crystals. This correction

depends in some way on the width of the rocking curve in the (1, −1) position of the spectrometer. For wave-lengths 2.4 to 3.2A the width of the (1, −1) curve is almost constant,[2] 18.2 seconds of arc, which is but 1/5 of the width of the (1, +1) curve for the same wave-length.

It is interesting to note that the region of elements in which occur these curious variations in widths, asymmetry and peak intensity ratios is the one in which the incompleted subshell of electrons, the *3d* electrons of the *M* level, is being filled. Every element studied has just two *N* electrons, of the 4*s* type, except Cr, which has but one. Of course these atomic configurations are derived from the optical spectra of the elements in the gaseous form, and the explanation of the effects reported here may very likely be in terms of the distortions of the atom as it exists in the solid form—distortions of the symmetry of the electric and magnetic fields surrounding the atom which may cause subdivision of the energy levels of the atomic states in question.

The author is at present studying the rocking curves of the $K\alpha$ doublet from an element in various alloy targets. The results so far seem to indicate that the calcium data given here are not correct for pure Ca but rather apply to calcium plus a surface layer of oxide. Calcium oxidizes rather readily and in spite of the fact that the surface of the target was filed clean of oxide just previous to the recording of each rocking curve, some oxide had certainly formed before the tube could be pumped out. Such a layer of oxide on a manganese target has been found to increase the width of the $K\alpha_1$ line of Mn 5 to 15 percent depending upon the relative amount of oxide present; the corresponding increase in the width of $K\alpha_2$ is somewhat less than for that of α_1. In all cases except calcium the data here reported apply to pure elements.

The author is pleased to express his indebtedness to Professor S. K. Allison for the privileges of working in his laboratory and for his valuable criticism of the manuscript.

Energy Distribution in Cosmic Rays

W. G. POLLARD, *The Rice Institute, Houston, Texas*

(Received July 24, 1933)

The experimental evidence from the distribution of cosmic rays with magnetic latitude and from their absorption in the atmosphere demands that they have some sort of energy distribution. Examination shows that passage through interstellar space would not have appreciably distorted an energy band in cosmic-ray particles which have been travelling for 5×10^{12} years. Consequently, it seems probable that they have preserved the energy distribution with which they were originally emitted. A Maxwell distribution in energy corrected for relativity is applied to functions which approximate Lemaitre's and Vallarta's curves for the latitude effect and fairly good agreement with Compton's observations is obtained when 16.7 percent of the radiation has the Maxwell distribution, the remainder being composed of particles unaffected by the earth's magnetic field. These results are applied to Lemaitre's theory of the radioactive origin of the radiation. The distribution found has many features which suggest such an origin although the recent findings of Johnson and those of Alvarez and Compton, indicating that there are more positive than negative electrons in the rays, seem to discredit such a theory.

TWO bodies of experimental evidence give information concerning the distribution of energy in cosmic rays: (1) distribution with magnetic latitude; (2) absorption in the atmosphere and in water. Both lines of evidence indicate that cosmic rays as they enter the earth's atmosphere have a wide spread of energy. J. Clay[1] and A. H. Compton[2] have proposed energy distributions which bring the observed latitude distribution into partially satisfactory agreement with Lemaitre's and Vallarta's curves,[3] while a number of observers have proposed energy distributions to account for the observed absorption of cosmic rays in the atmosphere and in deep lakes. The distributions postulated by Clay and Compton are purely *ad hoc* assumptions and their authors made no attempt to justify them. It is the purpose of this paper to examine more fully the information which may be derived from latitude measurements concerning the distribution of energy in cosmic rays. The question of the origin of this distribution involves a discussion of what effect passage of cosmic rays through interstellar matter may have on any original distribution of energy. We propose to examine this question first.

[1] J. Clay, Proc. Amsterdam Acad. December 17, 1932.
[2] A. H. Compton, Phys. Rev. **43**, 387 (1933).
[3] G. Lemaitre and M. S. Vallarta, Phys. Rev. **43**, 87 (1933).

Energy Losses Through Collisions with Interstellar Matter

Bohr[4] has shown that when high velocity β-rays are passed through matter of thickness t, the losses in energy which they suffer are distributed about a mean value according to the law

$$W(E)dE=(2\pi Pt)^{-\frac{1}{2}}e^{-(E-E_0)^2/2Pt}dE,$$

where $W(E)dE$ is the probability that a β-particle has lost energy between E and $E+dE$, E_0 is the mean loss of energy to be expected from the passage and P for this particular problem is given by $P=\pi e^4Nn$ in which e is the electronic charge, N the number of atoms per unit volume and n the average number of electrons in the atoms composing the matter. This law is only valid when a great many collisions have occurred.

If T is the time during which these particles moving with nearly the velocity of light have been coursing through space, the distance which they have traversed is cT. H. A. Wilson[5] has estimated that there is one calcium atom in every 2.3×10^7 cc in interstellar space. Assuming that interstellar matter is all calcium, we have $N=0.435\times10^{-7}$, $n=20$, and $Pt=\pi e^4NcnT=4.3\times10^{-33}T$. The energy losses E and E_0 are con-

[4] N. Bohr, Phil. Mag. **30**, 581 (1915).
[5] H. A. Wilson, Astrophys. J. **68**, 423 (1928).

veniently expressed in electron-volts, so we must multiply them by $e/300$. We have then

$$W(E) = (6\times 10^{15}/T^{\frac{1}{2}})e^{-(3\times 10^{9}/T)(E-E_0)^2}.$$

To make Lemaitre's and Vallarta's theory fit Compton's observed results, there must be a maximum variation from the mean energy of at least 5×10^9 electron-volts. $W(E)$ must therefore be appreciable when $E-E_0$ is between 0 and 5×10^9. This condition is satisfied only if T is of the order of 10^{28} seconds or 10^{21} years. This is certainly too long a time, since Jeans' and Edington's independent estimates of the age of the universe both give only about 5×10^{12} years. With this value for T, a density of matter equivalent to five calcium atoms per cc in interstellar space would be required to give the necessary range of energy.

These considerations show that it is quite probable that any original distribution in energy which the radiation may have had has remained unaltered so far as passage through interstellar space is concerned. There may, however, be enough matter around the stars to produce an energy variation in a single band of the required magnitude but the scarcity of data on such matter and the fact that it is distributed in lumps throughout the universe puts this explanation outside the domain of a rigorous theoretical treatment. All that can be said is that it is highly improbable that there is enough of it to form the equivalent of 100 electrons per cc throughout all space.

Theory for Any Law of Distribution

Let the total number of particles be N and let the number having components of momentum between p_x and p_x+dp_x, p_y and p_y+dp_y, p_z and p_z+dp_z be

$$dN = Nf(p_x, p_y, p_z)dp_x dp_y dp_z.$$

Transforming to spherical coordinates and letting φ be the magnitude of the momentum gives

$$dN = Nf(\varphi)\varphi^2 d\omega d\varphi,$$

which represents the number of particles in a solid angle $d\omega$ whose momenta lie between φ and $\varphi+d\varphi$.

For particles moving with nearly the velocity of light, $\epsilon = c\varphi$ where ϵ is the energy of a particle. Hence $\varphi^2 d\varphi = \epsilon^2/c^3 d\epsilon$ and

$$dN = (N/c^3)f(\epsilon/c)\epsilon^2 d\epsilon d\omega. \tag{1}$$

Lemaitre and Vallarta point out that since Liouville's theorem applies to the case of particles moving in the earth's magnetic field,[6] the intensity at any point is proportional to the total solid angle at the point inside of which the particles can reach the earth. Let $i_\lambda(\epsilon)$ be the fractional intensity of the radiation at magnetic latitude λ expressed as a function of its energy. Since, when $i_\lambda = 1$, $\omega = 2\pi$,

$$\omega_\lambda = 2\pi i_\lambda(\epsilon). \tag{2}$$

The resultant fractional intensity I_λ of all energies at magnetic latitude λ is then

$$I_\lambda = (1/N)\int dN = (1/c^3)\int_0^\infty \int_0^{\omega_\lambda} f(\epsilon)\epsilon^2 d\epsilon d\omega = (2\pi/c^3)\int_0^\infty f(\epsilon) i_\lambda(\epsilon)\epsilon^2 d\epsilon \tag{3}$$

from (1) and (2). In general two arbitrary constants appear in the distribution function. These are determined by the usual conditions

$$N = (N/c^3)\int_0^\infty \int_0^{2\pi} f(\epsilon)\epsilon^2 d\epsilon d\omega$$

or

$$c^3/2\pi = \int_0^\infty f(\epsilon)\epsilon^2 d\epsilon \tag{4}$$

and, if $\bar{\epsilon}$ is the mean energy of the radiation

$$\bar{\epsilon} = (1/N)\int \epsilon dN = (2\pi/c^3)\int_0^\infty f(\epsilon)\epsilon^3 d\epsilon. \tag{5}$$

Maxwell Distribution

Suppose for example that the function $f(\epsilon)$ is taken to be

$$f(\epsilon) = Ae^{-h\epsilon},$$

which leads to a Maxwell distribution. The above conditions (4) and (5) give $A = c^3h^3/4\pi$ and $\bar{\epsilon} = (h^3/2)\int_0^\infty e^{-h\epsilon}\epsilon^3 d\epsilon = 3/h$. Eq. (3) becomes for

[6] See also, W. F. G. Swann, Phys. Rev. **44**, 224 (1933).

this special case

$$I_\lambda = (h^3/2)\int_0^\infty e^{-h\epsilon} i_\lambda(\epsilon)\epsilon^2 d\epsilon, \quad h = 3/\bar{\epsilon}. \tag{6}$$

Fair agreement with Lemaitre's and Vallarta's curves is obtained when we use for $i_\lambda(\epsilon)$ the functions defined as follows

$$\begin{aligned} i_\lambda(\epsilon) &= 0, && 0 \leqslant \epsilon \leqslant \epsilon_0 \\ &= (A_\lambda\epsilon^2 + B_\lambda\epsilon + C_\lambda)/\epsilon^2, && \epsilon_0 \leqslant \epsilon \leqslant \epsilon_1. \\ &= 1, && \epsilon \geqslant \epsilon_1 \end{aligned} \tag{7}$$

in which the constants A_λ, B_λ, C_λ, ϵ_0, and ϵ_1 have the values given in Table I.

TABLE I. *Values of constants.*

λ	A_λ	B_λ	C_λ	ϵ_0	ϵ_1
0	1.222	−1.111	−0.111	1.09	5.10
10	1.207	−0.995	−0.156	0.96	4.96
20	1.215	−0.859	−0.089	0.80	4.10
30	0.940	0.455	−0.870	0.75	3.82
40	0.660	0.930	−0.630	0.50	1.50
50	1.000	0.173	−0.093	0.23	0.54

TABLE II. *Comparison of Lemaître-Vallarta curves with the approximate functions i_λ.*

ϵ \ λ	0	10	20	30	40	50
0.238						0.10 0.08
0.536					0.18 .20	1.00 1.00
0.954			0.084 .216	0.443 .46	.95 .95	
1.49	0.35 .426	0.40 .47	.56 .60	.86 .85		
2.145	.68 .69	.71 .71	.85 .79	.965 .963		
2.92	.83 .83	.84 .85	.92 .91	.99 .99		
3.82	.97 .93	.975 .94	.983 .986			
4.83	.99 .99	.995 .994				

Table II gives the intensities i_λ as a function of the energy ϵ in electron-volts $\times 10^{10}$ and the magnetic latitude λ. The first value given in each case was taken from Lemaitre's and Vallarta's curves. The second value is that calculated from the functions $i_\lambda(\epsilon)$.

By carrying out the integration of Eq. (6) and by using the approximate functions (7), we get

$$I_\lambda = (h^3/2)\int_{\epsilon_0}^{\epsilon_1} (A_\lambda\epsilon^2 + B_\lambda\epsilon + C_\lambda)e^{-h\epsilon} d\epsilon + (h^3/2)\int_{\epsilon_1}^\infty e^{-h\epsilon}\epsilon^2 d\epsilon$$

or

$$\begin{aligned} I_\lambda = (h^2/2)\{ & A_\lambda e^{-h\epsilon_0}(\epsilon_0^2 + 2\epsilon_0/h + 2/h^2) \\ & - (A_\lambda - 1)e^{-h\epsilon_1}(\epsilon_1^2 + 2\epsilon_1/h + 2/h^2) \\ & + B_\lambda e^{-h\epsilon_0}(\epsilon_0 + 1/h) - B_\lambda e^{-h\epsilon_1}(\epsilon_1 + 1/h) \\ & + C_\lambda e^{-h\epsilon_0} - C_\lambda e^{-h\epsilon_1}\}. \end{aligned} \tag{8}$$

This Eq. (8) has been solved for various values of $\bar{\epsilon}$ and λ. If the cosmic radiation is regarded as consisting entirely of electrons or positrons with a Maxwell distribution of energy, curve I, Fig. 1 is obtained. In this case $\bar{\epsilon}$ was 5.17×10^{10} electron-volts and was chosen so that the value I_0 at the magnetic equator agreed with Compton's observed value. This curve obviously does not agree with Compton's observations at all.

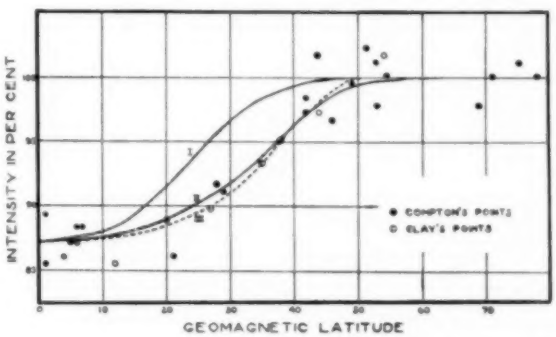

FIG. 1. Intensity distribution as a function of latitude. Curve I, Maxwell distribution of electrons (or positrons); curve II, 16.7 percent of radiation possessing Maxwell distribution; curve III, Compton's experimental curve.

As a matter of fact, no distribution with only one maximum which includes all the rays can give the observed results. If the reduction in intensity at the equator is to be made about 13 percent, the distribution function must have a maximum around 4 or 5×10^{10} electron-volts. This, however, forces the curve for I_λ to approach unity between 30 and 40 degrees magnetic latitude. In order to make it approach unity at 50

degrees, as Compton's curve does, the distribution function must have a maximum around 10^{10} electron-volts which forces the reduction in intensity at the equator to about 80 percent.

Curve II, for which $\bar{\epsilon}$ is 1.2×10^{10} electron-volts, represents 16.7 percent of the radiation with a Maxwell distribution. It passes through Compton's observed points very well and very nearly fits curve III which he obtained by assuming the energy distribution to be a discrete spectrum of four lines.[7] The remaining 83.3 percent of the radiation can be regarded as consisting of either positive or negative electrons with an energy greater than 6×10^{10} electron-volts and of neutral particles (photons or neutrons) of any energy.

The actual values obtained by solving Eq. (8) are given in Table III. The intensities I_λ are given in percent of the total intensity which would be observed in the absence of the magnetic field.

TABLE III.

		Curve II	
λ	Curve I	Actual values	I_0 increased to 87.2 percent
0	87.2	23.3	87.2
10	88.0	26.1	87.6
20	91.5	34.8	89.1
30	96.5	50.3	91.7
40	99.2	77.1	96.2
50	99.9	95.1	99.2

THEORIES OF THE ORIGIN OF COSMIC RAYS

Once it is known that the cosmic radiation has preserved the energy distribution of its original emission, we have a valuable means of checking any theory of its origin. If such a theory offers anything definite as regards the energy distribution which would be expected in the emission of the particles composing the radiation, that distribution should conform to the one which it now possesses.

The distribution which we have just proposed is very suggestive of Lemaitre's theory[8] that these rays were produced in the breakdown of some radioactive super-element which completely disappeared long ago. The 83 percent not affected by the earth's field could be regarded as consisting of high energy disintegration electrons and γ-rays. The other 17 percent could be associated with the continuous β-ray spectrum which has an energy distribution roughly approximated by a Maxwell distribution in most known radioactive substances.

The recent independent findings of Johnson[9] and of Alvarez and Compton[10] indicating that the larger part of the radiation affected by the earth's field consists of positive electrons seem, however, to discredit this theory. Nevertheless, one might perhaps argue that α-rays emitted with energies of the order of 10^{10} electron-volts would disintegrate into four neutrons and two positrons. The latter might then be regarded as forming the 17 percent affected by the earth's field.

Swann[11] has proposed that the cosmic rays originated in stellar vortices similar to sun spots. Unfortunately, all that can be gathered from his theory about their energy distribution is that it would roughly follow the distribution of stellar intensities which has been continuously changing for 10^{12} years. As a result it would be difficult to obtain any very definite information from his theory of the sort that this analysis demands.

Nothing much can be done in this direction until a more detailed theory of the origin of cosmic rays and more precise data on their present energy distribution is available. All that we desire to do here is to point out the applicability of these results to such a theory and to suggest a distribution of common occurrence which agrees with all observations so far made.

In conclusion, I wish to thank Dr. L. M. Mott-Smith for the large amount of information which he placed at my disposal, and Marcella Pollard for her assistance in making the calculations involved in this paper. I am deeply indebted to Professor H. A. Wilson for the interest he has shown in this work and for his many valuable suggestions.

[7] Compton, reference 2, note 20, p. 399.
[8] G. Lemaitre, Nature **128**, 704 (1931).
[9] T. H. Johnson, Phys. Rev. **43**, 834 (1933); T. H. Johnson and E. C. Stevenson, Phys. Rev. **44**, 125 (1933).
[10] Luis Alvarez and A. H. Compton, Phys. Rev. **43**, 835 (1933).
[11] W. F. G. Swann, Phys. Rev. **43**, 217 (1933).

The Positive Ion Excitation of Mercury Vapor

ERNEST J. JONES, *University of Minnesota, Minneapolis and the Bureau of Chemistry and Soils, Washington, D. C.*

(Received July 13, 1933)

Mercury vapor was bombarded by Li^+ and K^+ ions and the resulting spectra photographed with a quartz spectrograph and the plates photometered to give an approximate intensity-velocity curve. Voltages used ranged from 150 to 1500 volts. The results indicate that the velocity rather than the energy is the important factor to be considered in the mechanism of the collision process. A preference seems to exist for the excitation of levels of higher L values. The spark lines 2847, 2260 and 2224 appear at 1000 volts for Li^+ ions. A powerful source of positive ions has been developed.

EXPERIMENTS on the effect of positive ion impact in gases[1] have usually been directed toward measuring the resulting ionization as a function of the kinetic energy of the ions. The purpose of the present investigation is to study the somewhat more general problem of the probabilities of excitation of an atom to its various energy states by positive ion impact.[2] The excitation of the spectrum lines of the mercury atom by impact with the positive ions of lithium and potassium was the specific problem attacked.

Source of Positive Ions

A first essential was the development of a copious and constant source of the ions. The material which proved most satisfactory was the alkali aluminum silicates. Hundley was the first to use these compounds in studying the emission of lithium ions from spodumene. In the present work the system $Li_2O \cdot Al_2O_3 \cdot SiO_2$ was studied and a mixture of the composition $3Li_2O \cdot Al_2O_3 \cdot 3SiO_2$ proved to be most satisfactory. A similar mixture $3K_2O \cdot Al_2O_3 \cdot 3SiO_2$ was used as a source of potassium ions. With these sources it was possible to maintain a remarkably constant current of about 4×10^{-4} amp./cm^2 for periods of forty hours. The mixtures were prepared from pure chemicals by heating the constituents on a platinum gauze. A further study[3] is in progress concerning the whole problem of emission of alkali ions from their corresponding aluminum silicates.

Apparatus

Fig. 1 gives the plan of the experimental tube and the arrangement of the electrodes and is self-explanatory. It was evacuated by a two-stage diffusion pump. The tube was placed in the magnetic field of a pair of Helmholtz coils which have a field of about 150 gauss parallel to the direction of observation. This field was ample to prevent any electrons from entering the region under observation.

The spectrograph was a medium size Hilger quartz instrument. The slit width was 0.5 mm. A Zeiss step filter covered the slit and allowed the photographic plate to be calibrated for intensities. The plates used were Seed 23 and were developed 5 minutes at 16°C.

Procedure

An exposure time of eight hours was chosen as standard. Each exposure was made on a sepa-

[1] J. Franck, Verhand. der Deut. Phys. Ges. **16**, 57 (1914); Zeits. f. Physik **25**, 312 (1924).
J. J. Thomson, J. Phys. Soc. London **27**, 94 (1914); Phil. Mag. **48**, 1 (1924).
Pawlow, Proc. Roy. Soc. **A90**, 348 (1914).
A. J. Dempster, Proc. Nat. Acad. **2**, 374 (1916); Phys. Rev. **8**, 651 (1916).
W. J. Hooper, J. Frank. Inst. **201**, 311 (1926).
R. M. Sutton, Phys. Rev. **33**, 364 (1928).
O. Beeck, Ann. d. Physik **6**, 1001 (1930).
J. C. Mouzon, Phys. Rev. **41**, 605 (1932).

[2] J. T. Tate, Phys. Rev. **23**, 293 (1924).
E. J. Jones, Phys. Rev. **29**, 611 (1927).
C. H. Kunsman, J. Frank. Inst. **203**, 635 (1927).
Kirchstein, Zeits. f. Physik **60**, 184 (1930).
E. T. S. Appleyard, Proc. Roy. Soc. **A128**, 330 (1930).
J. L. Hundley, Phys. Rev. **30**, 864 (1927).

[3] E. J. Jones and S. B. Hendricks, Chicago meeting, 1933, American Physical Society. Phys. Rev. **44**, 322A (1933).

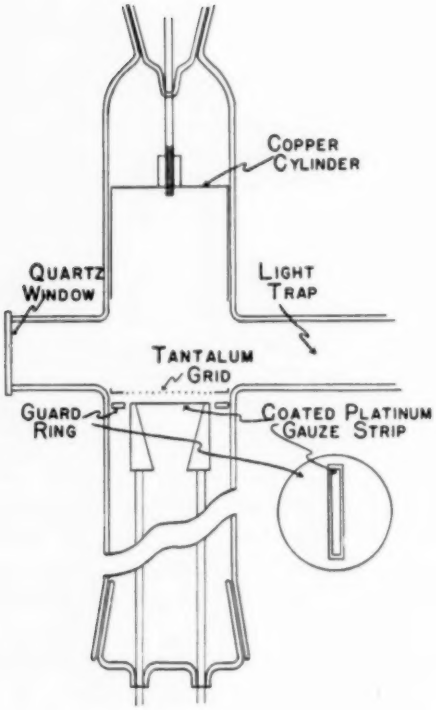

FIG. 1. A diagram of the apparatus.

rate plate. While this procedure made photometric comparison of one exposure with another less accurate, it was adopted to facilitate the taking of a large number of plates. For each exposure a time record of the ionic current was made with a recording microammeter. The current was of the order of 3×10^{-4} amp. and was held to this value as closely as possible by adjusting the temperature of the filament. From the integrated value of the positive ion current it was possible to reduce the intensity measurements to a comparable basis. The photometric measurements were made with a photoelectric photometer. The transmission of the clear part of the plate on each side of the line and of the line itself was obtained for each step of the step filter. The characteristic curve of the plate was obtained by plotting the logarithm of the blackening against the logarithm of the intensity.

RESULTS

A series of exposures from 150 to 1500 volts for lithium positive ions and from 300 to 1500 volts for potassium positive ions was taken as described. (Below 300 volts, for K^+ ions, space charge made it impossible to obtain currents of the magnitude chosen as a standard.) The plates were then measured and the blackening of each line relative to that of the line 2537 was calculated. To obtain the intensities relative to a fixed standard it is necessary to compare exposures taken on different plates. However, the plates were all from the same batch and were developed in exactly the same way. The curves showing the variation of the intensity of 2537 with both voltage and velocity are given in Figs. 2 and 3. In Fig. 4 are plotted the intensities of various other

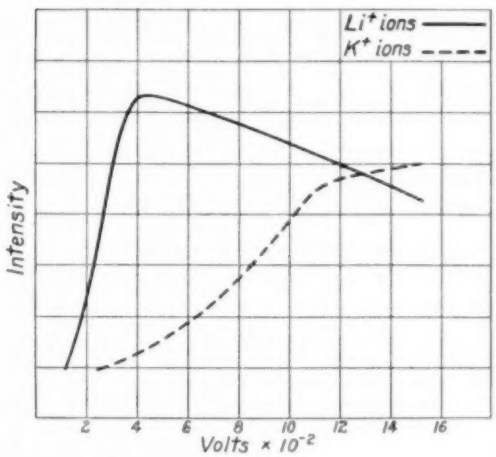

FIG. 2. The intensity of 2537 (arbitrary scale) as a function of voltage.

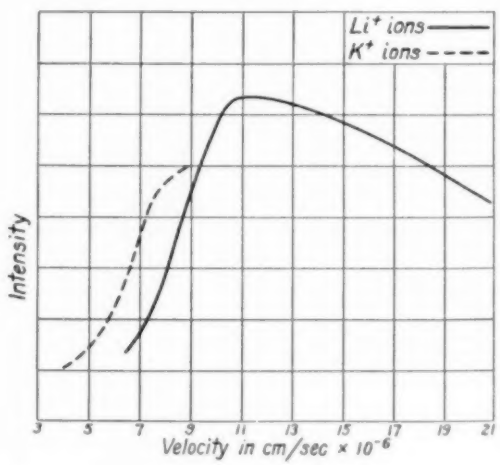

FIG. 3. The intensity of 2537 (arbitrary scale) as a function of velocity of the impacting ion.

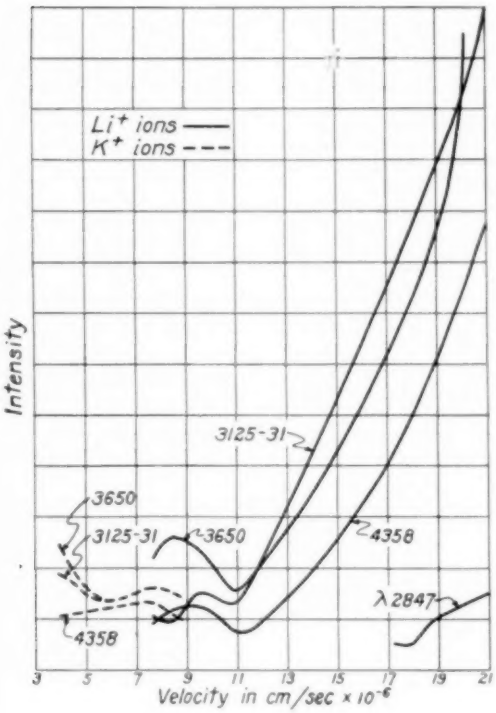

FIG. 4. The absolute intensities (arbitrary scale) of the prominent mercury lines as a function of the velocity.

mercury lines. These intensities were calculated by multiplying the intensities of each line relative to 2537 by the corresponding intensity of that line. The effect of the magnetic field in preventing stray electrons from exciting mercury vapor is seen in Fig. 5. In exposure *A* the magnetic field failed for 90 minutes. As may be seen the spectrum has the familiar appearance of that of the ordinary arc. An interesting feature which is illustrated in these photographs is the appearance of 2857 of the arc spectrum and 2847 of the spark spectrum in *A* while in *B* (pure positive ion excitation) only the spark line 2847 appears.

The following characteristic differences between the mercury spectrum excited by positive ion impact and the spectrum excited by electron impact may be pointed out. The most conspicuous of these is the relatively great intensity of the line 2537 in positive ion bombardment. Up to 1500 volts this line is more than three times as intense as any other line on the plate. This effect is, of course, not due to any lack of energy on the part of positive ions.

Another interesting feature of positive ion excitation is that the lines do not appear in the order of the energy necessary for their excitation. Table I illustrates this point. It will be noted that

TABLE I. *Order of appearance of Hg levels by positive ion excitation.*

Term	Energy	Order of appearance	Term	Energy	Order of appearance
2^3P_1	4.9	1	3^1S	9.2	absent
2^3S	7.7	3	4^1D & ^3D	9.3	4
2^1S	7.9		4^1S	9.7	absent
3^1D & ^3D	8.8	2	Hg II		
3^3S	9.1	7	$2S$	22	5
			$3d$	23	6

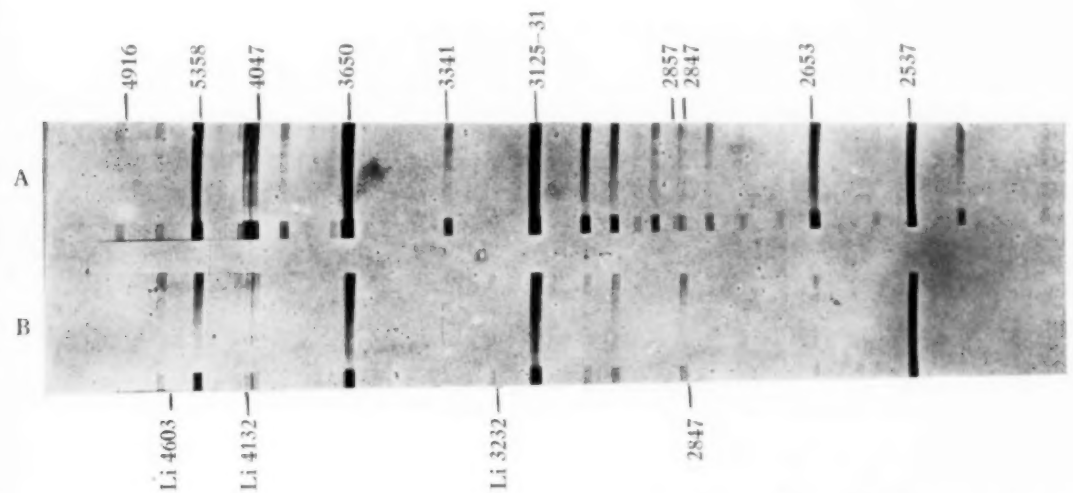

FIG. 5. Plate showing the effect of secondary electrons; *A*, magnetic field off 1½ hours. Total exposure time 8 hours. *B*, magnetic field on 8 hours.

there is a preference for levels of higher L values and this suggests the possibility that in collisions of this type there is a preference for the transfer of larger amounts of angular momentum.

Attention should be drawn also to the early appearance of the spark lines. Some of them appear before lines of the arc spectrum which appear early in electronic excitation. Lithium arc lines appeared on the plates and their presence is probably due to the bombardment of lithium vapor arising from the lithium compounds by lithium ions. Capture of an electron by a lithium ion to yield the arc spectrum seems to be ruled out.

Finally, it is apparent from Figs. 2 and 3 that for this type of excitation the velocity of the ions rather than their energy is the variable which reduces the excitation produced by different ions to a comparable basis.

Acknowledgment

The author is deeply grateful to Dr. F. G. Cottrell and Dr. C. H. Kunsman who so kindly put the facilities of the Fixed Nitrogen Research Laboratory at his disposal for the performance of these experiments. He also takes pleasure in acknowledging the advice and assistance of Professor John T. Tate who suggested the problem and its principal method of attack.

Doppler Effect in Spectra of Positive Rays of Uniform Velocity in Argon, Neon, Helium

ANNA I. MCPHERSON, *Ryerson Physical Laboratory, University of Chicago*
(Received June 19, 1933)

Ions of argon, neon, helium, formed in a low voltage arc have been accelerated to high speeds in a short electric field, forming beams of positive ions which all have the same energy. The spectra of the beams of positive rays of uniform energy observed in the direction of motion show a characteristic Doppler effect, with displaced lines fully as sharp as the rest lines. With the exception of the very intense λ3418 of neon, the arc lines of argon and neon have no Doppler effect, while the lines of the first spark spectrum are accompanied by sharp displaced lines only slightly less intense than the rest lines, whose separation corresponds accurately to the speeds acquired by singly charged ions in the accelerating field, for velocities 9000 to 28,000 volts and several lines of higher spark spectra were observed with displaced lines also corresponding to singly charged ions. Satisfactory observations are made at pressure about 5×10^{-3} mm, the intensity and sharpness of the displaced lines diminishing with increasing pressure. In helium, the arc lines show relatively faint displaced lines corresponding to singly charged ions; one spark line λ4686 was accompanied by a relatively intense displaced line, while the only other spark line observed, λ4541, had no Doppler effect.

CANAL rays in passing through a gas excite a spectrum characteristic of the gas at rest and also radiate themselves. Viewed in the direction of motion, the spectrum from the moving particles exhibits a Doppler displacement towards the shorter wave-lengths. As usually produced, the canal ray particles do not all have the same speed, because of change of charge within the accelerating field; hence the spectral lines showing the Doppler shift are correspondingly diffuse, their maximum displacements less than anticipated from the magnitude of the accelerating field. In general, the displaced lines of the spark spectra are more intense than the displaced lines of the arc spectra for high voltages.[1]

In the present experiments, the Doppler effect has been investigated in argon, neon and helium for beams of positive rays in which all the particles have nearly the same energy. In marked contrast to previous observations, the displaced lines are sharp and their positions are calculable from the magnitude of the accelerating field within the accuracy of observation. The beam of uniform energy was obtained by the method developed by Dempster, in which ions formed in a low-voltage arc traverse an accelerating field too short for an appreciable number of particles to change charge.[2, 3, 4]

APPARATUS AND METHOD

The discharge tube shown in Fig. 1 is Pyrex glass, 45 cm long by 4 cm diam. One end is ground smooth and fitted with a quartz window

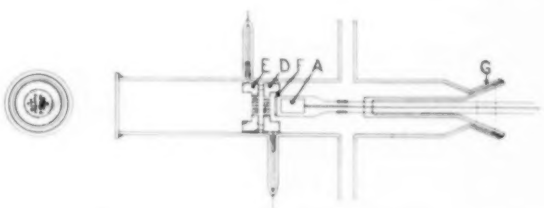

FIG. 1. Discharge tube for production of beams of positive ions of uniform energy.

waxed in position. F is an oxide-coated filament; D, E, are steel electrodes held in place by glass rods. The perforations in D, E, are similarly cut as shown in the end-on view, in such a way that the solid strip in the center of the electrodes conceals the filament F. Before mounting the

[1] Handbuch d. Physik **24**, 112–136, and Wien-Harms Handbuch d. Experimentalphysik **14**, 643 and following.

[2] H. F. Batho and A. J. Dempster, Astrophys. J. **75**, 34 (1932).

[3] Philip Rudnick, Phys. Rev. **38**, 1342 (1931).

[4] H. F. Batho, Phys. Rev. **42**, 753 (1932).

electrodes were partially outgassed by heating in vacuo to redness. The waxed joint G allowed easy removal of the anode and the filament for renewal or adjustment.

The filament F and the perforated electrode D were kept at ground potential throughout, the anode A was kept about 100 volts positive, while the electrode E was highly negative, from 9000 to 28,000 volts. Thus positive ions were formed in the arc AF, drifted into the narrow accelerating space $DE-3.75$ mm—then passed into the observation space beyond.

The vacuum was produced by a Gaede mercury diffusion pump, backed by a Cenco Hyvac oil pump. Pressures were measured with a McLeod gauge. A trap immersed in liquid air served to keep mercury vapor from the discharge tube.

High negative potential from a 2.4 kilowatt transformer, rectified and smoothed by a kenotron and condenser, reached electrode E through a high resistance. For convenience in estimating the voltage across DE, before the experiment was begun a micrometer spark gap with inch spheres was connected across DE, a voltmeter across the primary of the transformer. The primary voltage was calibrated over the range used, in terms of the spark gap for breakdown and the equivalent high potential.[5] The applied high potential was kept constant by maintaining steady voltmeter readings across the primary of the transformer.

The gases were purified by evaporating a small bit of magnesium metal in a side-tube of the storage vessel with an induction heater; the system was usually refilled for each photograph.

Two spectrographs were used, for the visible a Steinheil instrument with three large glass prisms, dispersion 58.3A per mm at $H\beta$, 32.4 at $H\gamma$; and for the ultraviolet, a Hilger quartz single prism spectrograph, type E-3, dispersion 37A per mm at λ4000, 14.6 at λ3000. The positive ray beam, which was about 12 cm long, was viewed end-on, the image of the unperforated central strip of electrode E being formed on the slit of the spectrograph so that no light from the filament of the arc behind it could enter the spectrograph directly. Eastman 40 plates were used.

[5] W. Peek, *Dielectric Phenomena in High-Voltage Engineering*, McGraw-Hill (1929).

Experimental Results

Photographs were taken, with the two spectrographs, of the canal ray spectra of neon, argon, and helium, covering the range of wave-lengths from about 2500 to 5000A. The applied potentials varied from 9000 to 28,000 volts. Gas pressures between 10^{-2} and 10^{-3} mm Hg, requiring exposure times from one hour to about 20 hours, gave satisfactory pictures. The effect of increasing the pressure as far as 3×10^{-1} mm was studied in neon.

The appearance of the photographs taken at the lower pressures is characteristic, each spectrum appearing to consist mainly of doublets. The displaced line in all cases is as sharp as the undisplaced line, indicating the uniformity of speed among the moving particles, and is usually slightly less intense. The intensity of both the rest lines and the displaced lines increases appreciably with increasing speeds of the moving particles. The only impurity lines were $H\beta$ and $H\gamma$ and Hg 4358.

Neon

Doppler effects in neon canal rays were observed by Dorn[6] in 1909 for a few lines in the red part of the arc spectrum and in 1931 by Romig[7] who, with unhomogeneous rays of 24,000 volts maximum velocity found the effect for many lines of the spark spectrum and strongly for two lines of the arc spectrum.

In the present experiments, the neon photographs showed sharp, intense Doppler lines, but

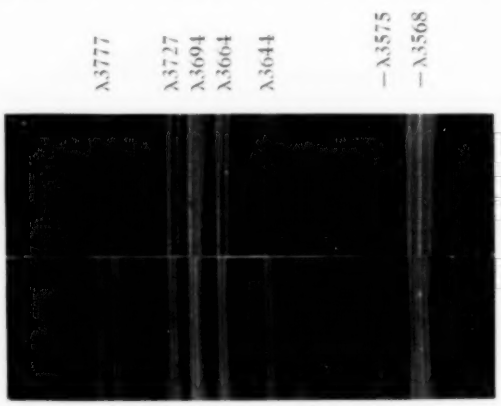

Fig. 2. Doppler effect spectra of neon canal rays, 26,350 and 9100 volts.

[6] E. Dorn, Phys. Zeits. **10**, 614 (1909).
[7] W. Romig, Phys. Rev. **38**, 1709 (1931).

TABLE I. *Neon lines which show Doppler effect.*

International A	Intensity	International A	Intensity
4569.02	5	3355.09	7
4522.65	4	3345.49	3
4428.56	6	3344.44	5
4409.31	7	3334.89	10
4397.94*x*	6	3327.22	5
4391.94	7	3323.79	7
4379.47	6	3319.76	3
4322.66	1	3297.74	8
4322.26	2	3244.15	5
4290.40	6	3232.38	3
4231.61	5	3230.13	5
4219.74	6	3224.84	5
3942.19	3	3218.22	8
3777.14	8	3214.33?	5
3766.28	8	3198.58	6
3751.25	4	3097.15	2
3734.94	7	3093.99	4
3727.09	9	3059.15*x*	3
3713.07	10	3054.70	5
3709.66	7	3047.60	6
3694.19	10	3034.49	5
3664.05	9	3028.90	4
3643.90	5	3027.07	4
3594.15	2	3001.72	7
3574.65	5	2967.20	3
3568.47	6	2955.77	7
3542.89	7	2866.60 II Spark	6
3481.97	6	2822.97 II Spark	4
3477.66	3	2792.04	4
3417.90 Arc	10	2777.60 II Spark	5
3418.00 Arc	6	2678.65 II Spark	3
3406.88	5	2677.90 II Spark	5
3404.77	4	2613.41 II Spark	4
3392.81	7	2610.04 II Spark	5
3388.47	5	2595.66 II Spark	6
3378.28	5	2593.57 II Spark	6
3367.25	6	2590.01 II Spark	7
3360.63	5		

the appearance of the spectrum was quite unlike the normal neon Geissler tube spectrum. That this was neon was verified from the displacements of the lines, which agreed with that of singly charged ions of atomic weight 20. The spectrum was found to be the first spark spectrum, with a few higher order spark lines and some of the more intense arc lines. The two typical pictures of Fig. 2, in which the rest lines are matched and appear continuous, show clearly the sharpness and intensity of the Doppler lines, and the different displacements at two different speeds.

Table I lists the lines which show the Doppler effect. Unless otherwise specified, all lines belong to the first spark spectrum. Lines marked *x* show Doppler effect, but the position of neighboring lines prevented measurement of the displacement. The wave-length and classification of Bloch[8] were followed for the spark lines, those of Paschen[9] for the arc. While most of these lines belong to the first spark spectrum, several lines of the second spark spectrum also exhibit Doppler effect, as do the very intense unresolved arc lines 3417.9 and 3418.0. The appearance of their displaced lines was not distinguishable from that of the displaced first spark lines in respect to sharpness, intensity or distance of separation. In no case was more than one displaced line observed associated with a line. It would not have been possible in these experiments to resolve the displaced line corresponding to the less abundant neon isotope of mass 22.

Measurement of the separations on two spectrograms with applied voltages 26,350 and 9100 showed that all the displacements corresponded to the velocity acquired by a singly charged ion traversing the entire accelerating field. From the first plate, calculating from the voltage 26,350, the value of $d\lambda/\lambda$ is 0.00168 while the average measured value is 0.00164; from the other, voltage 9100, the values are 0.00099 and 0.00101.

Effect of pressure. A series of photographs was made, the pressure of the neon being increased to 3×10^{-1} mm, when sparking took place between the electrodes, then 1.5 mm apart. With increase of pressure the observed Doppler lines became less sharp and decreased in intensity relative to the rest lines. At pressure 3×10^{-1} only the most intense lines were accompanied by displaced lines, which were faint and diffuse and extended a considerable distance towards the rest lines.

The appearance of the displaced lines and their extension towards the rest lines suggest that most of the moving ions have lost charge in the accelerating field, attaining all velocities up to the maximum. The weakening of the displaced lines may also be due to the fact that the normal rate of decay of radiation from the group of excited particles is hastened by collision and neutralization of the radiating particles, since the time of decay of radiation intensity to $1/e$ of its initial value is about 10^{-8} seconds,[10] the same

[8] L. Bloch, J. de Physique et le Radium **7**, 129 (1926).

[9] F. Paschen, Ann. d. Physik **60**, 405 (1919).

[10] W. Wien, Ann. d. Physik **73**, 483 (1924); H. Kerschbaum, Ann. d. Physik **79**, 465 (1926).

order of duration as the life before neutralization of a moving ion at the speed and pressure here considered.[3, 4]

Argon

Dorn,[11] Stark and Kirschbaum[12] and Friedersdorff[13] have studied Doppler effects in argon canal rays under various conditions, the latter workers reporting broad diffuse displaced lines accompanying both the "red" and the "blue" spectra, with regions of maximum intensity apparently corresponding to velocities of multiply charged ions. In the present experiments, photographs were taken with both spectrographs. All the blue, first spark lines of considerable intensity were accompanied by sharp displaced lines of slightly less intensity, while no red arc lines showed any Doppler effect whatever.

Table II lists the argon lines for which Doppler effect was observed; separations were not measured for lines marked *x*, owing to the proximity of other lines. Wave-length tables of Rosenthal[14] and Bloch, Bloch and Dejardin[15] were used for the blue spectrum, that of Meissner[16] for the red spectrum.

In distinction to the earlier observations, the shifted lines were sharp, and their displacements corresponded accurately to those calculated from the velocity acquired by a singly charged argon ion falling through the entire applied potential difference. For example, at 20,400 volts the average measured value of $d\lambda/\lambda$ is 0.00101, the calculated value is 0.00106; at 26,000 volts the measured value is 0.00119, that calculated is 0.0012; and at 28,000 volts these values are 0.00124 and 0.00123.

TABLE II. *Argon lines showing the Doppler effect.*

Internat'l. A	Intensity	Internat'l. A	Intensity	Internat'l. A	Intensity
49 65.12	7	43 09.25	3	35 82.35?*x*	8
49 33.24	6	43 09.11	2	35 76.62	10
48 79.9	12	43 00.66	6	35 61.04	6
48 67.59*x*	3	42 77.55*x*	8	35 59.53	6
48 47.90	8	42 66 53	10	35 45.84 }	9
48 06.07	20	42 37.23*x*	7	35 45.58 }	10
47 64.89	10	42 28.18	7	35 14.39	9
47 35.93	15	41 89.67?	4	34 91.54 }	8
47 26.91	10	41 31.73	8	34 91.24 }	6
46 57.94	9	41 03.91	10	34 76.74	6
46 37.25	6	40 76.96 } *x*	4	33 88.54	7
46 09.60	15	40 76.64 } *x*	5	32 81.72	6
45 89.93	9	40 72.40 }	7	{ 31 28.00	4 }
45 79.39	8	40 72.01 }	9	{ Rowland's Sys., II Spark }	
45 47.78*x*	5	40 52.94*x*	5	30 99.97	4
45 45.08	10	40 42.91*x*	8	30 93.41	8
44 81.8	8	40 38.82	7	30 85.05	4
44 33.83	5	40 13.87?	10	30 82.99	4
44 31.02*x*	8	39 46.10*x*	7	29 42.90	8
44 30.18*x*	9	38 68.53	8	{ 28 84.21?	2 }
44 26.01	15	38 50.57	15		II Spark }
44 01.02 }	7	{ 38 19.04?	4 }		
44 00.09 }	6	{ Rowland's Sys., II Spark }			
43 83.79	4	38 09.49	7		
43 79.74*x*	8	37 99.39	6		
43 75.96	5	37 80.84	8		
43 71.36	8	37 65.27*x*	6		
43 70.76	6	37 37.89*x*	6		
43 62.07?	5	37 29.29	10		
43 52.23	6	37 17.17	5		
43 48.11	20	36 22.15	6		
43 31.25	10	35 88.44*x*	10		

[11] E. Dorn, Phys. Zeits. **8**, 589 (1907).

[12] J. Stark, H. Kirschbaum, Ann. d. Physik **42**, 255 (1913).

[13] K. Friedersdorff, Ann. d. Physik **47**, 737 (1915).

[14] A. H. Rosenthal, Ann. d. Physik **4**, 49 (1930).

[15] L. Bloch, E. Bloch and G. Déjardin, Ann. de Physique **2**, 480 (1924).

[16] K. W. Meissner, Zeits. f. Physik **39**, 172 (1926).

The three second spark lines which appeared, 3819.30, 3128.00, 2884.21, all have displaced lines whose separations correspond to singly charged ions. No line was observed whose displacement corresponded to a multiply charged ion.

Helium

Doppler effects have long been known for some lines in the visible spectrum of helium canal rays.[17] Stark[18] reported two maxima of intensity in the displaced strip when the helium ions were sent into mixtures of helium with hydrogen or iodine vapor.

In the present experiments, the results obtained with helium differed markedly from those with neon and argon. The plates showed displaced lines accompanying the lines of the arc spectrum, apparently all of the same intensity relative to the rest lines, very much less intense but quite as sharp.

TABLE III. *Helium lines for which Doppler effect is observed.*

International A	International A	International A
5047.7*x*	4437.552*x*	4009.270*x*
5015.68	4387.931	3964.732
4921.9	4168.965*x*	3888.649
4713.373	4143.759	3867.631 *x*
4713.143	4120.989	3867.477
4685.75 Spark	4120.817	3819.761 *x*
4471.681	4026.363	3819.614
4471.479	4026.189	3187.744*x*

Table III lists the helium lines for which the Doppler effect was observed, lines not previously reported are marked *x*.

Since at least one line is here represented belonging to each singlet series and each doublet series of the helium spectrum, presumably all the arc lines show the Doppler effect. Insufficient intensity probably caused the earlier failures to observe many of the displacements.

The spark line 4686 appearing on several of the plates differed from the arc lines in that the displaced line was of intensity comparable to the rest line, in accordance with Rau's[19] observation of its characteristic appearance. The same plates also showed the Pickering spark line 4541, stronger than 4686, but this line had no accompanying displaced line.

DISCUSSION

The observed sharpness of the displaced lines was anticipated, as the measurements of Rudnick and Batho on the distance travelled by a positive ion before neutralization show that few ions change their charge in the length of the accelerating field at these pressures and speeds and thus the beam contains particles of sensibly uniform energy. The absence of displacements corresponding to velocities of multiply charged ions accords with the observations of Bleakney[20] that most of the ions formed by single electron impact in a 100-volt arc in neon, argon, helium, are singly charged.

The beam of moving particles for most of its observed length has its equilibrium distribution mostly neutrals, some positive ions;[21] but the almost entire lack of Doppler effect in the arc spectrum indicates that the excitation of the moving neutrals by collision with particles at rest does not result in arc radiation in considerable intensity, nor does the neutralization of the moving positives. Collisions between moving neutrals and neutrals at rest must result on the average in the same degree of excitation of the moving particles and the rest particles. If the greater number of such collisions produces an excited ion and a normal atom, or two excited ions, as is possible on closely interpenetrating collisions,[21] this could account for the observed Doppler effect in the spark spectrum, with the displaced and rest lines of comparable intensity.

The behavior of the three gases is probably similar and it is possible that the neon and argon as well as the helium have Doppler effect in their

[17] H. Rau, Phys. Zeits. **8**, 360 (1907); G. F. Hull, Astrophys. J. **25**, 1 (1907); H. Gerdien, R. Holm, Ann. d. Physik **27**, 844 (1908).

[18] J. Stark, Jahrbuch der Radium und Elektronik **14**, 139 (1917).

[19] H. Rau, Ann. d. Physik **73**, 271 (1924).

[20] W. Bleakney, Phys. Rev. **36**, 1303 (1930).

[21] W. Weizel and O. Beeck, Zeits. f. Physik **76**, 3–4, 250 (1932).

arc spectra but with displaced lines too faint to be perceived in the present experiments, except for the strong neon arc lines at 3418.

From the measured displacement of the displaced spark lines of order higher than the first, observed in the spectra of neon and argon, these lines were radiated from particles which passed through the accelerating field with only a single charge, afterwards becoming more highly charged and excited in the observation space.

The writer acknowledges with pleasure the gracious assistance and encouragement of Professor A. J. Dempster, at whose suggestion these experiments were performed.

Electron Diffraction by Hydrocarbons

H. R. NELSON, *Department of Physics, Cornell University*

(Received August 7, 1933)

Thin films of vaseline, paraffin, and tap grease were prepared (1) by evaporation from a heated filament on to a metal surface, (2) by allowing an ether solution to evaporate from a water or metal surface leaving the hydrocarbon film behind and (3) by smearing the greases on metal surfaces. When 25 to 50 kv electrons were reflected at grazing incidence from these films the diffraction patterns consisted of rows of spots similar to an x-ray single crystal rotation picture. The resolving power of all but the smeared films is much better than has been reported previously. Observed reflections are in good agreement with the structure of normal hydrocarbon crystals found by Müller. The patterns indicate that the films are largely, if not completely, crystalline, with the long axes of individual crystals perpendicular to the plane of the film.

INTRODUCTION

IT is well known that the molecules in thin films of various organic acids have a definite orientation in the film.[1] Trillat and Nowakowski have shown that the molecules in films of normal hydrocarbons are similarly oriented.[2] Recently Trillat and Hirsch[3] and Garrido and Hengstenberg[4] have made electron diffraction pictures by transmission through paraffin films produced by allowing an ether solution of paraffin to evaporate on water. Their experiments indicate that the films contain minute single crystals oriented with the long axis of the orthorhombic cell perpendicular to the plane of the film. Thomson and Murison[5] have recently obtained diffraction patterns by reflecting electrons at grazing incidence from a plane metal surface on which various greases have been smeared. Their pictures indicate that the hydrocarbon molecules are lined up perpendicular to the surface on which they lie. The present paper describes diffraction experiments similar to those of Thomson and Murison. The hydrocarbon films used have considerably greater resolving power for the various crystal reflections than has been achieved heretofore.

[1] For a résumé of the field see N. K. Adam, Kolloid Zeits. **57**, 125 (1931).

[2] Trillat and Nowakowski, Ann. de Physique **15**, 455 (1931).

[3] Trillat and Hirsch, J. de Physique **4**, 38 (1933).

[4] Garrido and Hengstenberg, Zeits. f. Krist. **82**, 477 (1932).

[5] Thomson and Murison, Nature **131**, 237 (1933).

EXPERIMENTAL PROCEDURE

The pictures were taken in an electron diffraction camera essentially like that described by Thomson and Fraser.[6] An oxide coated platinum strip serves as the electron source. A full-wave rectifier with smoothing condensers supplies the accelerating potential which is measured by an electrostatic voltmeter.

25 to 50 kv electrons ($0.08\text{A} < \lambda < 0.055\text{A}$) were reflected at grazing incidence from a plane metal surface on which a very thin hydrocarbon film had been deposited. Equally good pictures were obtained from films of tap grease, vaseline, and a commercial paraffin called Parowax. These substances were deposited on the metal base (1) by evaporation from a tungsten filament placed near the metal base in the evacuated camera, (2) by allowing an ether solution of the hydrocarbon to evaporate on water and catching the resulting film on the metal base, (3) by allowing the ether solution to evaporate directly from the metal leaving the film behind and (4), in the case of the grease and vaseline, by smearing them on the metal. The quality of the pictures seems to be quite independent of the various ways in which the films were produced although it was difficult to obtain good results from those films which were smeared on the metal base. Films which were barely visible gave the best patterns. Thicker films charged up and distorted the pattern.

[6] Thomson and Fraser, Proc. Roy. Soc. **A128**, 641 (1930).

Results

An electron beam striking the film at grazing incidence will pass through several crystals in a direction perpendicular to their long c axes. Since, however, the a and b axes of individual crystals are oriented at random, the diffraction pattern is similar to that which would be obtained if a single crystal were rotated about the c axis during exposure. Better pictures are obtained if the film is rotated in its own plane during the exposure. The spot at the right end of the line at the bottom of Fig. 1 was made by

Fig. 1. Diffraction pattern formed by Parowax on aluminum.

the undeflected electron beam after the picture was taken. The horizontal row of spots immediately above the undeflected spot corresponds to the first layer line of an x-ray rotation picture. Three other layer lines appear above the first. The equatorial line lies within the shadow of the metal base.

The length of the unit cell cannot be determined from the pictures because the wave-length is too small and because the resolving power in the direction of the c axis is very small, the film being only a few molecules thick. Furthermore, each film consists of a mixture of hydrocarbons which have c axes of different lengths. There is, however, a regular spacing along the c axis which is common to all hydrocarbons, *viz.*, the spacing between alternate carbon atoms in the chain. This is not a true spacing for it is broken at the ends of the molecules.[7] Nevertheless it is sufficiently regular to give rise to the layer lines. This pseudo-spacing, together with the mixture of crystals, undoubtedly accounts for the elongation of the spots in the direction of the c axis. Since all Bragg angles are small and the crystal-to-plate distance is large (40.3 cm), the layer lines and row lines appear straight.

The spacing between layer lines on 11 plates gives 2.51A for the distance between alternate carbon atoms in the chain. In order to identify the spots several pictures were taken by transmission through a film containing single crystals. Measurements of the rectangular array of spots

Table I. *Intensities: sss, very intense; ss, very strong; s, strong; m, medium; f, faint; ff, very faint; d, diffuse; ?, doubtful.*

r, (cm) (obs)	r, (cm) (calc)	Miller indices	Observed intensities
0.0	0.0	0 0 n	f
	0.70	1 0 n	
1.06	1.06	0 1 n	s
1.26	1.28	1 1 n	m
1.40	1.40	2 0 n	m
1.75	1.76	2 1 n	s
	2.10	3 0 n	
	2.13	0 2 n	
2.23	2.25	1 2 n	s
2.36	2.35	3 1 n	m
2.53	2.55	2 2 n	f
2.80	2.80	4 0 n	f
2.97	2.99	3 2 n	f
	3.00	4 1 n	
3.15	3.20	0 3 n	f
	3.27	1 3 n	
3.47	3.49	2 3 n	m
3.50	3.50	5 0 n	?
	3.52	4 2 n	
3.66	3.66	5 1 n	m
3.78	3.82	3 3 n	?
	4.10	5 2 n	
	4.20	6 0 n	
4.26	4.25	4 3 n	d, m
	4.27	0 4 n	
4.33	4.32	1 4 n	ff
	4.34	6 1 n	
	4.49	2 4 n	
4.71	4.71	6 2 n	f
0.00	0.00	0 0 2n	sss
	0.70	1 0 2n	
	1.06	0 1 2n	
1.26	1.28	1 1 2n	ss
1.42	1.40	2 0 2n	s
	1.76	2 1 2n	
2.09	2.10	3 0 2n	f
	2.13	0 2 2n	
	2.25	1 2 2n	
2.36	2.35	3 1 2n	ff
2.53	2.55	2 2 2n	ff

[7] A. Müller, Proc. Roy. Soc. **A120**, 437 (1928).

thus obtained gave $a = 7.35$A and $b = 4.83$A for the two short axes of the unit cell. These values are in good agreement with those obtained by Trillat and Hirsch by the same method but are about 2 percent less than Müller's. Reflections in the first layer line are of the form $h\ k\ n$; those in the second $h\ k\ 2n$, where n depends on the number of carbon atoms in the molecule. In the case of Parowax (m.p. 50°) whose principal constituents are probably $C_{23}H_{48}$ and $C_{24}H_{50}$, the values of n would range around 24 and 25.

Data from a typical plate are presented in Table I. The first column gives the observed distance, r, between a spot and its twin on the opposite side of the layer line's center. In the second column are tabulated all possible values of r computed from the spacings obtained in the transmission experiments. The 0 0 $2n$ planes pass through successive carbon atoms in the chain. They are, therefore, most rich in scattering points, a fact which accounts for the exceedingly intense spot in the center of the second layer line.

Missing reflections and the estimated intensities of those present are in good qualitative agreement with the structure of normal hydrocarbon crystals found by Müller. Very few of the smeared films gave well-resolved reflections on the layer lines. Films prepared by the other three methods, however, always gave well-defined spots. The intensity of these crystal reflections in comparison with the relatively weak general scattering indicates that the molecules composing these films are not only lined up perpendicular to the surface but most of them are grouped into actual crystals.

The author wishes to express his appreciation to Professor C. C. Murdock and Dr. A. G. Emslie for helpful suggestions and criticisms received in the course of this work.

New O_2^+ Bands. Dissociation Energy of O_2^+ and Ionization Potential of O_2

R. S. MULLIKEN AND D. S. STEVENS, *Ryerson Physical Laboratory, University of Chicago*

(Received August 10, 1933)

Three new bands are reported in the first negative and several in the second negative system of O_2^+. The numbering of the vibrational levels of the normal state of O_2^+, hitherto in doubt, is definitely established. The observed ionization potentials I of O_2 at 12.5 and 16.1 volts are discussed. From the known O_2^+ energy levels it is shown that the dissociation energy D of O_2^+ cannot be less than 6.0 volts; by extrapolation from the known levels we get 6.54 volts. The latter value, however, would require 12.11 volts as the ionization potential of O_2. We suggest $D=6.45\pm0.1$ and $I=12.2\pm0.1$ volt as a reasonable compromise (making D and I consistent, as they must be in reality) between the ionization potential and band spectrum data.

A. New O_2^+ Bands; Vibrational Numbering

THE O_2^+ band spectrum contains two band systems; the first negative bands, which lie mainly in the visible and (probably) the infrared, and the second negative bands which extend through the visible and throughout the ultraviolet to below λ2000.[1,2] The rotational structure of the first negative bands has never been analyzed, although it has been suggested that they may be $^4\Sigma^-_g \rightarrow {}^4\Pi_u$.[2] It is certain at any rate that they have no state in common with the second negative bands.

The second negative bands, whose rotational structure has been analyzed,[3] are of the type $^2\Pi \rightarrow {}^2\Pi$. In all probability their final state is the $^2\Pi_g$ normal state of O_2^+ and the bands are $^2\Pi_u \rightarrow {}^2\Pi_g$. The vibrational numbering of this system has never been satisfactorily established as regards v'', although the v' numbering is definitely known. This is because, on account of a large difference between r_e' and r_e'', bands having small v'' occur only for fairly large v' and these are weak and lie near λ2100, making them difficult to photograph. The only published data and photographs for the region near λ2100 in O_2^+ are those of Ellsworth and Hopfield.[4] Their reproduced photographs show bands of the system as far as λ2100 or perhaps as far as λ1975, but the authors give data only as far as λ2184 and state that the bands at shorter wave-lengths are too weak to measure.

Since a knowledge of the v numbering of the normal state of O_2^+ is necessary for an accurate knowledge of the values of r_e, ω_e and D (energy of dissociation) of O_2^+ and has a bearing on the ionization potential of O_2, we have taken new photographs of the O_2^+ spectrum under moderate dispersion with the object of photographing as many bands as possible, especially in the λ2100 region. (A description of the discharge tube used in this work will be published elsewhere by one of us.) In this way we have found several new bands of the second negative system, some near λ2100, others in the visible region.

We have also found three new bands which have the same structure as the first negative bands and extend the observed wave-length range of this system in both directions. Data on these bands are given in Table 1, together with v' and v'' assignments consistent with those now in use for the previously known bands of the system.

Our results on the second negative bands confirm the v'' assignment of Birge, which is that used by Ellsworth and Hopfield.[4] The new bands we have measured are given in Table I, with the values of v' and v'' which we believe to be correct.

[1] Cf. W. Jevons, *Report on Band Spectra of Diatomic Molecules* (Published by the Physical Society, London, 1932), for data and literature.

[2] R. S. Mulliken, Rev. Mod. Phys. **4**, 51 (Fig. 48) and 82 (Table 29) (1932). It should be noted that the v numbering and resulting constants, as given in references 1, 2, are based on the present work.

[3] D. S. Stevens, Phys. Rev. **38**, 1292 (1931).

[4] V. M. Ellsworth and J. J. Hopfield, Phys. Rev. **29**, 79 (1927).

TABLE I. *Bands of O_2^+ newly found or measured by us. (All data refer to heads, and are in cm^{-1} in vacuo.)*

v',v''	ν	v',v''	ν
A. Bands of the second negative system			
15,0	48536 dif 48334 dif	0,10	21368 21177
14,0	48042 dif 47824 dif	1,11	20714 20496
13,0	47520 47329	0,11	19855 19655
12,0	46969 46745	0,12	18367 18182
11,0	46383 46197	1,13	masked 17606
11,1	44559 44375	1,14*	16381 masked
*B. Bands of the first negative system.***			
3,0	**19972**	0,1	15574
2,0	18878	0,2	14581
1,0	17751	0,3	**13606**
0,0	16589	0,4	**12669**

* Others may also be present at this end of the system, masked by first negative bands.

** The measurements (cm^{-1} in vacuo) refer to the *most obvious head* in each case. The data are from Frerichs' paper,[5] except for the new bands (0,3), (0,4), and (3,0). Each most obvious head appears to be accompanied by several others, namely, one fainter head displaced about 20 cm^{-1} towards smaller frequencies, as already noted by Frerichs, and two or three strong, but not always well-marked heads (or possibly accidental accumulations of lines) displaced towards larger frequencies.

(The errors of measurement, which are fairly large, can be judged by the lack of constancy in the measured interval between the two heads of each band in Table I.) The bands (11,0), (12,0), and (13,0) are clear and definite, while (14,0) and (15,0) are weak and diffuse-looking on our plates, but probably genuine. No bands beyond (15,0) can be distinguished. Conceivably this and the diffuseness of (14,0) and (15,0) are the result of a Stark effect in the strong fields used to produce the O_2^+ bands.

It is of especial interest that the (11,0), (12,0) and (13,0) bands are also easily visible and measurable (with results which, we find, check ours) on the reproduction given by Ellsworth and Hopfield, even though these authors did not give measurements for them. The present measurements on these bands agree within the experimental error with values calculated by extrapolating from the previously measured series (6,0) to (10,0). This result disposes of the supposition of Ellsworth and Hopfield that the bands, not measured by them, which we identify as (11,0) to (13,0) belong to new progressions with lower v'' values than any of the measured bands. It was as a matter of fact just this supposition of Ellsworth and Hopfield that raised the question about the v'' numbering which, we hope, is now settled.

Specifically, the question which we had to decide was whether the series of bands which we call (v',0) really has $v''=0$ or whether it might be that they have $v''>0$. Our data, together with earlier data, give an unbroken series of (v',0) bands from $v'=6$ to $v'=15$. If $v''>0$ were correct for this series of bands, for instance if $v''=1$, then another series with v'' really zero should also appear and, as one sees by plotting all the known bands on a Condon parabola, at least a few of this series should be intense enough to be plainly visible in the region of the bands which we call (11,0) to (15,0). Actually, no such extra bands are to be seen on our plates, and we conclude that what we call $v''=0$ really is so.

The v'' numbering here established disagrees with that deduced by one of us and by Stueckelberg on the basis of the observed vibrational intensity distribution and the Franck-Condon principle.[6] The disagreement is, however, disposed of by the fact that these intensity considerations were based on an assumed value of r_e' (about 1.5A) which differs considerably from the later determined actual value (1.41A)[3] and because of other uncertainties in the $U(r)$ curves used.

The wrong v'' numbering just mentioned (two units too large) was adopted by one of us[3] in connection with the analysis of the O_2^+ bands. Hence the v'' numbering in that paper and the molecular constants and equations which depend

[5] R. Frerichs, Zeits. f. Physik **35**, 686 (1926). Although Frerichs gives probable band *origins* in his summarizing table, the heads can be found from his other tables.

[6] R. S. Mulliken, Phys. Rev. **32**, 213 (1928); E. C. G. Stueckelberg, Phys. Rev. **34**, 66 (1929).

on this should be changed. For example, the equation for B'' given there should be altered to:

$$B''=1.592-0.009v''.$$

These changes have already been included in the constants and figures of references 1 and 2.

B. Dissociation Energy of O_2^+ and Ionization Potentials of O_2

Measurements of the ionization potential of O_2 long gave conflicting results. Recent accurate measurements of Tate and Smith,[7] however, give two potentials, one at 12.5 and one at 16.1 volts (stated probable error ± 0.1 volt) in exact agreement with earlier measurements by Mackay, whose results on ionization potentials of other gases have proved unusually reliable. The existence of two potentials, near 12.5 and near 16.1 volts, may then be considered as well established. The potential 12.5 volts doubtless corresponds to the energy required to remove a π_g electron from the normal state of O_2, which is . . . $(\sigma_g)^2(\pi_u)^4(\pi_g)^2$, $^3\Sigma^-_g$, to give the normal state of O_2^+, . . . $(\sigma_g)^2(\pi_u)^4(\pi_g)$, $^2\Pi_g$.

The potential at 16.1 volts may reasonably be interpreted as corresponding to the energy required to remove a π_u electron from normal O_2 to give O_2^+ in the state . . . $(\sigma_g)^2(\pi_u)^3(\pi_g)^2$, $^4\Pi_u$. A $U(r)$ curve for such a state (which *may* be the lower state of the first negative bands of O_2^+) is sketched in Fig. 48 of reference 2. It should be noted that, although the configuration $(\pi_u)^3(\pi_g)^2$ must give several states $^4\Pi_u$, $^2\Pi_u$, $^2\Phi_u$, $^2\Pi_u$, $^2\Pi_u$, just the first two of these are to be expected if an electron is removed from *normal* O_2, in which the $(\pi_g)^2$ group is in the particular condition $^3\Sigma^-_g$. The remaining states $^2\Phi_u$, $^2\Pi_u$, $^2\Pi_u$ correspond to $^1\Delta_g$ and $^1\Sigma^+_g$ conditions of the group $(\pi_g)^2$. The $^4\Pi_u$ state should be lower than the corresponding $^2\Pi_u$ state, which is probably the upper state of the second negative bands of O_2^+ and which should be excited at a higher potential. Although $v=0$ of this $^2\Pi_u$ is only 4.73 volts above that of the normal state of O_2^+, one expects electronic excitation produced by electron impact to be accompanied with high probability by strong vibrational excitation, even to the point of dissociation (cf. reference 2, Fig. 48). This is in agreement with the observations of several writers who have found that O^+ ions begin to be produced from O_2 at about 19 to 20 volts (cf. Stueckelberg).[6]

The energy required to dissociate and ionize unexcited O_2 so as to give unexcited $O^+(^4S)+O(^3P_2)$ is exactly known: it is 18.65 volts. This is the sum of the ionization potential of O (13.56 volts for $^3P_2\rightarrow{}^4S$) and the energy of dissociation of O_2 (5.09 volts for O_2, $^3\Sigma^-_g\rightarrow 2\,O$, $^3P_2$). If from the value 18.65 volts we subtract 12.5 volts as the ionization potential of O_2, the remainder, 6.15 volts, should be the energy of dissociation, D, of $O_2^+(^2\Pi_g)$ into $O(^3P_2)+O^+(^4S)$.

An independent estimate of D for O_2^+ can be made from data on the second negative O_2^+ bands. Theory shows that both the upper ($^2\Pi_u$) and lower ($^2\Pi_g$) electronic states of these bands are permitted to, and almost certainly would, give unexcited $O(^3P_2)+O^+(^4S)$ on dissociation. [Assumption of excited O (^1D or ^1S) on dissociation runs counter to strict theoretical rules. If we assume excited $O^+(^2D$ or $^2P)$ we get, on using data for the total energy of excitation plus dissociation of excited O_2^+, based on the second negative bands, only 3.2 or 1.6 volts for the dissociation of O_2^+, into unexcited $O+O^+$, values which are ridiculously low.]

With the v'' numbering established here, the energy interval from $v''=0$ of normal $O_2^+(^2\Pi_{ig})$ to $v'=0$ of excited $O_2^+(^2\Pi_u)$ is 4.73 volts, while the energy interval up to the last level ($v'=15$) for which we have observed a band is 5.99 volts. (Note that for the $^2\Pi_u$ state, since it is of case b type,[3] the sub-levels $^2\Pi_{\frac{1}{2}}$ and $^2\Pi_{1\frac{1}{2}}$ fall together.) If we extrapolate the frequencies of the series of observed bands (6,0) to (15,0), we find that they converge approximately linearly toward a limit at 6.54 volts. Since the extrapolation beyond the last observed level is only 0.55 volt, our result should probably be not far from the correct value of D for the process $O_2^+(^2\Pi_{ig})\rightarrow O(^3P_2)+O^+(^4S)$. The corresponding value for D of the upper, $^2\Pi_u$, level is 1.81 volts. These values are somewhat higher than those (6.15 and 1.42 volts)[2] which we get from the ionization potential of O_2, using 12.5 volts for the latter. The disagreement is, however, within reason.

If we accept the D obtained from the ultra-

[7] J. T. Tate and P. T. Smith, Phys. Rev. **39**, 270 (1932).

violet bands as correct, the ionization potential of O_2 becomes 12.11 volts. In view of the general downward tendency in measured ionization potentials of molecules as the technique of measurement is improved,[8] it seems quite possible that the value 12.1 volts for O_2 may prove to be correct. The possibility of such downward shifts in measured ionization potentials may be ascribed in part to the action of the Franck-Condon principle, which often makes ionization with $v>0$ more probable than ionization with $v=0$, so that strong ionization sets in only gradually and at some distance above the true minimum ionizing potential. On the other hand it may be, in view of the fact that D values obtained by linear extrapolation are nearly always high, that the value $D=6.54$ volts is a little too high. We would therefore suggest as a reasonable compromise the following mutually consistent estimates for D of O_2^+ and the ionization potential of O_2: 6.45 ± 0.1 and 12.2 ± 0.1 volts.

[8] Consider, e.g., the results of Tate and associates[7] on N_2 and C_2H_2, as compared with earlier work; also J. T. Tate, P. T. Smith and A. L. Vaughan, Phys. Rev. **43**, 1054A (1933).

Analysis of Zeeman Patterns

RUSSELL A. FISHER, *Northwestern University*

(Received August 14, 1933)

A method for the representation and analysis of Zeeman patterns is explained. The method makes possible the representation in a simple graphical manner of the line distribution, intensities, polarization and g-values for Zeeman patterns occurring in all types of spectra. When applied to observed patterns the method offers a means of identification and analysis even if the patterns are imperfectly resolved.

INTRODUCTION

A GRAPHICAL method which was developed as an aid to the analysis of hyperfine structure patterns[1] has found considerable application by workers in that field. A similar device may be employed in the analysis of weak field Zeeman patterns. The graphical method applies to all types of such patterns and is particularly helpful when the observed patterns are imperfectly resolved. As applied to unresolved patterns this method allows a somewhat more accurate estimate of the uncertainty involved than does the frequently used method of Shenstone and Blair.[2]

EXPLANATION OF METHOD

The graphical method will be explained with reference to the Zeeman pattern formed in the transition between two terms identified by J-values of 2 and 1, respectively, in a weak magnetic field. The state having the inner quantum number J equal to 2 will consist of five uniformly spaced magnetic levels, the interval between adjacent levels being g_2 in Lorentz units. Here g_2 is the Landé splitting factor, the subscript designating the J-value of the term. Similarly the state having J equal to 1 will consist of three magnetic levels separated by g_1. The number of lines occurring in such a transition, when observed transversely to the field, will be nine. A graph which shows the possible line patterns resulting from such a transition is given in Fig. 1.

The graph represents the behavior of the line pattern as g_2 varies with respect to g_1, which is to be regarded as fixed. The vertical coordinate is the ratio g_2/g_1. The line pattern corresponding to any value of this ratio is found by drawing a line parallel to the base of the figure at the given value of g_2/g_1. The points at which this line is intersected by the vertical and diagonal lines of the figure give the positions of the spectral lines of the Zeeman pattern.

Construction of the graph. An outline of the manner in which the graph is constructed will illustrate its meaning. First, the line pattern arising when g_2 is zero and g_1 has a definite value is determined and marked out along the axis, $g_2/g_1=0$. This pattern will show simply the sepa-

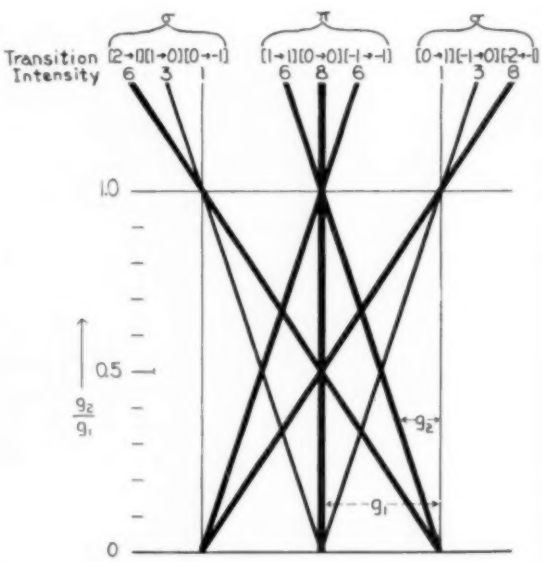

FIG. 1. Transition between $J=2$ and $J=1$; g_1 fixed, g_2 varying from 0 to g_1.

[1] Fisher and Goudsmit, Phys. Rev. **37**, 1057 (1931).

[2] Shenstone and Blair, Phil. Mag. **8**, 765 (1929). The present method is, in a sense, a graphical parallel of the analytical method of Shenstone and Blair.

ration of the term whose splitting factor is g_1. In the example under consideration the pattern is a triplet. When g_2 is zero certain lines which may be regarded as having independent existence fall into coincidence with one another. As g_2 increases from zero these lines separate, the manner in which they separate being represented by the diverging lines of the graph. The slopes of these diverging lines are found by considering the Zeeman pattern formed when $g_2/g_1=1$. This is always a triplet whose interval is the common g-value of the two terms. The appropriate straight lines may then be drawn joining the pattern at $g_2/g_1=0$ to that at $g_2/g_1=1$, thus showing the gradual transition from the one case to the other. The lines converging at $g_2/g_1=1$ form a triplet which is the normal triplet if g_1 and g_2 are unity. A little practice in the construction of such a graph will make the method more clear than would further explanation.

Changes in magnetic quantum number. Since each of the diagonal and vertical lines of the graph is identified with a particular transition between magnetic levels, each may be labeled by the change in magnetic quantum number, m to which it corresponds. The change in the magnetic quantum number is given in the bracket at the upper extremity of each line of the figure. Here it is assumed that the state having J equal to 2 is initial.

Polarization. Since the transition $\Delta m=0$ yields π-components and the transition $\Delta m=\pm 1$ yields σ-components when observed transversely, these two types are readily distinguished by the graph. The lines are divided into three groups according to their polarization. The polarization of each group is indicated at the top of the figure.

Intensity. Formulas for the relative intensities of the components within a Zeeman pattern which are in good agreement with experiment have been developed by Hönl[3] and by Kronig and Goudsmit.[4] These intensity relations depend only upon the J and m-values involved and not upon the electron configurations and type of coupling. With the aid of such formulas the expected relative intensities of the lines within the pattern may be found. The number beneath the bracket at the upper extremity of each line of the graph represents the expected relative intensity of that line. To make the representation more pictorial the widths of the lines are made roughly proportional to the theoretical intensities.

g-values. It is evident that the intervals between certain of the lines of the graph measure directly the intervals of the two magnetic level multiplets. Thus the interval between the lines $[1\to 1]$ and $[0\to 1]$ measures the interval between the two magnetic levels of the initial Zeeman multiplet identified by $m=1$ and $m=0$, respectively, which is g_2. Similarly, the interval between lines $[0\to 0]$ and $[0\to 1]$ is g_1. Examples of separations which yield directly the values of g_1 and g_2 are indicated in the lower portion of the figure.

The graph of Fig. 1, if extended to indefinitely large positive and negative values of g_2/g_1 would represent all conceivable Zeeman patterns of the type, $J=2\to J=1$. The negative portion of the graph may be omitted since negative g-values occur extremely rarely. Obviously all positive values of g_2/g_1 cannot be represented by a graph of finite extent. It is therefore convenient to limit the graph of Fig. 1 so that g_2/g_1 does not extend above unity and to represent those patterns arising when g_2 is greater than g_1 by a second graph for which the variable is g_1/g_2 and the value of g_2 is considered as fixed. Fig. 2 gives such a graph applying to the same transition in

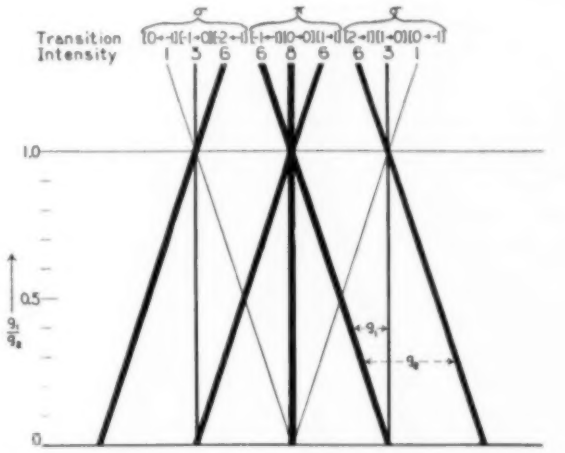

FIG. 2. Transition between $J=2$ and $J=1$; g_2 fixed, g_1 varying from 0 to g_2.

[3] Hönl, Zeits. f. Physik **31**, 340 (1925).

[4] Kronig and Goudsmit, Naturwiss. **13**, 90 (1925). The intensity formulas are to be found in convenient form in Pauling and Goudsmit, *Structure of Line Spectra*, p. 142.

J as is discussed above. For transitions in which J does not change, a single graph will represent all possible patterns.

Analysis of observed patterns. If one is provided with other graphs similar to Figs. 1 and 2 representing other transitions in J, he may readily identify an observed Zeeman pattern with one of the graphs since each type of pattern has distinguishing characteristics such as the number of lines, the relative intensities and the polarization. When a match between an observed pattern and a graph has been found, the g-values and other features of the states involved are at once available.

The graphs are particularly helpful in the analysis of imperfectly resolved patterns since even here a match may usually be found between the pattern and the graph. In such a case it is useful to compare the observed intensity maxima in the unresolved pattern with the centers of gravity of any close group of lines in the graph. The center of gravity of any close group of lines of the graph may be represented by a single line when desired.

The approximate identification of an observed pattern with a position on the graph is usually possible by inspection. To make the match more accurate a drawing of the measured line pattern on the same scale as the graph can then be made. This drawing may then be shifted along the graph until the match is found.

In obtaining a match with an observed pattern one always finds that there is a certain range upon the graph within the limits of which the match may be said to occur. The extent of this range gives one immediately a measure of the limit of error of his analysis.

It frequently occurs that the lines of a graph show symmetry about some horizontal axis as does Fig. 1 about the line $g_2/g_1=0.5$. Thus, if the intensity and polarization characteristics of an observed pattern are neglected, there may be two alternative analyses. Fig. 1, for example, gives the same line pattern when g_2/g_1 is equal to 0.3 and to 0.7 except for the differences in polarization and slight differences in the intensities of the components. Since the intensities in such alternative cases may not be materially different the correct analysis of a pattern may often depend entirely upon a knowledge of the polarization of the components.

In conclusion it is to be remarked that the graphs discussed above serve as an alternative means for the representation of the fundamental Zeeman types (Grundtypen) which have been discussed completely by Back and Landé.[5] Thus Figs. 1 and 2 are examples of Grundtypus 1 and Grundtypus 2, respectively, of Back and Landé. A more complete set of graphs representing other transitions in J would illustrate all of Back and Landé's fundamental types.

[5] Back and Landé, *Zeemaneffekt*, p. 162 ff.

Characteristic Values of the Two Minima Problem and Quantum Defects of *f* States of Heavy Atoms

TA-YOU WU, *University of Michigan*

(Received August 14, 1933)

The characteristic value problem with two unequal minima in the potential field has been solved by the approximate method of Wentzel, Kramers and Brillouin. The result is applied to the calculation of the quantum defects of the *f* states of heavy atoms and explains the fact that these quantum defects are all very close to unity.

THE quantum mechanical problem in which the potential field possesses two symmetrical minima has been treated by various authors[1] and the results successfully applied to the doubling of energy levels of the ammonia molecule.[2] But the case in which the two valleys in the potential field are not alike has not yet been treated in the literature. This is apparently due to lack of application to physical problems. In the present paper the expression for the eigenvalues of a wave equation with two unsymmetrical potential minima is obtained with the W-K-B method. It is shown that the result finds application in the calculation of certain atomic energy states and, in particular, in the explanation of the fact that the quantum defects of the *f* states of heavy atoms are all near unity.

I.

Consider the one-dimensional wave equation of a particle of total energy E with a potential function which has two minima. On writing $2mE-2mV=P^2$, the wave equation takes the form

$$d^2\psi/dx^2+(4\pi^2/h^2)P^2\psi=0.$$

The solution of this equation is, in the first approximation,

$$\psi=c_1P^{-1}\exp(2\pi i/h)\int^x Pdx + c_2P^{-1}\exp(-2\pi i/h)\int^x Pdx.$$

Consider a characteristic value E (Fig. 1) such that in the region I where $x_1>x$, $P^2<0$; in the region II where $x_1<x<x_2$, $P^2>0$; in the region III where $x_2<x<x_3$, $P^2<0$; in the region IV

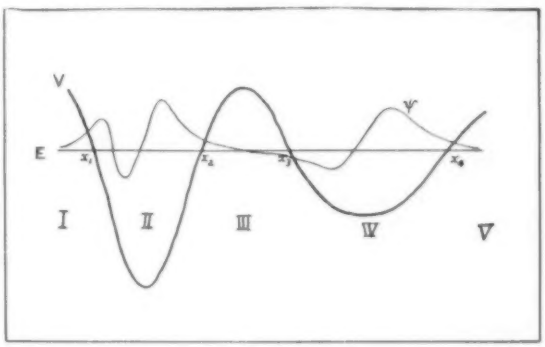

FIG. 1.

where $x_3<x<x_4$, $P^2>0$; and in the region $x_4<x$, $P^2<0$. In the regions II and IV where $P^2>0$ and motion is possible classically, ψ has an oscillatory character. In the regions I and V where motion is impossible classically, ψ falls off exponentially; in region III a linear combination of two exponentials must be used.

The relations between the exponential and the oscillatory functions are given by the "connection formulae" of Kramers and Zwaan,[3] obtained

[1] P. M. Morse and E. C. G. Stueckelberg, Helv. Phys. Acta **4**, 337 (1931); P. M. Morse and N. Rosen, Phys. Rev. **40**, 1039A (1932); D. M. Dennison and G. E. Uhlenbeck, Phys. Rev. **41**, 313 (1932).

[2] D. M. Dennison and G. E. Uhlenbeck, reference 1; D. M. Dennison and J. D. Hardy, Phys. Rev. **41**, 313 (1932).

[3] H. A. Kramers, Zeits. f. Physik **39**, 828 (1926); Zwaan, Utrecht Dissertation 1929; L. A. Young and G. E. Uhlenbeck, Phys. Rev. **36**, 1154 (1930).

from considerations of the behavior of the functions in the complex x-plane. The result may be summarized as follows: At a point x_0 where the exponentially increasing or the exponentially decreasing function is to be connected with the oscillatory function, the following formulae hold

$$P^{-\frac{1}{2}} \exp \frac{2\pi}{h}\int_{x_0}^{x} P dx \rightarrow P^{-\frac{1}{2}} \cos\left[\frac{2\pi}{h}\int_{x}^{x_0} P dx + \frac{\pi}{4}\right], \tag{1}$$

$$P^{-\frac{1}{2}} \exp \frac{-2\pi}{h}\int_{x_0}^{x} P dx \rightarrow 2P^{-\frac{1}{2}} \cos\left[\frac{2\pi}{h}\int_{x}^{x_0} P dx - \frac{\pi}{4}\right].$$

Here, and in all that follows, P is taken to mean $(|2mE-2mV|)^{\frac{1}{2}}$.

Now at x_1, the exponentially decreasing function in the region $x<x_1$

$$\psi_{\mathrm{I}} = AP^{-\frac{1}{2}} \exp(-2\pi/h)\int_{x}^{x_1} P dx$$

is connected with the oscillatory function to the right of x_1

$$\psi_{\mathrm{II}_a} = 2AP^{-\frac{1}{2}} \cos\left[(2\pi/h)\int_{x_1}^{x} P dx - \pi/4\right].$$

At the right of x_2, we have a linear combination of increasing and decreasing exponentials

$$\psi_{\mathrm{III}_a} = DP^{-\frac{1}{2}} \exp(2\pi/h)\int_{x_2}^{x} P dx + EP^{-\frac{1}{2}} \exp(-2\pi/h)\int_{x_2}^{x} P dx.$$

By (1) the continuation of this into region II is

$$\psi_{\mathrm{II}_b} = P^{-\frac{1}{2}} \cos\left[(2\pi/h)\int_{x}^{x_2} P dx - \pi/4 + \delta\right],$$

where

$$\tan\delta = D/2E. \tag{2}$$

As ψ_{II_a} and ψ_{II_b} are the same function, they, together with their derivatives, must be equal and hence

$$(d\psi_{\mathrm{II}_a}/dx)/\psi_{\mathrm{II}_a} = (d\psi_{\mathrm{II}_b}/dx)/\psi_{\mathrm{II}_b}.$$

From this it follows that

$$(2\pi/h)\int_{x_1}^{x_2} P dx = (n+1/2)\pi - \delta. \tag{3}$$

At x_4, the decreasing function

$$\psi_{\mathrm{V}} = BP^{-\frac{1}{2}} \exp(-2\pi/h)\int_{x_4}^{x} P dx$$

is connected with the oscillatory function to the left of x_4

$$\psi_{\mathrm{IV}_a} = 2BP^{-\frac{1}{2}} \cos\left[(2\pi/h)\int_{x}^{x_4} P dx - \pi/4\right].$$

To extend the solution ψ_{III_a} into region IV, it may be noted that ψ_{III_a} may be written in the form

$$\psi_{\mathrm{III}_b} = D\alpha^2 P^{-\frac{1}{2}} \exp(-2\pi/h)\int_{x}^{x_3} P dx + E\alpha^{-2} P^{-\frac{1}{2}} \exp(2\pi/h)\int_{x}^{x_3} P dx, \tag{4}$$

where

$$\alpha^2 = \exp(2\pi/h)\int_{x_2}^{x_3} P dx.$$

By (1) the continuation of ψ_{III_b} into region IV is

$$\psi_{\mathrm{IV}_b} = P^{-\frac{1}{2}} \cos\left[(2\pi/h)\int_{x_3}^{x} P dx - \pi/4 + \epsilon\right],$$

where

$$\tan\epsilon = E/2D\alpha^4. \tag{5}$$

As ψ_{IV_a} and ψ_{IV_b} are the same function, we have as before

$$(2\pi/h)\int_{x_3}^{x_4} P dx = (n+1/2)\pi - \epsilon. \tag{6}$$

From (2) and (5) we obtain the relation between δ and ϵ

$$\tan\delta \tan\epsilon = 1/4\alpha^4. \tag{7}$$

The characteristic value E is then given by (3), (6) and (7) which, on combining, may be written in the form

$$(2\pi/h)\int_{x_1}^{x_2} P dx = (n+1/2)\pi - \arctan\left[(1/4)\exp\left\{(-4\pi/h)\int_{x_2}^{x_3} P dx\right\} \cdot \tan(2\pi/h)\int_{x_3}^{x_4} P dx\right]. \tag{8}$$

An immediate result of this equation is that when the two minima of the potential field are exactly symmetrical,

$$\delta = \epsilon, \qquad \text{and} \qquad \delta = \pm \tan^{-1}(1/2\alpha^2).$$

This shows that to a first approximation, each energy level is split in two symmetrically with respect to the one that would exist if there is only one valley in the field. Furthermore, this splitting, which results from the resonance between the two energy states in the two potential valleys, increases as the square root area under the potential hill decreases. This agrees with the results of Dennison and Uhlenbeck[1] on the doubling of the vibrational levels of the ammonia molecule.

II.

The above result finds application in the calculation of certain atomic energy levels. In a central field the wave equation satisfied by the radial wave function ψ/ρ is

$$d^2\psi/d\rho^2 + (E - V)\psi = 0 \qquad \text{with} \qquad V = v + l(l+1)/\rho^2, \tag{9}$$

the energy E and the potential energy v being in units of the ionization potential of hydrogen and the atomic distance ρ in units of the first Bohr radius of hydrogen. With the aid of an atomic field, such as that of Fermi-Thomas, the energies can be obtained by solving Eq. (9) with the W-K-B method.

To calculate the energy values in the arc spectrum, one may consider the electron as moving in the field of the singly ionized atom and for v one may use the Fermi potential[4] for a singly charged positive ion. Thus

$$v = -(2Z/\rho)\varphi(\gamma\rho) - 2/\rho_0, \quad \rho < \rho_0; \qquad v = -2/\rho, \quad \rho > \rho_0$$

where $\gamma = (128\,Z/9\pi^2)^{\frac{1}{3}}$, ρ_0 is the distance beyond which the field is of Coulombian character, i.e., $\varphi(\gamma\rho_0) = 0$, and φ is the Fermi function for a singly ionized atom of nuclear charge Z. Thus φ satisfies the equations

$$d^2\varphi/dx^2 = \varphi^{\frac{3}{2}}/x^{\frac{1}{2}}, \quad x < x_0; \qquad d^2\varphi/dx^2 = 0, \quad x > x_0$$

subject to the conditions $\varphi(0) = 1$, $-x_0(d\varphi/dx)_{x_0} = 1/Z$, where $x = \gamma\rho$.

Solution of Eq. (9) by the W-K-B method leads to the phase integral of the classical quantum theory with half integer quantization in all cases in which V possesses one minimum. But in certain cases, such as the d states of the elements of the third and the fourth periods and the f states of the heavy atoms, the V function has two valleys separated by a potential hill. The curves of V for the f states of Hg, U, U^+, U^{++} and U^{+++} are given in Fig. 2. The inner valley is a very deep and narrow one; in the case of uranium its minimum lies at -79.5 and can not be conveniently shown in the figure.

From the curves of V it is evident that the energies of the f states of heavy neutral atoms must be calculated by means of Eq. (8) which, after a transformation to the atomic units is made, takes the form[5]

$$\int_{\rho_3}^{\rho_4} Q\,d\rho = (n - l - 1/2)\pi - \arctan\left[(1/4)\left\{\exp\left(-2\int_{\rho_2}^{\rho_3} Q\,d\rho\right)\right\} \tan\int_{\rho_1}^{\rho_2} Q\,d\rho\right], \tag{8a}$$

where

$$Q = \{\,|E - v - (l+1/2)^2\rho^{-2}|\,\}^{-\frac{1}{2}}.$$

Here $\int_{\rho_1}^{\rho_2} Q\,d\rho$, $\int_{\rho_3}^{\rho_4} Q\,d\rho$ are the phase integrals taken over the inner and the outer regions of possible classical motion, respectively, and $\int_{\rho_2}^{\rho_3} Q\,d\rho$ is taken over the potential barrier between them. In the calculation of E for the f states, a great simplicity sets in, as the field in the region $\rho_3 < \rho < \rho_4$ is of

[4] E. Fermi, *Mem. della reale Acad. d'Italia* I (1930); A. Sommerfeld, Zeits. f. Physik **78**, 283 (1932).

[5] The result of Sugiura and Urey, Kgl. Danske Vid. Selsk. **7**, 13 (1926), concerning the energy levels of the f states of elements of the 6th and the 7th periods must be modified by replacing the Sommerfeld phase integral by Eq. (8) above. See T. Y. Wu and S. Goudsmit, Phys. Rev. **43**, 496 (1933).

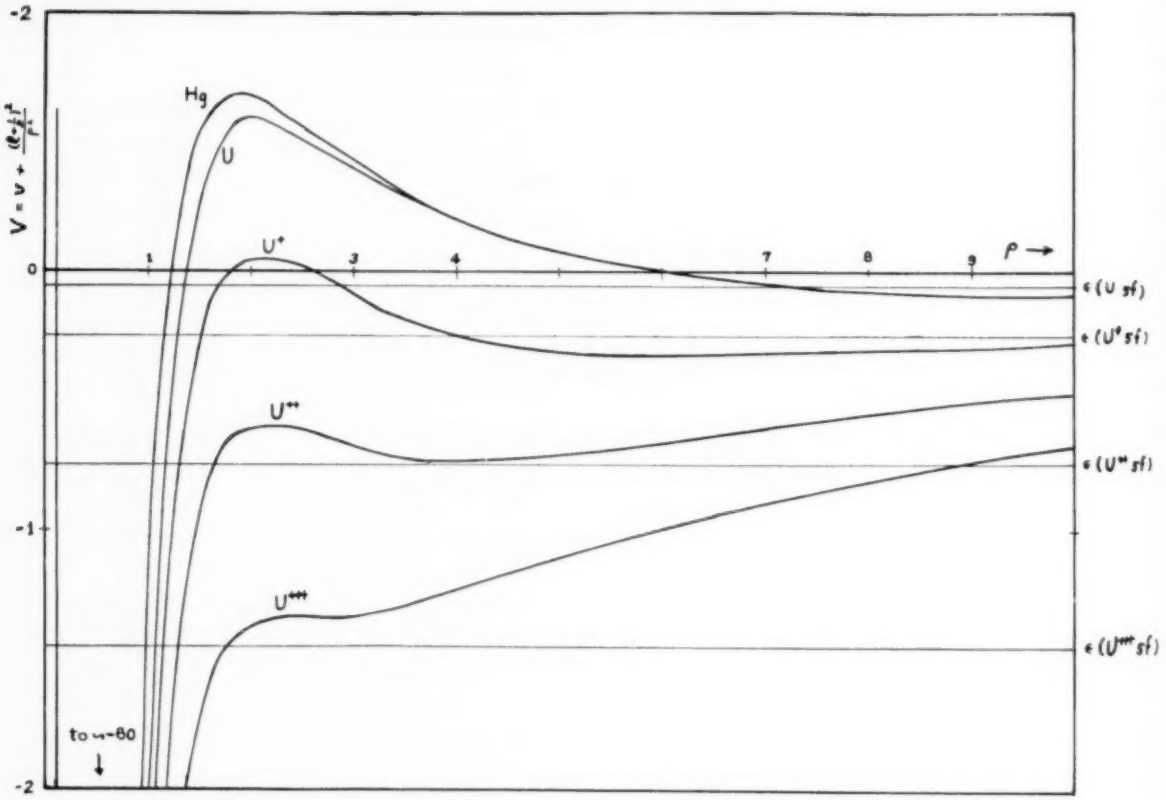

FIG. 2. Curves of $V=v+(l+\frac{1}{2})^2\rho^{-2}$ for f states of heavy atoms and ions.

Coulombian nature. The integral $\int_{\rho_3}^{\rho_4} Q d\rho$ can be evaluated directly giving

$$\int_{\rho_3}^{\rho_4} [E-2/\rho-(l+1/2)^2\rho^{-2}]^{\frac{1}{2}} d\rho = \pi(-E)^{-\frac{1}{2}} - \pi(l+1/2). \tag{10}$$

Writing

$$\arctan\left[(1/4)\left\{\exp\left(-2\int_{\rho_2}^{\rho_3} Q d\rho\right)\right\} \tan \int_{\rho_1}^{\rho_2} Q d\rho\right] = \Delta\pi, \tag{11}$$

we have, on combining Eqs. (8a) and (10)

$$E = -1/(n-\Delta)^2. \tag{12}$$

It can be easily shown that when one's attention is confined to the discrete states, Δ is a very slowly varying function of E. Hence the above expression may be regarded as a Rydberg formula with a quantum defect Δ.

The values E are found by so adjusting them that Eq. (8a) is satisfied. Then Δ is calculated according to Eq. (11). The calculations can be carried out with the aid of a planimeter. It is found that for all neutral atoms from Au ($Z=79$) to U ($Z=92$), the integral $\int_{\rho_1}^{\rho_2} Q d\rho$ over the inner classical region varies from 1.0π to 1.2π and the potential hill is so large that the factor $\exp(-2\int_{\rho_2}^{\rho_3} Q\, d\rho)$ ranges from 0.0027 to 0.0025. A little consideration will hence show that $\Delta=1.00$ for the f states of all these atoms. The experimental values of Δ of these states are listed in Table I.[6] The difference between the observed values and the expected values 1.00 of the quantum defects may be attributed

[6] The closeness of the effective quantum numbers of these states to 4 has led many authors to assign the value 4 to the principal quantum numbers. See, for example, Hund's *Linienspektren und periodisches System der Elemente*, p. 42.

to the effect of polarization of the atomic core, which has been neglected, and the approximate nature of the calculation.

TABLE I. *Experimental values of* Δ.

Z	79	80	81	82	86
Atom	Au	Hg	Tl	Pb	Rn
Δ	1.03	1.03	1.02	1.04	1.02

SOME REMARKS ON THE CALCULATION OF ENERGY LEVELS WITH THE FERMI POTENTIAL FOR POSITIVE IONS

Calculations of the energy levels of the heaviest atoms and ions have been made[5] with the Fermi potential for positive ions. Further calculations show that the calculated levels invariably lie above the observed positions by amounts which are different for the s, p, d, f states and which are quite large in the case of atoms of medium atomic weights but become smaller for the heavy atoms, as shown by Table II.

TABLE II.

	$6s$ Cs	$7s$ Tl	$6p$ Cs	$7s$ Ra^+	$7p$ Ra^+	$6d$ Ra^+	$5d$ Ce^{+++}	$4f$ Ce^{+++}
Calc. E	−0.215	−0.188	−0.145	−0.54	−0.47	−0.55	−1.65	−1.08
Obs. E	−0.286	−0.209	−0.184	−0.795	−0.56	−0.665[7]	−1.90	
Difference	0.071	0.021	0.039	0.255	0.09	0.115	0.25	

The energies here are expressed in terms of the Rydberg constant. It is seen that energy levels obtained with the statistical potential are at best qualitative. In spite of the consistent discrepancy between the calculated and the observed values, the relative positions of the $5d$ and the $4f$ levels of Ce^{+++} seem to be correct; for it does not seem very likely that the correction for the calculated $4f$ level is so large as to reverse them. This is of some interest, for on the other hand, the data on the magnetic susceptibilities of tri-valent cerium salts, hydrated or in solution, apparently show that the lowest states of Ce^{+++} are $4f\,{}^2F$. Spectroscopically the $4f$ levels have not yet been found[8] and these rough calculations indicate that they are approximately 60,000 cm^{-1} above the $5d$ levels. Further analysis of the spectrum of Ce^{+++} is desirable.

Calculations of doublet separations and values of $\psi^2(0)$ for s electrons have been made with the Fermi potential for positive ions. The characteristic functions needed are obtained by solving the wave equation by the W-K-B method. The results are in better agreement with observed values or with Breit's more accurate calculations than are those obtained with the use of the Thomas-Fermi potential for neutral atoms, as shown by the Table III.

TABLE III.

	Calc. with potential for positive ions	Obs.	Calc. with potential for neutral atoms
$\Delta\nu(6p\,{}^2P_{\frac{3}{2}}-6p\,{}^2P_{\frac{1}{2}})$ Cs	400 cm^{-1}	554 cm^{-1} Breit[11]	1022 cm^{-1} [9]
$\psi^2(0)$ for $6s\,{}^2S_{\frac{1}{2}}$ Cs	1.51×10^{25}	1.8×10^{25}	2.7×10^{25} [10]
$\psi^2(0)$ for $7s\,{}^2S_{\frac{1}{2}}$ Tl	1.88×10^{25}	1.7×10^{25}	

The writer is very grateful to Professor S. Goudsmit for his advice and interest in this problem.

[7] W. Albertson, Phys. Rev. **39**, 385 (1932).

[8] Freed, also Serber, have attributed the absorption at 2400Å of cerium salts to the transition $4\,{}^2F\rightarrow5\,{}^2D$, taking $4\,{}^2F$ as the normal state. Cf. C. J. Gorter, Phys. Zeits. **34**, 238 (1933).

[9] G. Gentile and E. Majorana, Accad. Lincei. Atti **8**, 229 (1928).

[10] E. Fermi, Zeits. f. Physik **60**, 320 (1930).

[11] G. Breit, Phys. Rev. **42**, 348 (1932).

Configuration Interaction in Complex Spectra

C. W. UFFORD, *Palmer Physical Laboratory, Princeton University*

(Received August 2, 1933)

The electrostatic interaction is calculated between the terms in Russell-Saunders coupling of the electron configurations $nd^2n's$, nd^3, $ndn's^2$ and $nd^2n''s$. The first order eigenfunctions, for the terms of these configurations in the LSM_LM_S scheme with $M_L=0$, $M_S=\frac{1}{2}$ are given in terms of the zero order functions of Slater. The matrix elements between the quartets of d^2s and d^3 are found to vanish. The sums over closed shells in non-diagonal matrix elements of electrostatic interaction are found to vanish except when the two electrons not in closed shells have the same value of l. This sum is evaluated in general and for the configurations $nd^2n's-nd^2n''s$. The matrix elements of magnetic spin orbit interaction are given between the initial states without configuration interaction. The electrostatic energies and magnetic splittings are then calculated for the terms of $nd^2n's$, nd^3 and $ndn's^2$; and compared with the values observed in Ti II and Zr II. Zr II agrees particularly well, especially if the observed ^2D terms are rearranged.

THIS paper will treat the electrostatic interaction between the terms in Russell-Saunders coupling of the electron configurations $nd^2n's$, nd^3, $ndn's^2$ and $nd^2n''s$. The method of treating the interaction of d^2s and d^3 has been outlined by Condon.[1] A previous paper[2] shows how to calculate the matrix of electrostatic interaction. The matrix elements between the quartets of d^2s and d^3 are found to vanish. Since there is no electrostatic interaction between different kinds of terms, interactions exist between all the doublets and between the quartets of $d^2n's$ and $d^2n''s$. This means that these terms cannot be assigned to any single electron configuration but have eigenfunctions which are linear combinations of those of the terms belonging to each configuration separately. Secular equations are obtained for the term energies, the order of each equation being equal to the number of terms of the same kind which occur in all the electron configurations. The energies obtained as solutions of these equations still contain integrals over the radial parts of the central field eigenfunctions as parameters. With these energies the eigenfunctions for the new states may be found from the matrix of electrostatic interaction. With these eigenfunctions, the separations of the different levels within a term may be found approximately, since the coupling is Russell-Saunders, by using only the diagonal elements of the spin orbit interaction of each electron.

The energy levels and separations thus found for the configurations d^2s, d^3 and ds^2 are compared with the experimental values from Ti II and Zr II.

1. THE MATRIX OF ELECTROSTATIC INTERACTION

Before giving the matrix elements of electrostatic interaction, it will be necessary to consider in general the sums over closed shells which enter into them.

Slater[3] has shown that, in computing the diagonal elements of the matrix of electrostatic interaction, the sum over pairs of electrons, one of which is an outer electron whereas the other runs over the individual electrons in a closed shell, gives the same value for each zero order state. This value has been calculated by Shortley.[4] Thus these sums do not affect the separation between terms. These sums exist for the non-diagonal matrix elements only when the states differ with respect to the individual sets of quantum numbers of just one electron[1] but can be shown to be zero except where the two electrons not in closed shells have the same value of l. Where these non-diagonal sums

[1] E. U. Condon, Phys. Rev. **36**, 1121 (1930).

[2] C. W. Ufford and G. H. Shortley, Phys. Rev. **42**, 167 (1932), referred to as I below.

[3] J. C. Slater, Phys. Rev. **34**, 1293 (1929).

[4] G. H. Shortley, Phys. Rev. **40**, 185 (1932).

are different from zero they will affect the separation between terms. To see when these sums vanish and to evaluate them when they do not, the procedure is identical with that used by Shortley[4] for the diagonal elements, except that the two electrons not in a closed shell have different individual sets of quantum numbers. Following Shortley's calculation and using the orthogonality of the surface spherical harmonics one obtains for the sum over a single closed shell in a non-diagonal matrix element where the states differ only in the individual sets of quantum numbers of one electron:

$$\begin{aligned}
&\sum_{m_s'} \sum_{m_l'=-l'}^{l'} \delta(m_s', m_s'') \Big[\int\int \bar{v}_1(nlm_l)\bar{v}_2(n'l'm_l')(e^2/r_{12})v_1(n''l''m_l'')v_2(n'l'm_l')d\tau_1 d\tau_2 \\
&\quad - \delta(m_s, m_s') \int\int \bar{v}_1(nlm_l)\bar{v}_2(n'l'm_l')(e^2/r_{12})v_1(n'l'm_l')v_2(n''l''m_l'')d\tau_1 d\tau_2 \Big] \\
&= \delta(l, l'')\delta(m_l, m_l'') \Big[2(2l'+1) \int_0^\infty \int_0^\infty (e^2/r_>)R_1(nl)R_1(n''l)R_2^2(n'l')dr_1 dr_2 \qquad (1) \\
&\quad - (2l'+1/2l+1) \sum_k C^l{}_{l'k} e^2 \int_0^\infty \int_0^\infty (r_<^k/r_>^{k+1})R_1(nl)R_1(n'l')R_2(n'l')R_2(n''l)dr_1 dr_2 \Big] \\
&= 2(2l'+1)R^0(nl, n'l'; n''l, n'l') - (2l'+1/2l+1) \sum_k C^l{}_{l'k} R^k(nl, n'l'; n'l', n''l).
\end{aligned}$$

This expression reduces to the diagonal value given by Shortley when $n = n''$. The condition $\delta(m_s, m_s'')\delta(m_l m_l'')$ is always fulfilled since the states differ by only one electron and have the same values of M_L and M_S. This sum over closed shells has the same value whenever it occurs, within a single pair of configurations, since it depends only on the n and l quantum numbers of the electrons.

With this value for the sum over a closed shell, we now return to the matrix of electrostatic interaction for the configurations $nd^2n's$, nd^3, $ndn's^2$ and $nd^2n''s$ in question. Using first order eigenfunctions in the $LS\,M_LM_S$ scheme, one obtains the following non-diagonal matrix elements of electrostatic interaction:[5]

$$nd^2n's - nd^2n''s$$

$$\begin{aligned}
(nd^2n's_1^4F\,|\,e^2/r_{12}\,|\,nd^2n''s_1^4F) &= R_0 - 2\,''R, \\
(nd^2n's_1^4P\,|\,e^2/r_{12}\,|\,nd^2n''s_1^4P) &= R_0 - 2\,''R, \\
(nd^2n's_1^2G\,|\,e^2/r_{12}\,|\,nd^2n''s_1^2G) &= R_0 - {}''R, \\
(nd^2n's_1^2F\,|\,e^2/r_{12}\,|\,nd^2n''s_1^2F) &= R_0 + {}''R, \\
(nd^2n's_1^2D\,|\,e^2/r_{12}\,|\,nd^2n''s_1^2D) &= R_0 - {}''R, \\
(nd^2n's_1^2P\,|\,e^2/r_{12}\,|\,nd^2n''s_1^2P) &= R_0 + {}''R, \\
(nd^2n's_1^2S\,|\,e^2/r_{12}\,|\,nd^2n''s_1^2S) &= R_0 - {}''R,
\end{aligned} \qquad (2)$$

[5] The order of the eigenfunction is indicated by the subscript on the left. The zero order eigenfunctions are Slater's[3] determinants of one-electron central field functions. The first order eigenfunctions are those in which the matrix of electrostatic interaction is diagonal in each configuration with respect to the different kinds of terms occurring in Russell-Saunders coupling. These may be found from the zero order functions by the methods of Gray and Wills, Wigner or Johnson (cf. I). Second order eigenfunctions are those belonging to terms of the same kind within a con-

where[6]

$$R_0=(nd^2n's,\ nd^2n''s)\{2R^0(nd,\ n's;\ nd,\ n''s)+\sum_{n_l'l'}[2(2l'+1)R^0(n's,\ n_l'l';\ n''s,\ n_l'l')$$
$$-R^{l'}(n's,\ n_l'l';\ n_l'l',\ n''s)]\}$$

and

$$''R=(nd^2n's,\ nd^2n''s)\tfrac{1}{5}R^2(nd,\ n's;\ n''s,\ nd),$$

$nd^2n's-nd^3$

$$(nd^2n's\,{}^4_1F\,|\,e^2/r_{12}\,|\,nd^3\,{}^4_1F)=0,$$
$$(nd^2n's\,{}^4_1P\,|\,e^2/r_{12}\,|\,nd^3\,{}^4_1P)=0,$$
$$(nd^2n's\,{}^2_1G\,|\,e^2/r_{12}\,|\,nd^3\,{}^2_1G)=2\tfrac{1}{2}5\,'R_2,$$
$$(nd^2n's\,{}^2_1F\,|\,e^2/r_{12}\,|\,nd^3\,{}^2_1F)=10\tfrac{1}{2}3\,'R_2, \qquad (3)$$
$$(nd^2n's\,{}^2_1D\,|\,e^2/r_{12}\,|\,nd^3\,{}^2_2D^+)=(5/2)^{\frac{1}{2}}(-3\tfrac{1}{2}3\alpha_-+7\tfrac{1}{2}\alpha_+)\,'R_2,$$
$$(nd^2n's\,{}^2_1D\,|\,e^2/r_{12}\,|\,nd^3\,{}^2_2D^-)=(5/2)^{\frac{1}{2}}(-7\tfrac{1}{2}\alpha_--3\tfrac{1}{2}3\alpha_+)\,'R_2,$$
$$(nd^2n's\,{}^2_1P\,|\,e^2/r_{12}\,|\,nd^3\,{}^2_1P)=(35)^{\frac{1}{2}}3\,'R_2,$$

where

$$'R_2=(nd^3,\ nd^2n's)(1/35)R^2(nd,\ nd;\ nd,\ n's),$$
$$\alpha\pm=+\left(\frac{1}{2}\pm\frac{4F_2+120F_4}{Ra}\right)^{\frac{1}{2}},$$
$$Ra=2[193F_2^2-1650F_2F_4+8325F_4^2]^{\frac{1}{2}},$$
$$F_2=(d^3)(1/49)F^2(nd^2),$$

and

$$F_4=(d^3)(1/441)F^4(nd^2).$$

$nd^2n's-ndn's^2$ (4)

$$(nd^2n's\,{}^2_1D\,|\,e^2/r_{12}\,|\,ndn's^2\,{}^2_1D)=(70)^{\frac{1}{2}}\,'R_2,$$

figuration in which the matrix of electrostatic interaction for these terms is diagonal. Second order eigenfunctions for the two ^2D's of d^3 have been found in I. Finally third order eigenfunctions are those in which the matrix of electrostatic interaction is diagonal for more than one configuration at a time. Thus, second order functions arise only when more than one term of the same kind occurs in a single configuration and third order eigenfunctions arise only when the non-diagonal elements of electrostatic interaction between terms of the same kind lying in different configurations are not zero. Each order of function can be expressed as a linear combination of the functions of lower order. When only two second or third order functions of the same kind occur it is sometimes convenient to indicate them by plus and minus superscripts on the right. The + and − superscripts on the right indicate the function belonging to the term with higher or lower energy, respectively.

[6] $\Sigma_{n_l'l'}$ is the sum over all the closed shells occurring in the atom, l' taking on the values 0, 1, 2, ⋯ for the s, p, d, ⋯ shells. n_l' distinguishes the different shells with the same value of l'.

In the R's, the first two electrons in the integral belong to the first configuration in the bracket, and the second two electrons to the second configuration except in $\Sigma_{n_l'l'}$. In $\Sigma_{n_l'l'}$ the first two electrons belong to the atom with its electrons outside closed shells in the first configuration given in the bracket and the second two electrons to the atom in the second configuration. In each pair, the electron with l given is outside a closed shell, the electron with $l=l'$ belongs to one of the closed shells.

In the G's, the first electron in the integral belongs to the first configuration in the bracket and the second electron to the second configuration. In the case of the diagonal elements all the electrons belong to the same configuration which is given in a bracket before the integral.

where

$$'R_2=(nd^2n's,\ ndn's^2)(1/35)R^2(nd,\ nd;\ nd,\ n's).$$

$ndn's^2-nd^3$

$$(ndn's^2\ {}^2_1D\,|\,e^2/r_{12}\,|\,nd^3\ {}^2_2D^+)=-2\alpha_+{}'G_2, \tag{5}$$

$$(ndn's^2\ {}^2_1D\,|\,e^2/r_{12}\,|\,nd^3\ {}^2_2D^-)=2\alpha_-{}'G_2,$$

where

$$'G_2=(nd^3,\ ndn's^2)\,\tfrac{1}{5}G^2(nd,\ n's)$$

and $\alpha_\pm$ is given in Eq. (3). $ndn's^2-ndn's^2$ gives the diagonal element,

$$(ndn's^2\ {}^2_1D\,|\,e^2/r_{12}\,|\,ndn's^2\ {}^2_1D)=2'F_0+{}''F-{}'G_2, \tag{6}$$

where

$$'F_0=(ndn's^2)\,F^0(nd,\ n's),\qquad {}''F=(ndn's^2)\,F^0(n's^2),$$

and

$$'G_2=(ndn's^2)\,\tfrac{1}{5}G^2(nd,\ n's).$$

The other diagonal elements have been given by Condon and Shortley[7] and in I. The matrix elements for $nd^2n''s$ are obtained from those for $nd^2n's$ by replacing n' by n'' giving different radial integrals.

In order to determine the phases of the first order states required to give these non-diagonal matrix elements, the first order eigenfunctions for d^2s and d^3 in the $LS\,M_LM_S$ scheme are given in Table I for $M_L=0$ and $M_S=1/2$.

The zero order states A, B, $C\ldots$ for d^2s, d^3 and $ndn's^2\ {}^2D_{0,1/2}$ are given in Table II in the notation of I.

The secular equations for the third order energies may now be written and solved in terms of

TABLE I. *First order eigenfunctions* $M_L=0$, $M_S=\frac{1}{2}$.

The first order eigenfunctions in the first column on the left in each configuration are linear combinations of the zero order functions A, B, $C\cdots$ in the first row, the coefficient of each zero order function appearing in the column below it. The second column from the left gives the normalization factor of the whole linear combination. The zero order functions are normalized separately so that N is the reciprocal of the square root of the sum of the squares of the coefficients appearing in the same row.

		$nd^2n's$									nd^3								
	N	A	B	C	D	E	F	G		N	A	B	C	D	E	F	G	H
${}^4_1F_{0,\frac{1}{2}}$	$(15)^{-\frac{1}{2}}$	-1	-1	-1	2	2	2	0	${}^4_1F_{0,\frac{1}{2}}$	$(15)^{-\frac{1}{2}}$	-2	-2	-2	0	0	1	1	1
${}^4_1P_{0,\frac{1}{2}}$	$(15)^{-\frac{1}{2}}$	2	2	2	1	1	1	0	${}^4_1P_{0,\frac{1}{2}}$	$(15)^{-\frac{1}{2}}$	1	1	1	0	0	2	2	2
${}^2_1G_{0,\frac{1}{2}}$	$(70)^{-\frac{1}{2}}$	1	-1	0	-4	4	0	6	${}^2_1H_{0,\frac{1}{2}}$	$(42)^{-\frac{1}{2}}$	-1	2	-1	$-6^{\frac{1}{2}}$	$6^{\frac{1}{2}}$	2	-4	2
${}^2_1F_{0,\frac{1}{2}}$	$(30)^{-\frac{1}{2}}$	-1	-1	2	2	2	-4	0	${}^2_1G_{0,\frac{1}{2}}$	$(14)^{-\frac{1}{2}}$	$-2^{\frac{1}{2}}$	0	$2^{\frac{1}{2}}$	$-3^{\frac{1}{2}}$	$-3^{\frac{1}{2}}$	$2^{\frac{1}{2}}$	0	$-2^{\frac{1}{2}}$
${}^2_1D_{0,\frac{1}{2}}$	$(14)^{-\frac{1}{2}}$	2	-2	0	-1	1	0	-2	${}^2_1F_{0,\frac{1}{2}}$	$(30)^{-\frac{1}{2}}$	$-2^{\frac{1}{2}}$	$8^{\frac{1}{2}}$	$-2^{\frac{1}{2}}$	$-3^{\frac{1}{2}}$	$3^{\frac{1}{2}}$	$-2^{\frac{1}{2}}$	$8^{\frac{1}{2}}$	$-2^{\frac{1}{2}}$
${}^2_1P_{0,\frac{1}{2}}$	$(30)^{-\frac{1}{2}}$	-2	-2	4	-1	-1	2	0	${}^2_1D^a_{0,\frac{1}{2}}$	$(4)^{-\frac{1}{2}}$	-1	0	1	0	0	-1	0	1
${}^2_1S_{0,\frac{1}{2}}$	$(5)^{-\frac{1}{2}}$	1	-1	0	1	-1	0	1	${}^2_1D^b_{0,\frac{1}{2}}$	$(28)^{-\frac{1}{2}}$	$3^{\frac{1}{2}}$	0	$-3^{\frac{1}{2}}$	$-8^{\frac{1}{2}}$	$-8^{\frac{1}{2}}$	$-3^{\frac{1}{2}}$	0	$3^{\frac{1}{2}}$
									${}^2_1P_{0,\frac{1}{2}}$	$(210)^{-\frac{1}{2}}$	-4	8	-4	$54^{\frac{1}{2}}$	$-54^{\frac{1}{2}}$	1	-2	1

[7] E. U. Condon and G. H. Shortley, Phys. Rev. **37**, 1025 (1931).

TABLE II. *Zero order eigenfunctions* $M_L=0$; $M_S=\frac{1}{2}$.

$nd\,n's^2\,{}^2D_{0,\frac{1}{2}}$ $\quad \boldsymbol{A}\,u_1(0^+)u_2(0_s^+)u_3(0_s^-)$

d^2s	d^3
A $\boldsymbol{A}\,u_1(2^+)u_2(-2^-)u_3(0_s^+)$	A $\boldsymbol{A}\,u_1(2^+)u_2(0^+)u_3(-2^-)$
B $\boldsymbol{A}\,u_1(2^-)u_2(-2^+)u_3(0_s^+)$	B $\boldsymbol{A}\,u_1(2^+)u_2(0^-)u_3(-2^+)$
C $\boldsymbol{A}\,u_1(2^+)u_2(-2^+)u_3(0_s^-)$	C $\boldsymbol{A}\,u_1(2^-)u_2(0^+)u_3(-2^+)$
D $\boldsymbol{A}\,u_1(1^+)u_2(-1^-)u_3(0_s^+)$	D $\boldsymbol{A}\,u_1(2^+)u_2(-1^+)u_3(-1^-)$
E $\boldsymbol{A}\,u_1(1^-)u_2(-1^+)u_3(0_s^+)$	E $\boldsymbol{A}\,u_1(1^+)u_2(1^-)u_3(-2^-)$
F $\boldsymbol{A}\,u_1(1^+)u_2(-1^+)u_3(0_s^-)$	F $\boldsymbol{A}\,u_1(1^+)u_2(0^+)u_3(-1^-)$
G $\boldsymbol{A}\,u_1(0^+)u_2(0^-)u_3(0_s^+)$	G $\boldsymbol{A}\,u_1(1^+)u_2(0^-)u_3(-1^+)$
	H $\boldsymbol{A}\,u_1(1^-)u_2(0^+)u_3(-1^+)$

the radial integral parameters. One obtains quadratic equations for the ${}^4F$'s, ${}^4P$'s and ${}^2S$'s; cubic equations for the ${}^2G$'s, ${}^2F$'s and ${}^2P$'s; and a quintic equation for the ${}^2D$'s.

If $nd^2n''s$ be omitted, quadratic equations are obtained for the ${}^2G$'s, ${}^2F$'s and ${}^2P$'s; and a quartic equation for the ${}^2D$'s.

Next with the energies obtained as solutions of these secular equations, the third order states, in which the matrix of electrostatic interaction for all the configurations is diagonal, may be found by solving the simultaneous equations obtained from the matrix of the secular equation by substituting each energy value successively.

2. SEPARATIONS OF THE ENERGY LEVELS WITHIN TERMS

With the third order states of § 1, it is now possible to calculate the separations of the energy levels within each term approximately as was done for the two $d^3\,{}^2D$'s in I. The matrix elements of magnetic interaction calculated from the third order states are given in terms of the matrix elements of magnetic interaction of the first order states. Therefore the latter matrix elements needed in addition to those found for d^3 in Pauling and Goudsmit[8] and I are given here. For d^2s the diagonal elements of ${}^4F$, ${}^4P$ and ${}^2P$ are the same as those of d^3. The others are:

$$\begin{aligned}
&(d^2s\,{}^2_1G_{9/2},\,9/2\,|v^1|\,d^2s\,{}^2_1G_{9/2},\,9/2)=0,\\
&(d^2s\,{}^2_1F_{7/2},\,7/2\,|v^1|\,d^2s\,{}^2_1F_{7/2},\,7/2)=d^2s\zeta_{nd},\\
&(d^2s\,{}^2_1D_{5/2},\,5/2\,|v^1|\,d^2s\,{}^2_1D_{5/2},\,5/2)=0,\\
&(ds^2\,{}^2_1D_{5/2},\,5/2\,|v^1|\,ds^2\,{}^2_1D_{5/2},\,5/2)=ds^2\zeta_{nd}.
\end{aligned} \tag{7}$$

The non-diagonal elements, between the first order states of terms of the same kind having the same values of M_L and M_S, vanish for the configurations $nd^2n's$, nd^3, $ndn's^2$ and $nd^2n''s$ except that element between the two $d^3\,{}^2D$'s which is:

$$(d^3\,{}^2_2D_{5/2}{}^+,\,5/2\,|v^1|\,d^3\,{}^2_2D_{5/2}{}^-,\,5/2)=-\frac{(21)^{\frac{1}{2}}2}{3Ra}\,(4F_2+15F_4)d^3\zeta_{nd}, \tag{8}$$

where F_2, F_4 and Ra have the values given in Eq. (3).

If $nd^2n''s$ be omitted, the matrix elements of magnetic interaction of the quartet levels will be unaffected by the interaction of the configurations, since the non-diagonal elements of electrostatic interaction are zero for the first order quartet eigenfunctions. The elements affected will be those of ${}^2G$, ${}^2F$, ${}^2D$ and ${}^2P$. As in I, the separations of the energy levels within the term are obtained from the diagonal matrix elements of magnetic interaction by the Landé interval rule.

[8] L. Pauling and S. Goudsmit, *Structure of Line Spectra*, § 39. The a of this section is ζ_{nd}.

3. Comparison with Experiment

The experimental term values of Russell[9] for Ti II and of Kiess and Kiess[10] for Zr II were the only ones found complete enough to test the calculations.

It was found that the lack of all but a few experimental term values of $d^2n''s$, combined with the fact that this configuration lies high compared to $nd^2n's$, nd^3 and $ndn's^2$, made it impossible to determine the three additional radial integral parameters with a reasonable accuracy. Therefore the configuration $d^2n''s$ was omitted and only the three configurations $nd^2n's$, nd^3 and $ndn's^2$ compared with experiment.

In order to evaluate the parameters, those radial integrals which contained electrons of identical n and l values were taken as equal, regardless of the fact that these electrons belonged to different configurations.[11] Although this introduces some error, it may be expected to give the best values of the parameters which can be obtained without calculating them from the radial eigenfunctions.

The radial integral parameters occurring in the diagonal matrix elements were first evaluated by the method of least squares using the quartet terms, the doublet terms, $nd^2n's^2S$, $nd^3\,{}^2H$, the mean of the ${}^2G$'s, and the mean of the ${}^2P$'s or ${}^2F$'s since these two means are theoretically the same. In Ti II, $nd^2n's^2S$ is not used as it appears to be perturbed and would thus introduce a larger error in the parameters. With these parameters, the interaction parameter $'R_2$ is found by making the sum of the squares of the errors in the calculated values of the three doublet separations, $nd^3\,{}^2G - nd^2n's^2G$, $nd^3\,{}^2F - nd^2n's^2F$ and $nd^3\,{}^2P - nd^2n's^2P$, a minimum. The values of the parameters are listed in Table III. These parameters are then used to solve the quartic equation to find the ${}^2D$ energy levels.

The results for the energy levels of Ti II and Zr II are given in Fig. 1. In Ti II, $d^3\,{}^2H$ and $d^3\,{}^2P$ are now separated by the interaction but the

[9] H. N. Russell, Astrophys. J. **66**, 283 (1927).

[10] C. C. Kiess and H. K. Kiess, Bur. Standards J. Research **5**, 1210 (1930).

[11] I am grateful to Professor D. R. Hartree for pointing out that, while not entirely arbitrary, these integrals are not identical.

Table III. *Radial integral parameters $nd^2n's$, nd^3, and $ndn's^2$, values from experiment.*

$F_0 = F^0(nd^2)$. The values of the other parameters in terms of the F's, G's and R's of Slater[3] and I are given in Eqs. (3), (4), (5) and (6). In this table, all radial integrals in which the electrons have the same values of n and l are considered equal, even when the electrons belong to different configurations.

	Ti II	Zr II
F_0	6549.	5761.
F_2	938.7	705.7
F_4	68.03	50.44
$'F_0$	2249.	2527.
$''F$	21870.	9562.
$'G_2$	1097.	1873.
$'R_2$	191.8	387.3
α_+	0.8905	0.8888
α_-	0.4550	0.4583
Ra	20340.	15300.

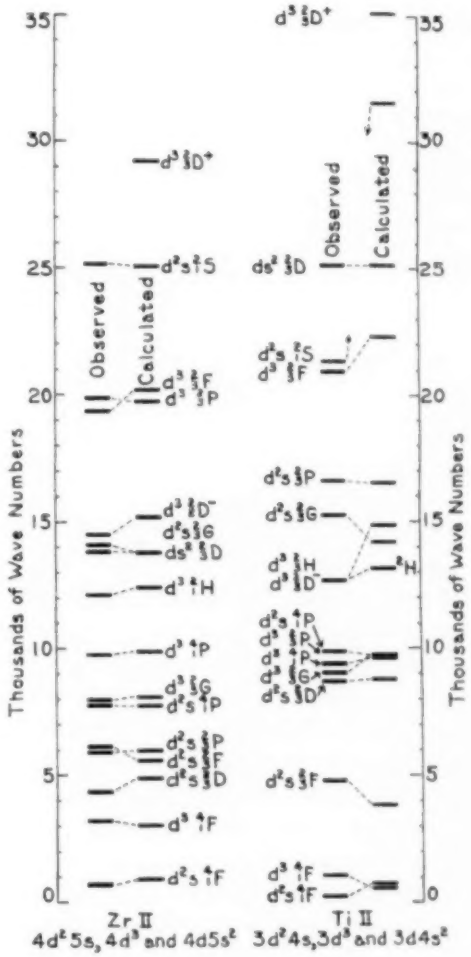

Fig. 1. Term values.

TABLE IV. *Energy level separations in Ti II and Zr II with interaction between d^2s, d^3 and ds^2.*

Term notation	Ti II	Zr II		Ti II	Zr II		Ti II	Zr II		Ti II	Zr II		Ti II	Zr II
$d^3\,{}^4_1F$	† Observed			128.37	458.02		103.41	404.59		75.84	322.84			
	Calculated			*133*	*512*		*104*	*398*		*74.1*	*284*			
$d^2s\,{}^4_1F$				167.75	558.47		131.53	448.77		93.94	314.67			
				170	*580*		*132*	*451*		*94.2*	*322*			
$d^3\,{}^4_1P$										122.29	225.85		32.05	189.70
										74.1	*284*		*44.5*	*170*
$d^2s\,{}^4_1P$										94.00*	322.14*		57.87	223.35
										94.2	*322*		*56.5*	*193*
$d^3\,{}^2_1H$	97.82*	375.20*	$d^3\,{}^2_3G$	120.46	315.06	$d^3\,{}^2_3F$	−59.89	−81.60	$d^3\,{}^2_3D^+$	—	—	$d^3\,{}^2_3P$	125.02	466.76
	97.8	*375*		*108*	*296*		*−48.8*	*−124*		*−43.6*	*−164*		*101*	*365*
			$d^2s\,{}^2_3G$	−8.07	130.69	$d^2s\,{}^2_3F$	268.99	714.69	$d^3\,{}^2_3D^-$	129.38	434.73	$d^2s\,{}^2_3P$	109.46	387.32
				12.2	*164*		*261*	*828*		*118*	*393*		*101*	*362*
									$d^2s\,{}^2_3D$	33.80	257.20			
										16.8	*300*			
									$ds^2\,{}^2_3D$	231.70*	734.40*			
										232	*734*			
11/2 *J* values		9/2			7/2			5/2			3/2			1/2

† Observed values are in Roman type, calculated values in italics.

* The observed separations marked with asterisks were used to calculate the following values of ζ_{nd}:

	Ti II	Zr II
$d^3\zeta_{nd}$	88.9	341
$d^2s\zeta_{nd}$	113	386
$ds^2\zeta_{nd}$	99.5	392

agreement is about the same as it was without considering interaction. However, omitting $ds^2\,{}^2D$ which has a unique parameter to determine its position, the calculated displacements of the remaining 15 levels from their center of gravity depend now on only 5 instead of 6 radial integral parameters. Thus equally good agreement is obtained for Ti II with one less parameter. The discrepancies still remaining in Ti II might be lessened if the interaction with higher configurations such as $nd^2n''s$ could be included. An accurate theoretical evaluation of the radial integral parameters may then be expected to give satisfactory agreement with experiment.

In Zr II, the experimental values of the ^2D's have been reassigned to give a more reasonable agreement with the theory. As no high ^2D was observed in d^3, this term has been omitted from the experimental list, as was the case in Ti II. The term assigned as the higher ^2D of d^3 is considered to be the lower one, $d^3\,{}^2D^-$. This means that one of the experimental terms is not a ^2D belonging to these configurations. As Kiess and Kiess remark that the assignment of $ndn's^2\,{}^2D$ is doubtful, this term is omitted and replaced by the level assigned as the lower ^2D of d^3 which is now considered to be $ndn's^2\,{}^2D$. As evidence for this change, $d^3\,{}^2D^-$ of Kiess and Kiess has its three strongest multiplets with dsp^2PDF so that by changing it to $ds^2\,{}^2D$ these become one electron transitions rather than the more improbable two electron jumps. It might be argued that the high lying $d^3\,{}^2D^+$, which has been calculated, should be pushed down because of the interaction with ^2D's lying above it. However, as Brillouin[12]

[12] L. Brillouin, J. de Physique **3**, 373 (1932).

has shown, it is impossible for such interaction to push it below $ds^2\ ^2D$. Therefore, since in Russell-Saunders coupling the magnetic interaction does not affect the center of gravity of each term, to get even rough agreement, the observed value of $d^3\ ^2D^+$ must lie above $ds^2\ ^2D$.

Now from these third order energies, the third order eigenfunctions may be calculated. The squares of the coefficients, in the linear combination of the first or second order eigenfunctions which must be taken to give the third order eigenfunctions, give the relative weights of the initial states that go to make up the final state. Except for the ^2P's, the original configuration assignment gives the state of greatest weight in the final state after configuration interaction. The final states of ^2P are made up of nearly equal weights of the initial states with these weights reversed from the original observed assignment. That configuration interaction should have the greatest effect on the ^2P's is to be expected since they disagreed badly with experiment in the configurations separately.

With the eigenfunctions, the separations of the levels with different J values within the terms can be found in terms of three radial integral parameters ζ_{nd}, one value coming from each of the configurations d^2s, d^3, and ds^2. ζ_{nd} is then found from the observed separation of a term which will give approximately an average value for each configuration. $d^3\zeta_{nd}$ is taken from $d^3\ ^2H$ as was done by Pauling and Goudsmit,[8] $d^2s\zeta_{nd}$ from $d^2s\ ^4P_{5/2-3/2}$ and $ds^2\zeta_{nd}$ from $ds^2\ ^2D$. The separations calculated with these parameters are compared with the observed values in Table IV.[13]

The separations of the ^2D's in Zr II present another argument in favor of rearranging the ^2D's as has been done here, since there was complete disagreement in the separations of the two ^2D's of d^3 before they were rearranged.

In conclusion it has been seen that the interaction of configurations in Russell-Saunders coupling has improved the calculated energies for the different terms of d^2s, d^3 and ds^2 in Ti II and Zr II. Zr II especially presents a striking effect from configuration interaction. Badly confused before, it comes out in satisfactory agreement with experiment after the interaction has been applied.

[13] In Ti II, the quartet separations and that for $d^3,^2H$ are those given by Pauling and Goudsmit.[8]

Relative Multiplet Transition Probabilities from Spectroscopic Stability

E. U. CONDON AND C. W. UFFORD, *Palmer Physical Laboratory, Princeton University*

(Received August 7, 1933)

A method analogous to the diagonal sum rule for term values is given for calculating the relative transition probabilities of the different multiplets in Russell-Saunders coupling. The method is based on the principle of spectroscopic stability. The relative multiplet transition probabilities are given for the transitions p^2d-p^3, d^2p-d^3, p^3d-p^4 and p^4d-p^5.

THIS paper will give a method, based on the principle of spectroscopic stability, of calculating the relative transition probabilities of different multiplets in Russell-Saunders coupling. This principle allows one to use a method of finding the transition probabilities in Russell-Saunders coupling in terms of the transition probabilities between the zero order states analogous to the diagonal sum rule used by Slater[1] for the energy values. This method gives the same results as that used by Ufford[2] but avoids using the eigenfunctions in Russell-Saunders coupling.

We have the theorem[3] analogous to the principle of spectroscopic stability, which states that the sum of the squares of the matrix elements connecting a set of states is invariant when these states are subjected to a unitary transformation. Since the transformation from zero order states to Russell-Saunders coupling states is unitary, this theorem will give us equations from which the matrix elements of the electric moment may be found in Russell-Saunders coupling. In cases where more than one term of a kind occurs in a configuration, this method will give only the sums of the squares of the matrix elements and not the elements themselves. The transition probabilities are proportional to the squares of these matrix elements of the electric moment. The transition probability for the entire multiplet may be determined from the transition probability for a transition between a single initial and final state by using the summation rules.

1. Calculation of the Matrix Elements of the Electric Moment in Russell-Saunders Coupling

We are to calculate the matrix elements of the electric moment between a set of states belonging to a first electron configuration and a set belonging to a second electron configuration differing from the first in regard to just one nl value with a change in l equal to unity. Call the first configuration αnl and the second $\alpha n'l'$. First, one draws up the zero-order scheme for each configuration, classified by M_L and M_S values; and the LSM_LM_S scheme for each configuration also classified by M_L and M_S values. As in the case of energies, only positive values of M_L and M_S need be considered.

The matrix components of $\mathfrak{er}$ will vanish between states of different M_S, so one may take each value of M_S separately, starting with the largest, and draw up the matrix for the different M_L values in each scheme. The matrix components of $\mathfrak{er}$ in the zero-order scheme may be obtained from the formulas given by Condon.[4] The only nonvanishing matrix components are those in which but one individual set of quantum numbers changes, so that this must be the individual set referring to $(nl)-(n'l')$, where $l'=l\pm1$.

[1] J. C. Slater, Phys. Rev. **34**, 1293 (1929).

[2] C. W. Ufford, Phys. Rev. **40**, 974 (1932).

[3] M. Born, W. Heisenberg and P. Jordan, Zeits. f. Physik **35**, 557 (1926); J. H. Van Vleck, Phys. Rev. **29**, 740 (1927).

[4] E. U. Condon, Phys. Rev. **36**, 1121 (1930). For the matrix elements between single electron states see for example, E. U. Condon and P. M. Morse, *Quantum Mechanics*, p. 100, McGraw-Hill (1929).

We want

$$|(nlm_l|e\mathbf{r}|n'l'm_l')|^2 = |(nl|er|n'l')(lm_l|\mathbf{r}|l'm_l')|^2, \quad (1)$$

where $(lm_l|\mathbf{r}|l'm_l')$ is the numerator of the factor given by Condon and Morse[4] in Eqs. (35) which contains the dependence of $(nlm_l|e\mathbf{r}|n'l'm_l')$ on m_l and m_l'. Therefore $(nl|er|n'l')$ must be defined to include the denominator of the factor given by Condon and Morse, thus

$$(nl|er|n'l') = [(2l+1)(2l'+1)]^{-\frac{1}{2}} \int_0^\infty erR(nl)R(n'l')dr. \quad (2)$$

Again in the LSM_LM_S scheme, we must separate from each matrix element $(LSM_LM_S|e\mathbf{r}| \times L'SM_L'M_S)$ the part, $(LM_L|\mathbf{r}|L'M_L')$, depending on M_L, so that the remaining part $(^{2S+1}L|er|^{2S+1}L')$ will be independent of M_L, and hence the same in each rectangle characterized by a different value of M_L. It is the squares of these factors independent of M_L which we are then able to calculate by the invariance of the sum of their squares. The dependence of $(LSM_LM_S|e\mathbf{r}|L'SM_L'M_S)$ on M_L may be obtained from formulas given by Güttinger and Pauli.[5]

Now in each rectangle characterized by a given value of M_SM_L and M_L' we write an equation.

$$|(nl|er|n'l')|^2 \sum_{\substack{\text{zero order}\\ \text{states}}} |(lm_l|\mathbf{r}|l'm_l')|^2 = \sum_{L\cdot S \text{ states}} |(LSM_LM_S|e\mathbf{r}|L'SM_L'M_S)|^2 = \sum_{L\cdot S \text{ states}} |(^{2S+1}L|er|^{2S+1}L')|^2 |(LM_L|\mathbf{r}|LM_L')|^2. \quad (3)$$

The factor $|(nl|er|n'l')|^2$ remains the same throughout the entire matrix so that, as we are interested only in relative values, it may be omitted. Also, the squares of the matrix elements contain the factor $\frac{1}{4}$ for the x and y components since $x=\frac{1}{2}(x+iy+x-iy)$ and the matrix element of either $x+iy$ or $x-iy$ is zero for a given transition. Since this factor, $\frac{1}{4}$, will occur in both the zero order and LSM_LM_S schemes, on each side of Eq. (3), it also may be omitted. Then, beginning in the rectangle with the largest M_L, we solve the equation of each rectangle for the $|(^{2S+1}L|er|^{2S+1}L')|^2$'s using the values obtained from the rectangles of higher M_L. Thus we obtain an equation for each rectangle with only one unknown as long as only one multiplet of the same kind occurs in a configuration. An equation for the sum of the squares of the matrix components of the multiplets of the same kind is obtained. In some rectangles it often happens that all the elements are known, so that a check is obtained on the work up to this point.

The relative transition probability for the entire multiplet is then obtained from

$$|(^{2S+1}L|er|^{2S+1}L')|^2$$

by multiplying by the factors given by Güttinger and Pauli[5] in Eq. (24) for the sum over the final states and by $(2S+1)(2L+1)$ for the sum over the initial states.

TABLE I. *Calculation of the matrix elements of the electric moment in Russell-Saunders coupling for the quartets of d^2p-d^3 with $M_S=3/2$.*

				d^3
	M_L			3
		Zero order states		$\|2^+1^+0^+\|$
			LSM_LM_S states	^4F
d^2p	4	$\|1_p^+2^+1^+\|$	^4G	$2=56\|(d^2p\,^4G\|er\|d^3\,^4F)\|^2$ $\|(d^2p\,^4G\|er\|d^3\,^4F)\|^2=\frac{1}{28}$
	3	$\|1_p^+2^+0^+\|$ $\|0_p^+2^+1^+\|$	^4G ^4F	$3+4$ $=7\|(d^2p\,^4G\|er\|d^3\,^4F)\|^2$ $+9\|(d^2p\,^4F\|er\|d^3\,^4F)\|^2$ $7=\frac{7}{28}$ $+9\|(d^2p\,^4F\|er\|d^3\,^4F)\|^2$ $\|(d^2p\,^4F\|er\|d^3\,^4F)\|^2=\frac{3}{4}$
	2	$\|1_p^+2^+-1^+\|$ $\|1_p^+1^+0^+\|$ $\|0_p^+2^+0^+\|$ $\|-1_p^+2^+1^+\|$	^4G ^4F ^4D ^4D	$2+12+6$ $=2\|(d^2p\,^4G\|er\|d^3\,^4F)\|^2$ $+6\|(d^2p\,^4F\|er\|d^3\,^4F)\|^2$ $+30\|(d^2p2\,^4D\|er\|d^3\,^4F)\|^2$ $20=\frac{2}{28}+6(\frac{3}{4})$ $+30\|(d^2p2\,^4D\|er\|d^3\,^4F)\|^2$ $\|(d^2p2\,^4D\|er\|d^3\,^4F)\|^2=\frac{15}{35}$

[5] P. Güttinger and W. Pauli, Zeits. f. Physik **67**, 743 (1931); p. 761, Eq. (25). The $a^{t}{}_{tt'}$ of this equation is $(^{2S+1}L|r|^{2S+1}L')$.

2. Detailed Calculation of Quartet Transitions in d^2p-d^3

The method of calculating relative multiplet transition probabilities is shown in Table I. To obtain, for example, the equation in the rectangle labeled $d^2p\,M_L=3$, $d^3\,M_L=3$, one has for the zero order states:[4]

$$\begin{aligned}|(|2^+0^+1_p{}^+|\,|\mathbf{z}|\,|2^+1^+0^+|)|^2&=|(1_p{}^+|\mathbf{z}|1^+)|^2=(1+1+1)(1-1+1)=3,\\ |(|2^+1^+0_p{}^+|\,|\mathbf{z}|\,|2^+1^+0^+|)|^2&=|(0_p{}^+|\mathbf{z}|0^+)|^2=(1+0+1)(1+0+1)=4.\end{aligned}\tag{4}$$

For the LSM_LM_S states:[5]

$$\begin{aligned}&|(d^2p4,\,3/2,\,3,\,3/2|e\mathbf{z}|d^33,\,3/2,\,3,\,3/2)|^2=(4^2-3^2)\,|(d^2p\,{}^4G|er|d^3\,{}^4F)|^2=7\,|(d^2p\,{}^4G|er|d^3\,{}^4F)|^2,\\ &|(d^2p3,\,3/2,\,3,\,3/2|e\mathbf{z}|d^33,\,3/2,\,3,\,3/2)|^2=3^2\,|(d^2p\,{}^4F|er|d^3\,{}^4F)|^2=9\,|(d^2p\,{}^4F|er|d^3\,{}^4F)|^2.\end{aligned}\tag{5}$$

Equating the sum of the elements of Eq. (4) to the sum of the elements of Eq. (5) gives the required equation. The value of $|(d^2p\,{}^4G|er|d^3\,{}^4F)|^2$ from the previous rectangle $d^2p\,M_L=4$, $d^3\,M_L=3$ is then substituted in this equation and the equation solved for $|(d^2p\,{}^4F|er|d^3\,{}^4F)|^2$. Now the relative multiplet transition probabilities are obtained from these elements by multiplying by the factors to sum over the initial and final states. Thus[5]

$$\begin{aligned}(d^2p\,{}^4G,\,d^3\,{}^4F)&=1/28(4\cdot9)(4\cdot7)=36,\\ (d^2p\,{}^4F,\,d^3\,{}^4F)&=3/4(4\cdot7)(3\cdot4)=252,\\ (d^2p2\,{}^2D,\,d^3\,{}^4F)&=18/35(4\cdot5)(3\cdot7)=216.\end{aligned}\tag{6}$$

$(d^2p2^2D,\,d^3\,{}^4F)$ is the sum of the relative transition probabilities of the two ^4D–^4F multiplets.

3. Relative Multiplet Transition Probabilities

The relative multiplet transition probabilities are shown in the tables as follows: p^2d-p^3 in Table II, d^2p-d^3 in Table III, p^3d-p^4 in Table IV, and p^4d-p^5 in Table V.

It must be remembered that a transition such as $d^2p3\,{}^2D-d^32\,{}^2D$ in Table III represents the sum of the relative transition probabilities of six $d^2p\,{}^2D-d^3\,{}^2D$ multiplets. As before,[2] the intersystem transitions forbidden by the selection rule for the spin quantum number, $\Delta S=0$, are marked

Table II. *Relative multiplet transition probabilities in Russell-Saunders coupling for the transitions p^2d-p^3.*

p^2d	p^3	^4S	^2D	^2P
	^4F	y	x	$x,\ y$
	^4D	y	x	x
	^4P	24	x	x
	^2G	$x,\ y$	y	y
	$2\,{}^2F$	$x,\ y$	42	y
	$3\,{}^2D$	$x,\ y$	15	25
	$2\,{}^2P$	x	3	9
	^2S	x	y	2

Table III. *Relative multiplet transition probabilities in Russell-Saunders coupling for the transitions d^2p-d^3.*

d^2p	d^3	^4F	^4P	^2H	^2G	^2F	$2\,{}^2D$	^2P
	^4G	180	y	x	x	x	$x,\ y$	$x,\ y$
	^4F	1260	y	$x,\ y$	x	x	x	$x,\ y$
	$2\,{}^4D$	1080	520	$x,\ y$	$x,\ y$	x	x	x
	^4P	y	240	$x,\ y$	$x,\ y$	$x,\ y$	x	x
	^4S	y	320	$x,\ y$	$x,\ y$	$x,\ y$	$x,\ y$	x
	^2H	$x,\ y$	$x,\ y$	396	44	y	y	y
	$2\,{}^2G$	x	$x,\ y$	1584	576	180	y	y
	$3\,{}^2F$	x	$x,\ y$	y	1000	420	470	y
	$3\,{}^2D$	x	x	y	y	660	625	215
	$3\,{}^2P$	$x,\ y$	x	y	y	y	705	255
	^2S	$x,\ y$	x	y	y	y	y	70

TABLE IV. *Relative multiplet transition probabilities in Russell-Saunders coupling for the transitions $p^5d - p^4$.*

		p^4		
		^3P	^1D	^1S
p^5d	^5D	x	x	x, y
	^3G	y	x, y	x, y
	$2\,^3F$	y	x	x, y
	$3\,^3D$	120	x	x, y
	$2\,^3P$	45	x	x
	^3S	15	x, y	x
	^1G	x, y	y	y
	$2\,^1F$	x, y	63	y
	$2\,^1D$	x	30	y
	$2\,^1P$	x	7	20
	^1S	x	y	0

TABLE V. *Relative multiplet transition probabilities in Russell-Saunders coupling for the transitions $p^4d - p^5$.*

		p^4d							
		^4F	^4D	^4P	^2G	$2\,^2F$	$3\,^2D$	$2\,^2P$	^2S
p^5	^2P	x, y	x	x	y	y	19	9	2

x; and those forbidden by the selection rule for the total orbital angular momentum, $\Delta L = 0, \pm 1$, are marked y. Thus the method of spectroscopic stability is seen to aid effectively in the theoretical calculation of relative multiplet transition probabilities in Russell-Saunders coupling.

The Hyperfine Structure Intensities of the 2^3S_1–$2^3P_{0,1,2}$ Triplet in Optically Excited Mercury Vapor

M. L. Pool and S. J. Simmons, *Ohio State University, Columbus, Ohio*

(Received July 10, 1933)

The hyperfine structures of the mercury lines 5461, 4358 and 4047 in fluorescence emission were obtained in the second order of a 30,000 line, 21 ft. grating. The ratio of the intensity of the central component to the intensity of any one of the other components was found greater than a similar ratio for the emission from the exciting arc. This anomalous increase in intensity of the central component in fluorescence may be accounted for by making use of the absorption coefficients of the components of 4047.

Introduction

THE hyperfine structure of the visible triplet 5461, 4358 and 4047 of mercury emitted from optically excited fluorescent mercury vapor was first investigated by Collins.[1] With a Lummer-Gehrcke plate he found that 5461 for pure mercury consisted of the central component only, while with a few millimeters of nitrogen admixture, the central and the $+0.785$ cm^{-1} components appeared with about equal intensity. The lines 4358 and 4047 also were observed to have peculiar component intensities as compared with those of the arc.

More recently Mrozowski[2] also using a Lummer-Gehrcke plate and similar experimental set-up, observed for these three lines in fluorescence, the central component only.

In the experiment reported on in this paper the above-mentioned lines were observed in the second order spectrum of a 30,000 line, 21 ft. grating.

Apparatus and Procedure

The quartz resonance tube about 2.5 cm diameter and 25 cm long was of the conventional horn-shaped design. The total radiation from two water-cooled and magnetically deflected quartz mercury arcs* excited the mercury vapor in the resonance tube. The admixed nitrogen was kept moving slowly through the resonance tube and over P_2O_5 and hot copper and copper oxide. The temperature of the resonance tube was about 25°C. Photographic exposures ranged from one quarter to sixty hours, and the temperature of the grating was constant to less than 0.1°C. The shorter exposures were sufficient when a telephoto lens was used near the photographic plate.[3] Eastman 33 plates were used for 4047 and 4358, while G 1 and G 3 plates were used for 5461. The plates were put in a small prism spectrograph and density markings put on by the help of calibrated screens.[4] Density measurements were made by a photoelectric densitometer[5] particularly designed for hyperfine structure work. The ratio of the intensity of the central component to that of some other component for the fluorescence was compared with the like ratio for the exciting arc. The arc used as comparison was a water-cooled Uviarc running at three amperes. Since for an optimum photographic density the exposure time for the arc was a few seconds while that for the fluorescence was several hours, it was necessary to investigate a possible change in the contrast for such large differences in instantaneous energy falling on the plate. It was found[6] that when the intensity was increased by a factor of about 10,000 the ratio of a strong line to a weak line increased by a factor of about 1.3. This factor, though smaller than expected, has been incorporated in Table I.

[1] E. Hobart Collins, Phys. Rev. **43**, 753 (1928).

[2] S. Mrozowski, Zeits. f. Physik **78**, 826 (1932).

* Cooper-Hewitt Uviarc, horizontal type.

[3] J. B. Green, Phys. Rev. **37**, 473 (1931).

[4] G. R. Harrison, J. O. S. A. and R. S. I. **18**, 492 (1929).

[5] G. A. Rosselot built this photoelectric densitometer using two FP54 tubes.

[6] C. E. Hesthal and V. C. Wilson kindly made these measurements for us.

TABLE I. *Observed intensity quotients for fine structure components of Hg 4047, 4358 and 5461. These quotients represent the ratio of the intensities of the components to the intensity of the central component in fluorescence divided by the corresponding ratios for the arc.*

	Pressure N_2 (mm)	Exposure (hrs.)	+0.330, +0.270 (cm^{-1})	−0.394 (cm^{-1})	−0.743 (cm^{-1})	
4047						
	0	43	2.9	2.8	2.9	
	3.7	59	2.9	2.9	—	
	8.0*	36	3.5	2.0	—	
	27.7	21	2.0	—	—	
	41.8*	20	2.5	—	—	
			+0.505, +0.566			
4358			+0.836		−0.240	−0.555
	3.7*	59	7.0	2.9	—	—
	8.9	36	5.5	2.3	2.8	3.8
	15.5	24	—	3.2	3.8	—
	15.9	$\frac{1}{4}$	—	4.5	—	—
	42.0	19	—	4.1	—	—
5461			+0.790	−0.278		
	3.7	46	—	3.6		
	8.4*	34	3.4	—		
	15.5	24	—	2.3		
	39.2	22	—	4.4		

* These exposures are reproduced in Figs. 1, 2, 3, 4.

In order to test for scattered and reflected light there was placed between each arc and the resonance tube a glass plate which cut out the 2537 exciting line, thus terminating all resonance radiation, but which passed the visible triplet. After 20 hours, not a trace of even the central component was visible.

RESULTS

Typical photographs of the fine structure of λ4047, 4358 and 5461 in the arc and in fluorescence are shown in Figs. 1, 2, 3 and 4. In Table I are presented the essential details of the exposures together with the results of the intensity measurements. The "intensity quotients" represent the ratio of the intensity of the particular component to the intensity of the central component in fluorescence divided by the same ratio in the arc.

DISCUSSION

We have not been able to correlate the findings of Collins with those reported here. We were successful in obtaining only one measurable plate at zero nitrogen pressure, but except for a marked decrease in intensity of emission there seemed to be no marked difference in hyperfine structure intensity ratio whether nitrogen was present or not. Perhaps Mrozowski did not get components other than the central one because of insufficient exposure.

One should expect components in fluorescence as is evident from Fig. 5.[7] In the exciting source all the components are present and each with its absorption coefficient would contribute to its component in emission. In order to calculate the relative intensities of the components in emission it will be necessary to make use of the fact that the central component of 4047 has a much larger absorption coefficient than any of the other components, and that the other components have absorption coefficients that decrease with decrease in intensity of the component.[8]

A detailed account of the process involved is probably as follows: The components of 2537 put the various isotopic mercury atoms into the 2^3P_1 state. Since the absorption coefficients of the various components of 2537 are probably different, the relative concentrations of the isotopes in this state will not be the same as the relative number in the ground state. This concentration may be further modified by collisions of the second kind with nitrogen resulting in mercury being left in the metastable 2^3P_0 state. It is not necessary to know the relative number of isotopes in this 2^3P_0 state, since the linear absorption coefficients for the various components of 4047 have been measured for just such a concentration. From this metastable state the populating of the 2^3S_1 state will depend upon the absorption of 4047, the component with the greatest absorption contributing the most. The absorption of 4358 and 5461 is negligible.[9] For example the lower hyperfine level of the 2^3S_1 state of the 199 mercury isotope is populated by the $-0.743\ cm^{-1}$ component of 4047. There is no transfer of energy between the various isotopes because each isotope is isolated from all others for the life time of the 2^3S_1 state by the admixed

[7] Compiled from H. Schuler and J. E. Keyston, Zeits. f. Physik **72**, 423 (1931).

[8] M. L. Pool and S. J. Simmons, Phys. Rev. **43**, 1045 (1933).

[9] M. L. Pool and S. J. Simmons, Phys. Rev. **42**, 909 (1932).

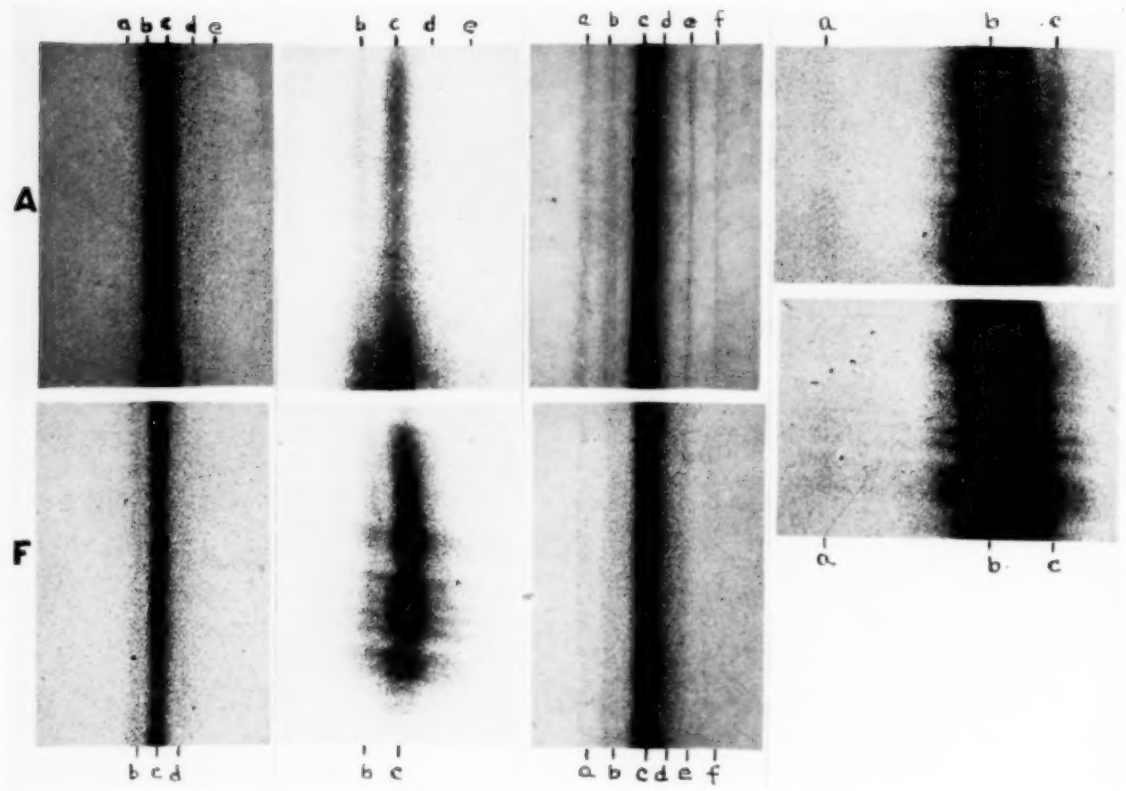

FIG. 1 FIG. 2 FIG. 3 FIG. 4

FIG. 1. The second order of λ4047 enlarged 50 times. *A* stands for arc and *F* for fluorescence. The components are *a*, +0.668; *b*, +0.270 and +0.330; *c*, 0; *d*, −0.394; *e*, −0.743 cm^{-1}.
FIG. 2. Second order of λ4047 as obtained with an additional telephoto lens near the plate.
FIG. 3. Second order of λ4358 enlarged 50 times. The components are *a*, +0.836; *b*, +0.505 and 0.566; *c*, 0; *d*, −0.240; *e*, −0.555; *f*, −0.960 cm^{-1}.
FIG. 4. Second order of λ5461 enlarged 50 times with telephoto lens in front of plate. The components are *a*, +0.799; *b*, 0; *c*, −0.278 cm^{-1}.

nitrogen. There also seems to be little chance of transfer of energy between the hyperfine levels of a given odd isotope.

In column three of Table II are listed the linear absorption coefficients. In column four are the values of $1-e^{-\mu}=A$ which are proportional to the total absorption of a particular component. These absorbed energies would give the relative concentrations in the various corresponding hyperfine levels of the $^3S_1$ state, see Fig. 5. The volume optically excited is approximately a two centimeter cube. In column five are the quotients, *Q*, formed by dividing the *A* of the central component by the *A*'s of column three. This quotient shows how much larger the ratio of the intensity of the central component to some other component in fluorescence is than a similar ratio in the exciting arc. As may be seen from Fig. 5, the first *Q* in Table II for each of the three

TABLE II. *Calculated intensity quotients.*

Pressure N_2	Component	μ	A	Q	Q'
2 mm	0 cm^{-1}	0.191	0.105		
	+0.330, +0.270	.036	.036	2.9	2.7
	− .394	.024	.024	4.4	4.0
	− .743	.010	.010	10.5	9.5
10 mm	0 cm^{-1}	.138	.139		
	+0.330, +0.270	.049	.045	2.9	2.6
	− .384	.036	.035	3.7	3.4
	− .743	.022	.021	6.2	5.5
40 mm	0 cm^{-1}	.164	.153		
	+0.330, +0.270	.054	.052	2.9	2.6
	− .394	.040	.039	3.9	3.5
	− .743	.028	.027	5.7	4.9

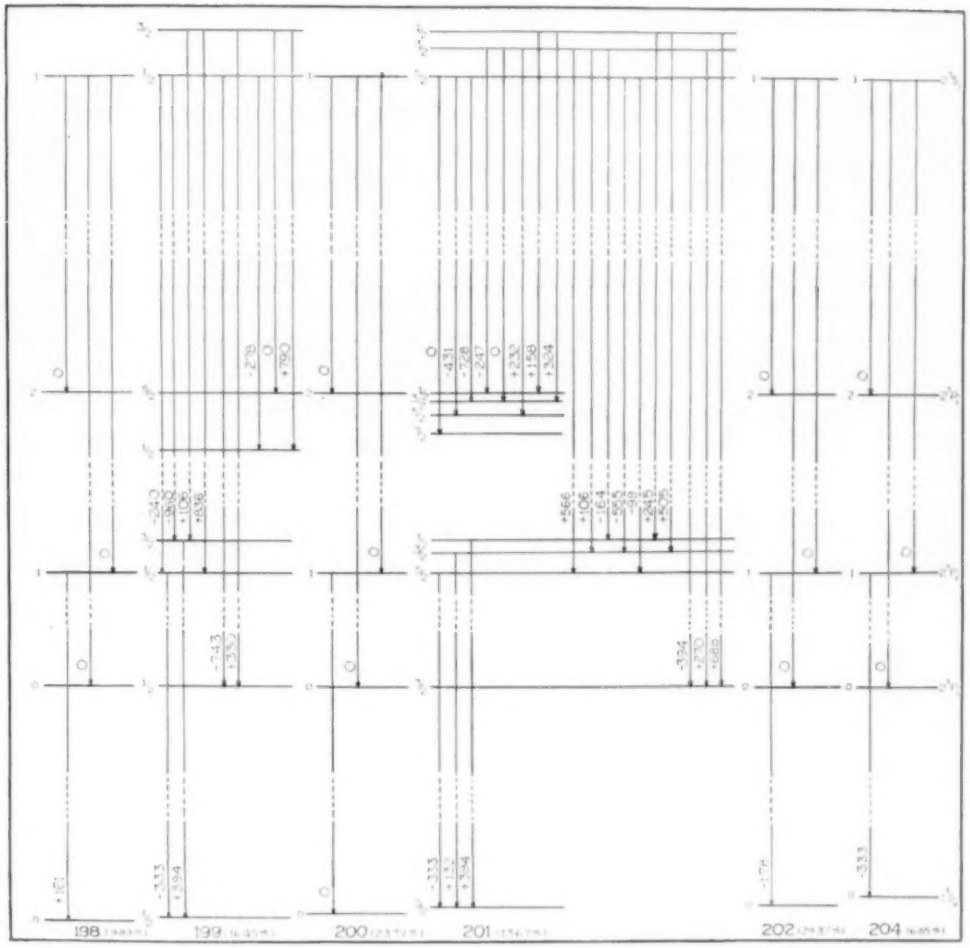

FIG. 5. Hyperfine energy level diagram of mercury.

nitrogen pressures applies to the $+0.566$ cm^{-1} component of 4358 and the $+0.790$ cm^{-1} component of 5461; the second Q applies to the -0.555 cm^{-1} of 4358; and the third to the -0.278 cm^{-1} of 5461 and -0.960 and -0.240 cm^{-1} of 4358. However, for the components of 4047 there is reabsorption, and the above quotients will be modified slightly as shown in column five. It is seen that the values of Q' of Table II compare favorably with the quotient values for 4047 in Table I and the values of Q in Table II are also reasonable with those for 4358 and 5461 in Table I.

The authors are grateful to J. B. Green and R. A. Loring for advice and assistance in the focussing of the grating and telephoto lens.

Pressure Effects of Nitrogen on Potassium Absorption Lines

WILLIAM W. WATSON AND HENRY MARGENAU, *Sloane Physics Laboratory, Yale University*

(Received August 7, 1933)

Pressure effects on the first three doublets of the principal series of the potassium absorption spectrum have been produced by nitrogen up to 30 atmospheres pressure. The 4045A and 3446A pairs show shifts of the absorption maxima to the red and half-widths more than twice as large as those for the resonance lines. In the range of nitrogen pressures above "relative density" 10 both the shifts and the half-widths increase more rapidly than linearly with density. The $^2P_{\frac{1}{2}}$ components exhibit this departure from the linear relation more markedly than the $^2P_{1\frac{1}{2}}$ components. Possible explanations of these variations are suggested. Quantitative results are summarized in the figures and tables.

IN a recent study[1] of the effects of foreign gases on the absorption of the D-lines of Na, the following observations were made: Shifts and half-widths are linear functions of the density of each perturbing gas; both members of the doublet show essentially the same behavior. The pressure range was limited by the close spacing of the D-lines, for overlapping begins at about 12 atm. The question whether or not the observed regularities extend to higher densities is an interesting one which can be decided by a study of the more widely spaced potassium resonance lines.

The effects of foreign gases on spectral lines are a measure of the intermolecular forces between the absorbing atom and its perturbers. The shift, in particular, may be thought of as the displacement between the average frequency of transition under the influence of foreign molecules, and the "normal" frequency. Formulae for the shift have been given previously;[2] they involve the interaction energy ϵ_k between the absorbing atom in its excited state (k) and the perturber. The dominant term in ϵ_k for large distances of separation r has the approximate form

$$-\frac{c}{r^6}\sum_\alpha \frac{f_{k\alpha}}{(E_\alpha - E_k)(\Delta F + E_\alpha - E_k)}, \qquad (1)$$

where c is a constant for a given pair of interacting particles, $f_{k\alpha}$ the f-value connecting the kth with the αth state of the absorbing atom, and the E's are unperturbed energies of the latter. ΔF represents a mean energy of transition of the perturbing molecule and is usually of the order of its ionization energy. The sum over the f-values is independent of k, the excited state in question. Hence the expression (1) will be greater the smaller the values of $(E_\alpha - E_k)$, and this, in turn, will lead to larger shifts.[3]

Let us now consider the arrangement of terms in an alkali atom. If k designates the lowest P-state, the most probable transitions (f-value nearly 1) are to the ground-state, and to higher S and D-states. If, on the other hand, k refers to one of the higher P-states, transitions to very near lying S and D-levels have a large probability, for we know that, while the sum of all $f_{k\alpha}$ must be approximately 1, the f relating to the large transition to the ground state is much smaller than 1. We must therefore expect expression (1) to be greater when k refers to the second or third P-state, for instance, than when it denotes the lowest one, because, on the average, the energy differences involved are smaller. Consequently, the higher members of the principal series should show larger shifts and greater widths than the resonance lines.

This matter can also be tested for potassium, because its resonance doublet, and the second and third members of the series, lie within a convenient spectral region. Since in this case the transitions permissible from the $5P$-state have on the whole energy differences roughly about $\frac{1}{2}$

[1] H. Margenau and W. W. Watson, Phys. Rev. **44**, 92 (1933).

[2] H. Margenau, Phys. Rev. **40**, 387 (1932).

[3] The quantity $f_{k\alpha}/(E_\alpha - E_k)$ is always positive.

of those from the 4 P-state, we should expect for the doublet λλ4044, 4047, shifts and half-widths of the order twice as large as for the resonance doublet. The higher lines, too, should be more strongly affected, but it is difficult to make numerical predictions regarding them.

Experimental Procedure

With minor variations, the technique in the present experiments on the potassium absorption lines was as outlined in reference 1. Nitrogen only was used as the perturbing foreign gas. For pressures above 200 lb./in.^{2} substitution of a higher-reading, less-sensitive pressure gauge was made, resulting in some reduction in the accuracy of determining the nitrogen pressures in this higher range. At pressures above 450 lb., with the temperature of the absorption tube about 200°C, the formation of some compound (probably K_3N) producing an opaque cloud in the tube prevented further exposures.

Eastman type IV-K plates were used for obtaining the spectrograms of the resonance lines at 7665A and 7699A in the first order of a 21-foot concave grating in a stigmatic mounting, the dispersion being 4.98A/mm. Second order Fe lines served as reference lines. Since the variation of the sensitivity of these infrared plates with wave-length is rather marked in this region, some care had to be taken in properly measuring the microphotometer traces of these line-contours and in reducing them to true absorption intensity curves. First verifying that the photographic density throughout the absorption regions fell on the straight line portion of the characteristic curve of the plates at this wave-length, the maximum of absorption was in each case determined with reference to the sloping base line of the photometer trace and then the wave-length of this peak was measured by interpolation between the Fe lines along the length of the plate.

In photographing the second member of the principal series of potassium of 4044A and 4047A the third order of the grating was used with Eastman Process plates which had been subjected to a slight prefogging in order to bring the time of exposure down to a reasonable value. The Hg lines at 4046A and 4077A served as a comparison spectrum. The fact that these two potassium lines are but 18 cm^{-1} apart, coupled with their great sensitiveness to foreign gas pressure, causes the two absorption lines to overlap appreciably at nitrogen pressures of about 10 atmospheres. This was then the upper limit of the pressure range that could be employed in this case. The temperature of the absorption tube at this highest pressure was 200°C.

Measurements of the pressure effect on the 3446 and 3447A lines were obtained with difficulty. Because of the absorption at this wave-length of the thick plate glass windows, the latter were replaced by 1 cm-thick Pyrex windows. Since the Pointolite lamp was of insufficient intensity to serve as the source of continuous radiation in this region, the positive crater of a carbon arc was used, thereby rendering any density calibration of our photographic plates impossible. Wave-length measurements were made by reference to a Ne comparison spectrum and to a near-by Ca line in the spectrum of the carbon arc. An upper limit of some 3 to 4 atmospheres pressure of nitrogen was set by the resulting fusion of the two absorption lines, which are but 8 cm^{-1} apart.

Results

Since the experimental accuracy of measuring shifts and widths is greater the larger the wave-length of the line, the resonance doublet of potassium is favorable for their study. The results are plotted in Fig. 1. Abscissae in this as

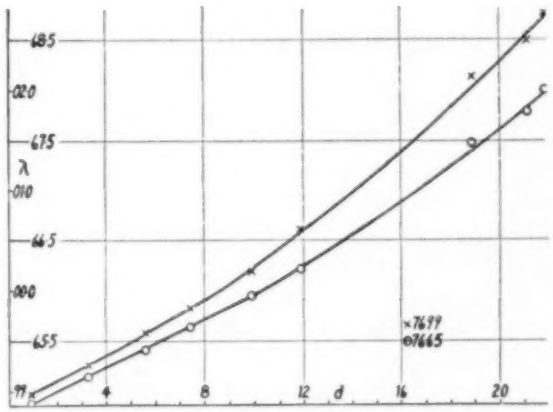

Fig. 1. Wave-lengths of maxima of potassium resonance lines *vs.* relative density of nitrogen gas.

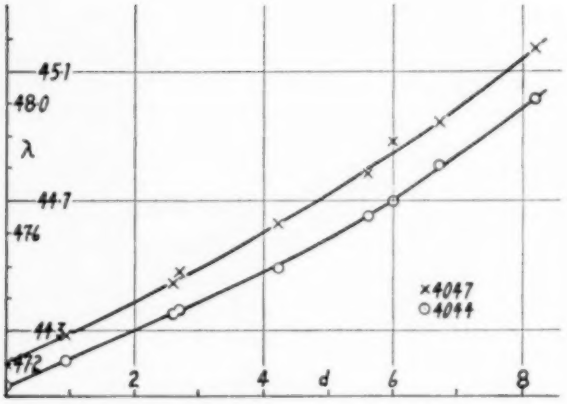

FIG. 2. Wave-lengths of maxima of the 4044A and 4047A lines of potassium *vs.* relative density of nitrogen gas.

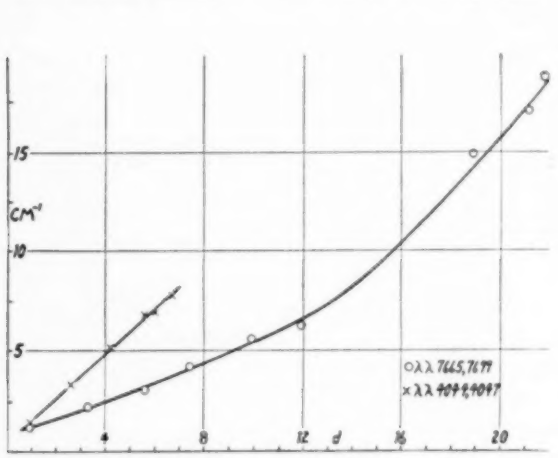

FIG. 3. Half-widths of the first and second members of the potassium resonance series *vs.* relative density of nitrogen gas. The points are average values for the two components of each doublet.

well as in Figs. 2 and 3 denote relative densities d, the unit being the density of the same quantity of N_2 as that used in the experiment but at 0°C and 1 atm. For small densities both lines of the resonance doublet show approximately equal shifts, as was found for the *D*-lines of sodium.[1] But for higher densities, Fig. 1 exhibits two features, not observed in any case previously. Shifts are no longer proportional to densities, and the two members of the doublet differ in their behavior. The curvatures set in at the highest densities used in connection with the *D*-lines and have, therefore, probably escaped detection in our previous work. The absence of experimental points in the pressure range from $d=12$ to 18 is accidental and caused by the use of a pressure gauge which was not previously calibrated. The test, made after the experimental work was finished, showed the gauge to read low by some two atmospheres in this region. The shift, in A, is larger than any that have been measured. Near the origin its value is 0.125A per unit relative density. In wave numbers, it amounts to 0.22 cm^{-1} as compared with 0.17 cm^{-1} in the case of the *D*-lines perturbed by N_2.

The shift of the next doublet is shown in Fig. 2, which again exhibits an upward curvature and a slight divergence of the two members at higher pressure. Both features are less pronounced because of the small density range to which observations were restricted by the close spacing of the doublet. While the wave-length shift is only 0.090A and 0.105A per unit relative density for λ4044 and 4047, respectively, the corresponding wave number shifts are 0.55 cm^{-1} and 0.64 cm^{-1}, that is nearly three times as large as the shifts of the first member of the series. The theoretical explanation discussed in the introduction is thereby verified.

The results for the third doublet, being somewhat sparse, have been omitted from the graphical representation. They are given in Table I. The values of $\Delta\lambda/\Delta d$ are 0.058A and 0.053A, respectively, corresponding to wave-number changes of 0.49 cm^{-1} and 0.45 cm^{-1}. Again, these latter values are much larger than the shifts of the resonance lines.

TABLE I. *Shifts of λ3446 and λ3447.*

d	λ	λ
0.84	3446.455	3447.462
2.15	3446.531	3447.525
3.58	3446.613	3447.606

In Fig. 3 the half-widths, defined as in reference 1, are plotted. Instead of giving individual values for each doublet component we are merely stating averages, the reason being that no significant difference between them has been detected. (It is clear that the determination of "line widths," i.e., accurate half-widths of the absorption coefficient, requires experimental corrections, such as those called for by nonlinear plate characteristics, which do not affect the line maximum, and is therefore slightly less accurate.) The lower curve starts upward at about the same

density as do the corresponding curves for the shifts. For the case of the second doublet no deviation from linearity with density has been found in the small pressure range permitted by its spacing. Line widths for the ultraviolet doublet could not be determined with sufficient accuracy to be listed.

To convey a picture of the line contours the absorption coefficient through λ7665 at two different densities of N_2 has been drawn in Fig. 4. At the lower density, the half-width is 3.1 cm^{-1}, at the higher, 17.0 cm^{-1}. The asymmetry of the contours may be measured by the ratio of the red "half-half width" to the violet "half-half width." This ratio is 1.25 for the lower, 1.60 for the higher density. It should be observed, however, that this simple characterization does not render adequately all the different features of the two curves. The ordinates in Fig. 4 are not measured in the same units; no reference as to

FIG. 4. Absorption intensity curves for λ7665 of potassium. Relative densities of N_2 are: *a*, 5.6, *b*, 21.1. The relative shift of the two maxima is 2.4A. Note the difference in the asymmetry of the two contours (cf. text).

total absorption in the two cases should be drawn from that figure. Determination of the latter has not been attempted because of obvious difficulties discussed in reference 1.

The lines λ4044 and λ4047 also show strong asymmetries to the red, comparable with those of the resonance doublet. Visual inspection of the third doublet, which could not be subjected to high pressures, disclosed no asymmetry. Thus there may have been a change from red asymmetry to symmetry in passing from the second to the third doublet of the series. While this work was in progress there appeared a letter by Füchtbauer and Goessler[4] in which a reversal of the symmetry from red to blue is reported for the corresponding Cs-lines. Such an effect has not been noticed in K. The latter authors discuss only one line of the doublet and make no mention of any nonlinearity of shifts and widths such as found in the present work.

Diverse possible explanations of the deviations from a linear law, observed in connection with the resonance lines, come to mind. It appears difficult, however, to make the speculations very definite before a greater amount of experimental data is available. It should be decided, by making similar experiments with different perturbing gases having very different polarizabilities, whether the curvature is primarily a function of the perturbing gas. It seems probable that the curvature is an indication of incipient non-additivity of the forces causing the shifts, which is to be expected at pressures for which the distances between particles give rise to appreciable first order interactions. Another fact is also worth mentioning. At high pressures the shift of the resonance lines acquires some of the features of Stark effect displacements: there appears to be an additional shift to the red for both lines, and the weaker one is shifted more strongly. This may suggest possible connections. The mutual polarization of the N_2-molecules taking place at high pressures certainly sets up intermolecular fields superimposed upon the attractive fields between the potassium-atom and the N_2-molecules; but it appears doubtful that these fields are strong enough to cause the additional shifts here observed.

Comparing both shifts and half-widths of the first and second doublets it will be observed that both quantities are increased (in energy units) by a factor almost three. This indicates a rather direct relation between shift and width. If, indeed, shifts and half-widths are calculated by

TABLE II. *Summary of pressure shifts and broadening of potassium doublets.*

	Shift		Half-width	
λ	$\Delta\lambda/\Delta d$ (A)	$\Delta\nu/\Delta d$ (cm^{-1})	$\Delta\lambda_{\frac{1}{2}}/\Delta d$ (A)	$\Delta\nu_{\frac{1}{2}}/\Delta d$ (cm^{-1})
7665	0.121	0.206	0.259A	0.44 cm^{-1}
7699	0.129	0.219		
4044	0.090	0.55	0.180A	1.10 cm^{-1}
4047	0.105	0.64		
3446	0.058	0.49		
3447	0.053	0.45		

[4] Chr. Füchtbauer and F. Goessler, Naturwiss. **21**, 315 (1933).

the principles outlined previously[2] this observation can be simply accounted for by assuming that the distance of closest approach between an excited K-atom and a N_2-molecule is approximately the same for both excited states ($4P$ and $5P$) of the K-atom, while the attractive forces increase by a factor between 2 and 3.

The experimental results are summarized in Table II. $\Delta\lambda/\Delta d$ and $\Delta\nu/\Delta d$ refer to the slopes for smallest densities.

Relative Intensity Tables for Spectrum Lines

H. E. WHITE AND A. Y. ELIASON, *University of California*

(Received August 1, 1933)

Relative intensities for a large number of multiplets have been calculated from well-known theoretical formulas. These intensities have been tabulated for future reference in making analyses of spectra. The tables are grouped under each resultant spin, from singlets $S=0$, to octets $S=7/2$ and include all probable values of L and J. It is shown how the same tables apply to jj-coupling, to hyperfine structure, and to related multiplets.

IN the analysis of the complex spectrum, or the hyperfine structure of a given element, theoretical intensities of the lines are frequently used to facilitate the work. In each instance numerous and tedious calculations are made by substituting various sets of quantum numbers in well-known intensity formulas. From a time-saving standpoint a tabulation of these intensities for all probable quantum numbers therefore seemed highly desirable.

The intensity formulas usually used were first derived by Kronig,[1] Russell,[2] and Sommerfeld and Honl,[3] from the classical model of the atom and from the sum rules of Ornstein,[4] Burger and Dorgelo.[5] They have since been derived on the quantum mechanics by Dirac.[6]

The tables here include those published by H. N. Russell in 1925.[7] The tables are grouped under each spin resultant from singlets, $S=0$, to octets, $S=7/2$. The values of L are given in heavy type, and the values of J in ordinary type, on either side and above or below each multiplet. The relative intensities calculated from the formulas have been reduced to the scale of one hundred for the strongest line of each multiplet. The sum rules make it possible to interchange the rôles of the initial and final states. The numbers are given to one decimal point except in a few cases of extremely low intensities where they have been given to two decimal places for the purpose of comparison.

These intensity tables may be applied to jj-coupling by replacing S by j_1, and L by j_2. Here j_1 is taken to be the quantum number which, for the transitions in question, does not change, i.e., $\Delta j_1=0$.

The intensity tables may be applied to hyperfine structure by replacing S by I, L by J, and J by F.

Kronig has shown that these same formulas apply to the relative intensities of related multiplets, where the coupling is Russell-Saunders, and the transitions involve a single electron transition. The formulas are modified by replacing S by L_0, L by l, and J by L, where L_0 is the L value of the parent term, l the orbital value of the transition electron, and L their resultant.

It should be pointed out that these tables give only the values in agreement with the sum rules, based upon the "*a priori* probabilities" of the energy states in question, and assume that temperature and ν^4 corrections have been made where necessary. In hyperfine structure, in particular, these certainly can be neglected.

[1] R. de L. Kronig, Zeits. f. Physik **33**, 261 (1925).
[2] H. N. Russell, Nature **115**, 735 (1925).
[3] A. Sommerfeld and H. Honl, Sitzsungsber. d. Preuss. Akad. d. Wiss. **9**, 141 (1925).
[4] L. S. Ornstein and H. C. Burger, Zeits. f. Physik **24**, 41 (1924).
[5] H. C. Burger and H. B. Dorgelo, Zeits. f. Physik **23**, 258 (1925).
[6] P. A. M. Dirac, Proc. Roy. Soc. **A111**, 281 (1926).
[7] H. N. Russell, Proc. Nat. Acad. Sci. **11**, 324 (1925).

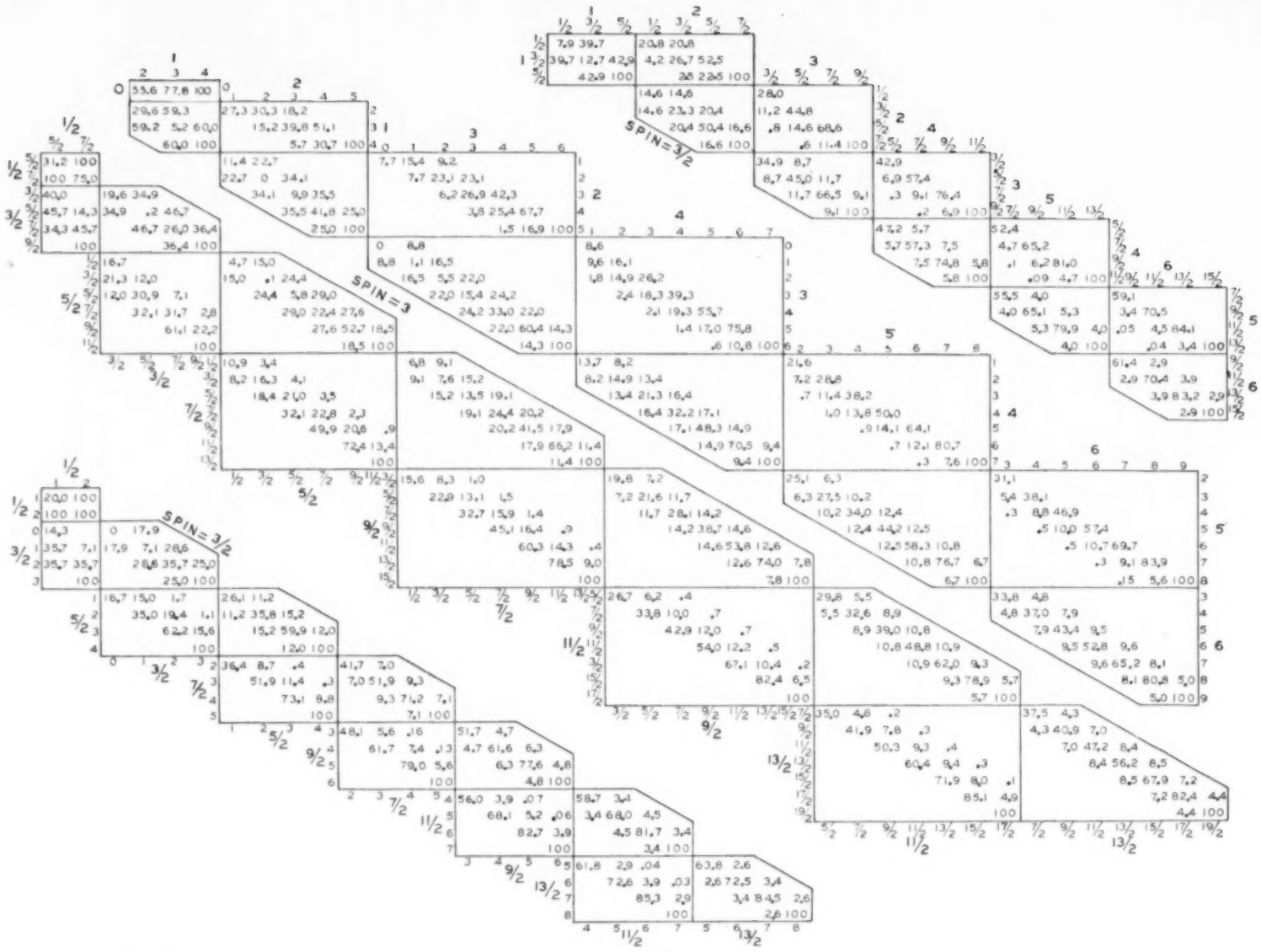
SPIN=3/2
SPIN=3
SPIN=3/2

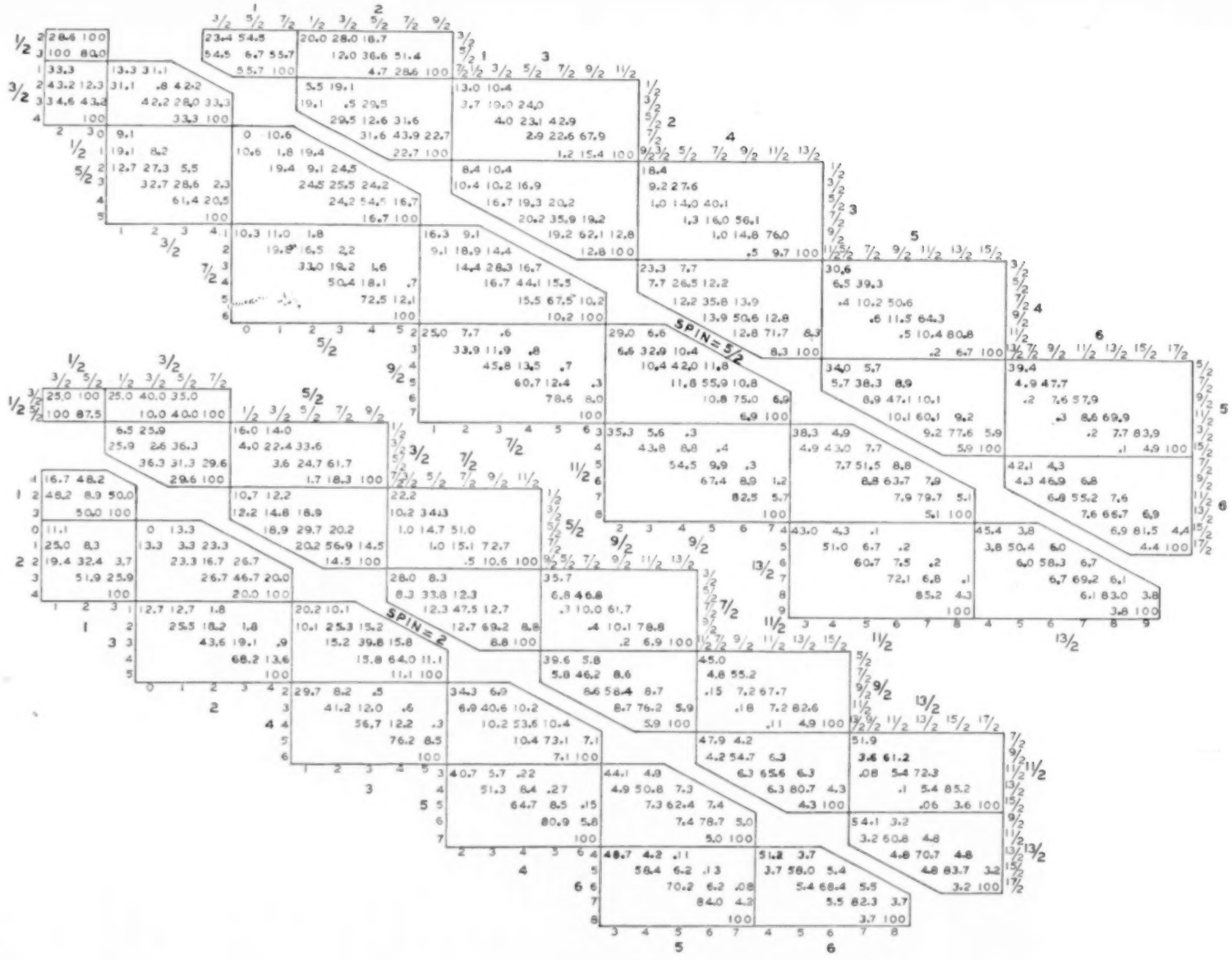
SPIN = 5/2
SPIN = 2

SPIN = 7/2
SPIN = 1/2

The Arc Spectrum of Sulfur in the Ultraviolet

J. E. RUEDY, *Cornell University*

(Received August 2, 1933)

A Schüler tube with a water-cooled aluminum cathode, with He gas for maintaining the discharge, was attached to a vacuum spectrograph employing a 1.5 meter grating of 15,000 lines per inch. The sulfur spectrum was excited by vaporizing some sulfur in the tube while the discharge was in operation. The wave-length range photographed was from 0–2600A, and in the region 1050–2400A many new lines were observed and classified. It was thus possible to establish the low singlet terms of the arc spectrum and some of the higher terms built on the doublet *P* and *D* states of the ion as well as some higher members of series built on the quartet *S* state of the ion.

AS a continuation of the work on the arc spectra of the elements of the oxygen group, it seemed desirable next to obtain more complete data for the vacuum region. The analyses of oxygen by Frerichs[1] and Hopfield[2] being the chief guide as to the nature of all these spectra, the next succeeding element, sulfur, was chosen as the first to be studied. The discharge tube used was, however, designed with the intention that it should be equally suitable for selenium and tellurium.

The essential features of the tube, which was of the Schüler type, are shown in Fig. 1. It was attached to a vacuum spectrograph employing a

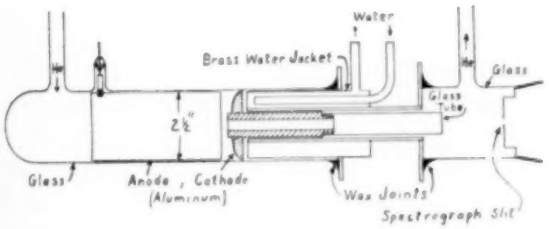

FIG. 1. Discharge tube.

1.5 meter grating, which gave a dispersion of about 11A per mm. Suitable provision was made for the circulation and purification of the helium used in maintaining the discharge. The power was supplied by an a.c. rectifier set which would deliver currents up to 2 amperes at potentials not exceeding 2000 volts.

The tube was first run at a high current density and the helium circulated until impurities had been removed as much as possible, after which it was taken apart and several grams of sulfur were placed in the anode end and then put back on the spectrograph. An oven was placed around the anode end, and while the discharge was in operation, the temperature was raised till the sulfur began to vaporize and its lines appeared in the visible spectrum.

A number of photographs were taken in the vacuum region with various densities of sulfur vapor and lengths of exposure up to 4 hours. As the current through the tube was increased some difficulty was experienced in making the bright glow remain in the hollow cathode and, for this reason, the maximum current employed for any length of time was limited to 1.8 amperes. When the vapor density was high, the sulfur lines became broad and in many cases showed strong reversal. Both the arc and first spark spectra were excited at all times and no distinguishing characteristics were observed but this caused no great difficulty, as there is little overlapping of the two in the region being examined.

Selenium was then used in place of sulfur in the same kind of tube and under the same conditions and several photographs were taken which served to identify many impurity lines in the sulfur pictures. A pure helium discharge did not show nearly as many such lines as did the helium and selenium combination.

Of the total wave-length range covered by these photographs (0–2600A), only that from 1050–2400A should contain arc lines and accurate

[1] R. Frerichs, Phys. Rev. **34**, 1239 (1929); Phys. Rev. **36**, 398 (1930).

[2] J. J. Hopfield, Phys. Rev. **37**, 160 (1931).

TABLE I. *Lines of S I. R=reversed; d=diffuse.*

Int.	λ (vac)	ν (vac)	Transition	Int.	λ (vac)	ν (vac)	Transition
15*R*	1914.68	52228.0	$3p^3P_1-4s(^4S)^5S_2$	4	1318.97	75817.0	
20*R*	1900.27	52624.1	$^3P_2-4s(^4S)^5S_2$	8*R*	1316.59	75954.0	$3p^3P_2-4d(^4S)^3D$
25*R*	1826.25	54757.0	$^3P_0-4s(^4S)^3S_1$	4	1313.25	76146.7	$^3P_0-6s(^4S)^3S_1$
25*R*	1820.37	54934.0	$^3P_1-4s(^4S)^3S_1$	5	1310.21	76323.4	$^3P_1-6s(^4S)^3S_1$
25*R*	1807.31	55331.0	$^3P_2-4s(^4S)^3S_1$	9*R*	1305.89	76576.1	$^3P_0-4s(^2P)^3P_1$
12*R*	1782.25	56109.0		4	1303.42	76721.4	$^3P_2-6s(^4S)^3S_1$
1	1713.54	58358.8		7*R*	1303.12	76738.9	$^3P_1-4s(^2P)^3P_0$
8	1707.13	58578.0	$^1D_2-4s(^2D)^3D_1$	6*R*	1302.86	76754.2	$^3P_1-4s(^2P)^3P_1$
8	1706.38	58603.5	$^1D_2-4s(^2D)^3D_3$	9*R*	1302.32	76786.2	$^3P_1-4s(^2P)^3P_2$
5	1704.99	58651.5	$^1D_2-3d(^4S)^5D$	5	1296.18	77150.0	$^3P_2-4s(^2P)^3P_1$
20*R*	1687.54	59258.0	$^1S_0-4s(^2P)^1P_1$	6	1295.62	77183.1	$^3P_2-4s(^2P)^3P_2$
25*R*	1666.68	59999.7	$^1D_2-4s(^2D)^1D_2$	0	1283.11	77935.6	
6	1641.30	60927.3	$^1D_2-3d(^4S)^3D$	4	1280.13	78117.3	$^3P_0-5d(^4S)^3D$
2	1592.72	62785.7	$^1D_2-3s3p^5\ ^3P_2$	5*d*	1277.24	78294.0	$^3P_1-5d(^4S)^3D$
15*R*	1487.12	67243.9	$^3P_0-4s(^2D)^3D_1$				$^3P_2-4s(^2P)^1P_1$
12	1485.61	67312.6	$^3P_0-3d(^4S)^5D$	1	1272.07	78612.0	$^3P_0-7s(^4S)^3S_1$
12*R*	1483.24	67420.0	$^3P_1-4s(^2D)^3D_1$	4	1270.78	78692.0	$^3P_2-5d(^4S)^3D$
15*R*	1483.05	67428.6	$^3P_1-4s(^2D)^3D_2$	2	1269.20	78789.5	$^3P_1-7s(^4S)^3S_1$
15*R*	1481.65	67492.2	$^3P_1-3d(^4S)^5D$	2	1262.83	79187.0	$^3P_2-7s(^4S)^3S_1$
6*R*	1474.54	67817.6	$^3P_2-4s(^2D)^3D_1$	2	1247.17	80181.5	
12*R*	1474.37	67825.6	$^3P_2-4s(^2D)^3D_2$	2	1241.95	80518.8	
15*R*	1473.98	67843.3	$^3P_2-4s(^2D)^3D_3$	15*R*	1204.30	83035.6	
15*R*	1472.97	67890.0	$^3P_2-3d(^4S)^5D$	2	1191.80	83906.7	
4	1471.82	67943.0	$^1D_2-4s(^2P)^3P_2$	2	1190.11	84025.5	
12*R*	1448.20	69051.4	$^1D_2-4s(^2P)^1P_1$	2	1171.91	85330.8	
6	1444.27	69239.3	$^3P_2-4s(^2D)^1D_2$	1	1157.37	86402.8	
12*R*	1436.94	69592.3	$^3P_0-3d(^4S)^3D$	2	1152.11	86796.9	
15*R*	1433.28	69770.0	$^3P_1-3d(^4S)^3D$	2*d*	1056.79	94626	
15*R*	1425.10	70170.7	$^3P_2-3d(^4S)^3D$	1	1055.15	94773	
12*R*	1412.85	70779.0	$^3P_0-5s(^4S)^3S_1$	1	1053.21	94948	
12*R*	1409.32	70956.2	$^3P_1-5s(^4S)^3S_1$	1	1052.60	95003	
10*R*	1401.50	71351.9	$^3P_2-5s(^4S)^3S_1$	2	1052.25	95215	
15*R*	1396.10	71628.1	$^3P_1-3s3p^5\ ^3P_2$	1	1049.77	95259	
12*R*	1392.59	71808.5	$^3P_0-3s3p^5\ ^3P_1$	1	1049.06	95323	
5*R*	1389.16	71986.1	$^3P_1-3s3p^5\ ^3P_1$	1	1048.43	95381	
12*R*	1388.39	72026.0	$^3P_2-3s3p^5\ ^3P_2$	1	1047.86	95433	
12*R*	1385.51	72175.6	$^3P_1-3s3p^5\ ^3P_0$	1	1047.56	95460	
15*R*	1381.55	72382.6	$^3P_2-3s3p^5\ ^3P_1$	2	1045.74	95626	
3	1363.04	73365.2		0	1036.41	96487	
1	1353.47	73883.9		1	1006.95	99310	
9*R*	1326.64	75378.4	$^3P_0-4d(^4S)^3D$	8	1006.15	99389	
10*R*	1323.52	75556.1	$^3P_1-4d(^4S)^3D$	2	1000.75	99925	

measurements were not made outside of these limits. After eliminating the lines indicated as impurities, it was possible to identify nearly all of the remaining ones in the selected region as definitely belonging to either S I or S II. Table I gives a list of all those lines which might belong to S I with their transition designations where known. No attempt was made to classify any new lines in S II and only those given by Ingram,[3] nearly all of which were found, were regarded as belonging to that spectrum.

While this work was being done, a paper by Frerichs[4] appeared extending the analysis of the S I spectrum in the long wave-length region and since he used a grating of high dispersion, his data are the most accurate yet reported for that region. His table of terms includes several established by the ultraviolet measurements of Hopfield,[5] although the present work indicates these should be slightly changed numerically, and yields a number of additional terms. All the term values given in Table II of this article constitute an addition to the term table given in Frerichs' paper. One correction should be made to the table as given in his paper; namely, the reduction by one of the total quantum numbers of all the *d* electrons, to which change he has expressed his agreement in a personal communication.

[3] S. B. Ingram, Phys. Rev. **32**, 172 (1928).
[4] R. Frerichs, Zeits. f. Physik **80**, 150 (1933).
[5] J. J. Hopfield, Phys. Rev. **22**, 523 (1923); Nature **112**, 790 (1923); Phys. Rev. **27**, 638 (1926).

TABLE II. *Multiplets and term values of S I.*

$3p^4$	$^3P_2$ 83560.7	(397.2)	$^3P_1$ 83136.5	(177.5)	$^3P_0$ 82986.0	(8665 1)	$^1D_2$. 74320.9	(9793.4)	$^1S_0$ 64527.5
$3p^3 4s(^4S)^5S_2$ 30936.9	52624.1 (20*R*)	(396.1)	52228.0 (15*R*)						
$3p^3 4s(^4S)^3S_1$ 28229.0	55331.0 (25*R*)	(397.0)	54934.0 (25*R*)	(177.0)	54757.0 (25*R*)				
$3p^3 4s(^2D)^3D_1$ 15743.3	67817.6 (6*R*)	(397.6)	67420.0 (12*R*)	(176.1)	67243.9 (15*R*)	(8664.9)	58578.0 (8)		
$3p^3 4s(^2D)^3D_2$ 15734.4	67825.6 (12*R*)	(397.0)	67428.6 (15*R*)						
$3p^3 4s(^2D)^3D_3$ 15716.7	67843.3 (15*R*)	(397.2)		(177.5)		(8665.1)	58603.5 (8)		
$3p^3 3d(^4S)^5D$ 15670.7	67890.0 (15*R*)	(397.7)	67492.2 (15*R*)	(179.6)	67312.6 (12*R*)	(8661.1)	58651.5 (5)		
$3p^3 4s(^2D)^1D_2$ 14321.3	69239.3 (6)	(397.2)		(177.5)		(8664.9)	59999.7 (25*R*)		
$3p^3 3d(^4S)^3D$ 13392.7	70170.7 (15*R*)*d*	(400.7)	69770.0 (15*R*)	(177.7)	69592.3 (12*R*)	(8665.0)	60927.3 (6)		
$3p^3 5s(^4S)^3S_1$ 12207.3	71351.9 (10*R*)	(395.7)	70956.2 (12*R*)	(177.2)	70779.0 (12*R*)				
$3s3p^5\ ^3P_2$ 11535.1	72026.0 (12*R*)	(397.7)	71628.1 (15*R*)	(177.5)		(8664.9)	62785.7 (2)		
$3s3p^5\ ^3P_1$ 11177.7	72382.6 (15*R*)	(397.5)	71986.1 (5*R*)	(177.6)	71808.5 (12*R*)				
$3s3p^5\ ^3P_0$ 10987.9			72175.6 (12*R*)						
$3p^3 4d(^4S)^5D$ 7606.7	75954.0 (8*R*)	(397.9)	75556.1 (10*R*)	(177.7)	75378.4 (9*R*)				
$3p^3 6s(^4S)^3S_1$ 6839.3	76721.4 (4)	(398.0)	76323.4 (5)	(176.7)	76146.7 (4)				
$3p^3 4s(^2P)^3P_0$ 6424.6			76738.9 (7)						
$3p^3 4s(^2P)^3P_1$ 6410.7	77150.0 (5)	(395.8)	76754.2 (6)	(178.1)	76576.1 (9)				
$3p^3 4s(^2P)^3P_2$ 6377.6	77183.1 (6)	(396.9)	76786.2 (9)	(177.5)		(8665.7)	67943.0 (4)		
$3p^3 4s(^2P)^1P_1$ 5269.5	78294.0 (5)*d*	(400.0)		(177.5)		(8665.1)	69051.4 (12*R*)	(9793.4)	59258.0 (20*R*)
$3p^3 5d(^4S)^3D$ 4868.7	78692.0 (4)	(398.0)	78294.0 (5)*d*	(176.7)	78117.3 (4)				
$3p^3 7s(^4S)^3S_1$ 4374.4	79187.0 (2)	(397.5)	78789.5 (2)	(177.5)	78612.0 (1)				

The only previous measurement and classification of ultraviolet lines of S I has been reported by Hopfield[5] but these results include none of the terms built on the ^2D and ^2P states of the ion. The location of such terms was the chief aim of this investigation. The terms built on the ^4S state of the ion were fairly completely identified. In some of the series only one or two members had been observed but they were all definitely fixed with respect to the limit by some combination with series containing more terms. From the present data, however, it was possible to identify immediately a number of these higher series members and also, by triplet intercombinations which were relatively weak, to locate the low ^1D term.

As an aid in locating the terms built on the two doublet limits, it was assumed that the terms arising from the same electron configuration would be at approximately equal distances from their respective limits, as was found to be the case in oxygen. The separations of the low levels of S II had been determined by Ingram[3] (the quartet-doublet separation by means of series limits and hence not very exactly), and these were used in placing the limits in Fig. 2. The expected positions of the various terms, as indicated by the assumption just mentioned, are marked by the circles. Two groups of strong lines were found which located the $4s(^2D)^3D$ and the $4s(^2P)^3P$ levels at almost exactly the predicted positions (the transitions being into the low ^3P levels). Furthermore, the outer separation of each triplet was very nearly equal to the separation of the doublet limit to which each series of such terms would converge.

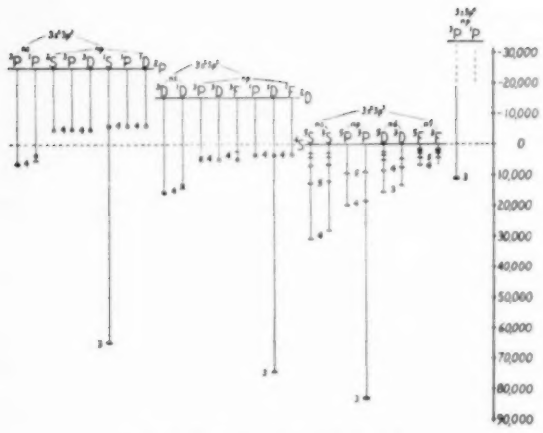

FIG. 2. Energy level of S I.

There were then remaining just three strong unclassified lines which lay anywhere near the positions expected for the corresponding singlet combinations. There was no doubt at all as to the identification of the transition $3p(^2D)^1D - 4s(^2P)^1P$ and since the $3p^1D$ term had been located by intercombinations, the $4s^1P$ was also fixed. The other two lines differed in frequency by only about 750 cm^{-1} and it would not be unreasonable to call either one the transition $3p(^2P)^1S - 4s(^2P)^1P$ or $3p(^2D)^1D - 4s(^2D)^1D$. The choice made was based on two reasons, neither of which alone is absolutely conclusive but taken together are almost so, and especially when there is nothing which gives any positive indication the other way. The reasons are these. First, the transition $3p(^2D)^1D - 4s(^2D)^1D$ should give a line of greater intensity than $3p(^2P)^1S - 4s(^2P)^1P$, since the ^1P term lies considerably higher in the term scheme and the corresponding triplet transitions followed the usual intensity relations. Second, an intercombination line is observed, $3p(^4S)^3P_2 - 4s(^2D)^1D$, if the classification as given is correct, whereas no such line is found with the alternative level assignment.

Table II gives all the identified transitions into the normal S I configuration, with the term values referred to the ^4S limit written below each term, and the frequency differences indicated in parentheses. The numbers under the radiated wave numbers are the estimated intensities, *R* meaning reversed and *d* diffuse.

Recognition of the fainter lines of sulfur was rendered difficult and in certain regions impossible by the presence of many impurity lines; that is, lines which were common to both the sulfur and selenium plates. These were so numerous in places as to give the impression of bands, though close observation showed that they were not. No line was included in the list as sulfur if it apparently coincided with a line of comparable intensity on the selenium plate, even though it fitted in as a member of a series or had a correct frequency difference from another line.

All the remaining unidentified terms would lie near or above the ^4S limit and hence the transitions from them would be expected to be weak. This may account for the failure to observe transitions involving higher terms of series going to either of the doublet limits. The two strong lines at λ1782 and λ1204 still remain unidentified and there is no place for them in the classification of the S I spectrum here reported.

The author wishes to acknowledge his indebtedness to Professor R. C. Gibbs, under whose direction this research was carried on, for his interest and advice during the course of the work.

Quenching of Iodine Fluorescence by Iodine and Argon

JAMES F. KOEHLER, *Smith College**

(Received August 14, 1933)

In iodine below pressures of 0.8 mm fluorescence was excited monochromatically by the mercury green and yellow lines and measured by photographic photometry with a spectrograph. Absorption measurements were made under similar conditions with two compensating photoelectric cells: Beer's law holds here; and argon does not alter the absorption of iodine. The ratio of probability of an excited molecule losing all energy in an iodine collision to probability of radiation is evaluated per unit time. The ratio exceeds unity for pressures above 0.05 mm. The yellow excited series is quenched more than the green by both iodine and argon. The complex nature of argon quenching is discussed.

IN analogy to the theory of Loomis and Fuller[1] on oxygen quenching, Turner has suggested that argon may also enhance a predissociation of the excited iodine molecule,[2] both of these phenomena being similar to the magnetic predissociation shown by Turner[3] and supported theoretically by Van Vleck.[4] The present investigation was undertaken to learn more of the action of argon upon iodine fluorescence. The resonance series excited in iodine vapor by monochromatic mercury light was discovered by Wood.[5] The accepted interpretation is that of Lenz,[6] *viz.*, that molecules are excited to one particular vibration and rotation state, and that transitions down to states of lower vibrational quantum numbers (with rotational quantum numbers differing by ± 1) give rise to the observed series.[7] With the hot arc used here the green line may be absorbed by as many as 12 lines in the iodine absorption spectrum, but exposures as short as 20 minutes are permitted. The use of either the green or yellow lines of a hot arc produced two distinctly separate groups of excited states, enabling one to find the effect of the quenching collisions on each group of vibration levels.

In general when a foreign gas quenches fluorescence radiation, it thereby shortens the mean lifetimes of the radiating molecules; and with this is associated a broadening of the absorption lines to those states. It was therefore necessary to know what effect the argon had on the amount of mercury light absorbed, and absorption experiments were made. This absorption work also showed how the exciting light was weakened by the iodine vapor before reaching the sheath from which the fluorescence was photographed. The absorption measurements will be discussed first.

An interpretation of the quenching of argon, as shown later, demands a knowledge of the quenching of iodine by itself. So the absorption of pure iodine and the autoquenching of pure iodine have been experimentally obtained. In fact this forms the major portion of this paper. No use could be made of the work of Wood and Speas[8] on iodine autoquenching, since they excited with the full mercury spectrum.

ABSORPTION MEASUREMENTS

Pure iodine

The absorption of the iodine was measured by dividing the light from the end of a mercury arc

* The experimental work was done in the Palmer Physical Laboratory of Princeton University.

[1] F. W. Loomis and H. Q. Fuller, Phys. Rev. **39**, 180 (1932).

[2] L. A. Turner, Phys. Rev. **41**, 627 (1932).

[3] L. A. Turner, Zeits. f. Physik **65**, 464 (1930).

[4] J. H. Van Vleck, Phys. Rev. **40**, 544 (1932).

[5] R. W. Wood, Phil. Mag. [6] **21**, 261 (1911); **35**, 236 (1918).

[6] W. Lenz, Phys. Zeits. **21**, 691 (1920).

[7] For a fuller account and bibliography through 1927, see P. Pringsheim, *Fluorescenz und Phosphorescenz*, p. 40 ff., Springer, Berlin, 1928.

[8] R. W. Wood and W. P. Speas, Phil. Mag. [6] **27**, 531 (1914).

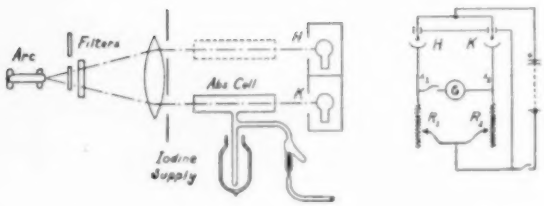

FIG. 1. Absorption apparatus and circuit.

into two parallel beams (see Fig. 1), each of which fell on a photoelectric cell (new G.E. type PJ14) with the absorption chamber in the path of one beam. The arc operated at 2.8 amperes under a drop of 90 volts. In both the absorption and fluorescence experiments the mercury green line (5462.23A) and the unseparated yellow lines (5771.2A and 5792.3A) were isolated by Zeiss monochromatic filters. These were mounted edge to edge on the end of a moveable arm, and afforded data for both the green and yellow absorption at each pressure of iodine. For the absorption work an additional filter of nickel nitrate solution was used to remove all but one percent of the wave-lengths longer than 6000A,[9] which are not absorbed by iodine.

Two evacuated sealed-off absorption cells were used, each constructed of 4 cm Pyrex tubing with internal lengths of 9.34 cm and 3.93 cm, and with optical Pyrex windows fused on. Iodine crystals were in a side tube immersed in a constant temperature bath, and the absorption cell was in an oven maintained at 50°C. Vapor concentration was calculated from pressure-temperature tables,[10] by using the formula

$$n_t = (P \cdot N)/(R \cdot T) = (P/T)9.72 \times 10^{18}$$

(P in mm of mercury).

The electrical circuit embodied a null compensation principle. (Fig. 1.) If i_1 is the current from the photoelectric cell receiving light directly from the arc; and if i_2 is the current from the cell in whose path is placed an *empty* absorption tube; and if R_1 and R_2 are the respective resistances in series with these cells: then at zero galvanometer deflection

$$i_1/i_2 = R_2/R_1 \quad \text{and again} \quad i_1'/i_2' = R_2'/R_1,$$

where the primed quantities indicate the presence of iodine in the tube. The transmission of the iodine is

$$(i_2' \cdot i_1/i_1')/i_2,$$

the factor i_1/i_1' representing the correction that must be applied to i_2' if the intensity of the mercury arc has changed. Therefore the transmission is $R_2R_1'/R_1R_2' = R_1'/R_1$ because the resistance R_2' is kept equal to R_2. With the circuit balanced variations in the intensity of the mercury arc affect both photoelectric cells alike and the balance is undisturbed. However, the shifting column of the arc did alter the light distribution, causing small galvanometer fluctuations which were overcome by averaging readings.

To overcome local e.m.f. disturbances within the circuit, the absorption cell and its bath were attached to a very accurate sliding platform, enabling the cell to be precisely fixed in either of the two optical paths (H or K). The procedure of the above paragraph was followed, first with the cell in H and again in K. This amounted to reversing the circuit; and an average of the two transmission values for each iodine concentration eliminated the effect of any local e.m.f. The apparatus measured transmissions with an extreme uncertainty <1.6 percent under green excitations, this being slightly larger for the yellow.

Data from runs made on two different days with the two tube lengths of 3.93 cm and 9.84 cm are plotted on Fig. 2 as a function of nL (L = tube length in cm). The agreement of data from tubes of two different lengths shows that the absorption is a function of the number of molecules in the line of sight (Beer's law), and that at least up to 0.7 mm the interaction between molecules does not affect the absorption. Any line broadening due to the numerous collisions (see later) must be negligible in comparison with the Doppler width. The validity of Beer's law for pure iodine has also been established by Miss Dlugosch[11] working with the

[9] L. A. Jones, J. Opt. Soc. Am. **16**, 259 (1928).

[10] C. P. Baxter, C. H. Hickey, W. C. Holmes, J. Am. Chem. Soc. **29**, 127 (1907).

[11] G. Dlugosch, unpublished Breslau dissertation (1922) which was made available through the kindness of Professor R. Ladenburg.

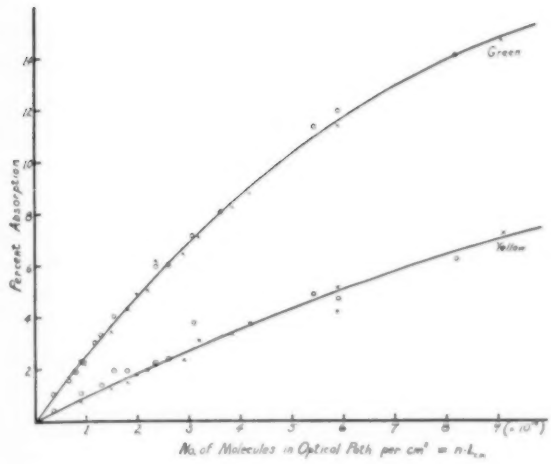

FIG. 2. Absorption in iodine: *circles* from 3.93 cm cell; *crosses* from 9.84 cm cell.

green and yellow lines of the mercury arc, but using an eleven-fold variation of tube length and a bath temperature variation from −20°C to +40°C. She reports collision broadening appearing at pressures above 1 mm.

The absorption should be given by

$$A = 1 - \int e^{-k_\nu n L} d\nu.$$

Here it is convenient to consider the absorption as approximately a linear function of nL for the small values of this product that appear in the following fluorescence work ($nL < 1 \times 10^{16}$). Dlugosch[11] has also shown that at the wave-lengths used here (longer than the dissociation continuum) a small part of the iodine absorption is continuous—a very small part below $p = 1$ mm. No explanation has been given. Because of this a part of the measured absorption does not excite fluorescence; but assuming this continuous absorption coefficient to be constant over a small wave-length region, the above approximation still holds: the absorption that does lead to fluorescence is $A = KnL$.

The absolute absorption values given by Dlugosch are considerably larger than those obtained here (at 25°C they are about 3/2 as large). No reason for this is at hand. But the calculations in this paper depend upon the proportionality of absorption to concentration, rather than on absolute values.

Iodine with argon

The previous absorption technique was followed. The iodine crystals were at 25.6°C and the oven at 50°C the same conditions under which the fluorescence with argon was photographed. The tube length was 3.93 cm. To vary the argon pressure, the moving absorption cell was connected to the vacuum system through the flexibility of 8 mm Pyrex tubing bent into a U-shape with $1\frac{1}{2}$ turns at the bend. The iodine, purified by distillation, was kept in sealed-off tubes which could be broken by a magnetically operated plunger after a satisfactory vacuum had been obtained. A magnetically controlled plunger valve slowed the diffusion of the iodine into the liquid air trap. Argon was purified in a misch metal arc.

Results of several measurements indicated that the argon up to pressures of 82 mm did not change the absorption of the iodine by more than 3 percent of that absorption.

From the fluorescence work an effect of some six times this magnitude would have been expected. In the fluorescence work the light came broadside from the arc; here it came from the end of the same arc similarly operated. But the possibility of the components of the mercury line being changed in intensity distribution depending on the part of the arc from which the light comes had been removed by Dlugosch.[11] She examined the mercury green and yellow lines under high dispersion and showed that the energy distribution changed very little with the voltage across the arc, i.e., with the total energy of the arc, and presumably therefore with regions of different energy density within the arc.

It was further found that the addition of oxygen at a pressure of 192 mm had no effect on the absorption of iodine (at a pressure of 0.3 mm), which seems to complicate the explanation of Loomis and Fuller.[1] Dlugosch,[11] using monochromatic mercury light, reports that nitrogen up to 10 mm does not change the iodine absorption.

FLUORESCENCE MEASUREMENTS

The fluorescence was produced in a Pyrex tube of diameter 3.9 cm with a window sealed to one end and the other drawn out to a horn (Fig. 3).

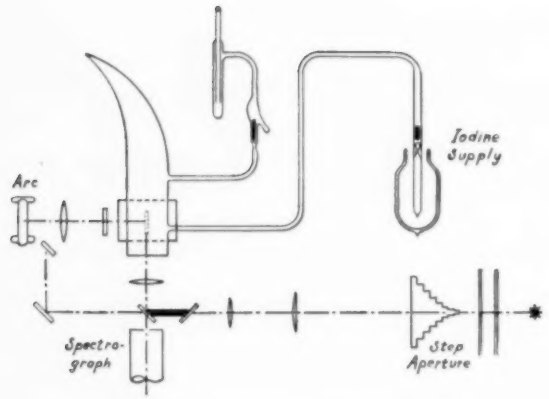

FIG. 3. Fluorescence apparatus.

The tube was horizontal, and blacked with Duco except for two opposite spaces near the window end, where the exciting light passed through it vertically. This gave a thin sheath of fluorescence parallel and end-on to the slit of a Steinheil spectrograph (high light power, dispersion about 80A per mm). A wide slit width was necessary for the argon work (see later) and was also used for pure iodine. The use of only a 2 mm height of this slit meant that the light came from a small trapezoidal region in the fluorescence sheath of average height 3.9 mm. Before reaching this effective part of the sheath, the mercury light was absorbed in a layer of molecules 5.65 mm high. On the lower half of the spectrograph slit fell a comparison beam directly from the arc.

Intensity marks were photographed on each plate, with the use of the step-diaphragm method developed by Hansen[12] and critically described by von Hippel.[13] The step aperture was made by milling the desired profile from two thin steel plates fastened face to face and framing them. The longest opening was 2 cm, and the eight steps were each 2 mm high.

Pure iodine

Each plate contained an intensity mark spectrum and six fluorescence spectra, the first and last of these taken with the iodine bath at 0°C, and the other four at any temperature up to 45°C. All exposures were 20 minutes. Prior to all 0°C pictures the iodine was entirely condensed into the bath tube. The fluorescence tube oven was at 50°C. The densitometer slit was moved across each spectrum on the plate at usually six wave-length regions. The intensities read from the plate characteristic curves were corrected from the comparison spectra for variations in the arc, and then divided by the average intensity of the first and last 0°C pictures. A further correction to account for the weakening of the mercury light in passing through the preliminary sheath of vapor was made by multiplying each relative intensity by $(100-A_0)/(100-A_t)$ where A_0 and A_t are the percent absorptions at the indicated temperature for a path length $L=0.565$ cm. Absolute absorption values are required for this, but the magnitude of the correction is under one percent. Measurements made on the green fluorescence between the third and fourteenth orders, and on the yellow between the third and eleventh orders, showed that within these limits for a given series and a given temperature the intensities were constant, i.e., no reabsorption. So it was possible to average the intensity values obtained from a given spectrum and thereby reduce the errors inherent in the densitometry. These relative intensities (I_t/I_0) were comparable even when derived from different plates.

Iodine with argon

Argon is one of the gases which Franck and Wood[14] found to produce a band spectrum background in iodine fluorescence by transferring some energy from the excited molecule to nearby vibrational or rotational states, from which radiation then occurs. These new band lines overlapped the original fluorescence lines, unless one employed large dispersion and prohibitively long exposure times. Since it was found difficult to correct for the intensity of this background because of the irregularity in its structure, no measurement could be made of the way in which the *original resonance series* lines were diminished. The method actually adopted was to open the slit of the spectrograph to a width of 2 mm, which blurred and overlapped the lines. A measurement at any fixed position in such a spectrum gave an intensity proportional

[12] G. Hansen, Zeits. f. Physik **29**, 356 (1924).
[13] A. von Hippel, Ann. d. Physik [4] **80**, 672 (1926).
[14] J. Franck and R. W. Wood, Phil. Mag. [6] **21**, 314 (1911).

not only to the adjacent lines of the original resonance series, but also to the energy that had been transferred and radiated. Any dimunition of this intensity, as argon was added, was then due entirely to *total-energy-removing collisions* of the argon on the iodine.

The iodine was held constant at 25.6°C, the oven at 50°C, and the argon pressure varied up to 16 mm. The procedure was as given above, except that no absorption correction was applied to the exciting light—the iodine density was constant, and no change in absorption was found to be caused by the argon. This yielded the ratios I_p/I_0, the reciprocals of which are plotted against argon pressure on Fig. 4

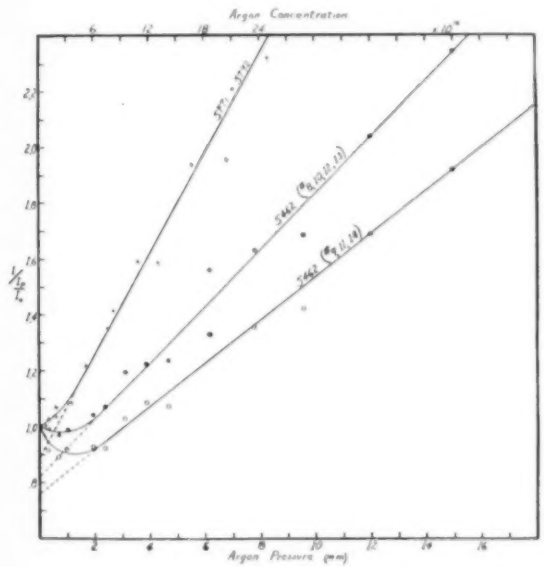

FIG. 4. Argon quenching of iodine fluorescence.

Reabsorption was noticeable at wave-lengths shorter than 6000A and measurements were made at longer wave-lengths. In the case of the green series it was noticed that for a given argon pressure, the I_p/I_0 ratios for wave-lengths above 6000A did not fluctuate about one constant value (as in pure iodine), but about *two* mean values, whose spacing increased with argon pressure. No meaning has been given to this phenomenon, but both green values are shown in Fig. 4.

When transfer occurs, the measurements made on the blurred spectrum tacitly assume that the transferred energy reappears in the close neighborhood of the fluorescence line to which it would otherwise have gone. While the appearance of early plates taken with a fine slit indicates that this is approximately true of the stronger transferred lines, still the presence of the reabsorption just mentioned seems only to be explained as a shifting of some energy to longer wave-lengths, as Franck[15] has suggested; for argon does not broaden the absorption lines. Therefore the I_p/I_0 values for the argon-iodine mixture are subject to a small but unknown error.

THEORY OF THE EXPERIMENT

The intensity of the fluorescence (after making all corrections) is proportional to the number of excited molecules and to their rate of radiation. The number of excited molecules present depends on the balance between the absorption and the rate of removal. In this latter connection the effect of collisions with other iodine molecules must be considered. Using the type of theory developed by Stern and Volmer[16] for the quenching of iodine fluorescence by itself, define:

n = number of normal iodine molecules per cc.

n' = number of excited iodine molecules per cc.

N = number of argon atoms per cc.

r = probability of one excited iodine molecule radiating in unit time.

b = probability of one normal iodine molecule making a total-energy-removing collision in unit time with one excited iodine molecule per cc.

a = probability of one argon atom making a total-energy-removing collision in unit time with one excited iodine molecule per cc.

A = the number of excited iodine molecules formed per cc in unit time (proportional to the absorption).

Then the equation for the equilibrium state of the fluorescence is:

$$A = rn' + bnn' + aNn' \qquad (1)$$

or

$$n' = A/(r + bn + aN). \qquad (2)$$

[15] J. Franck, Ergebnisse der Exakten Naturwissenschaften **2**, 118 (1923).

[16] O. Stern and M. Volmer, Phys. Zeits. **20**, 183 (1919).

Collisions with the walls are negligible, as Stern and Volmer[16] have shown. Under the condition of a wide slit the quantities n', r, b and a do not refer to only the original excited states to which the iodine is raised directly by the exciting line, but they may also include the nearby states from which energy is radiated after transfer. Since r, b and a are a kind of average for all the excited states producing fluorescence, and since the number of such states will vary with the amount of transfer occurring, and because the amount of transfer depends on the concentration, r, b and a, in the event of transfer, are not constants, but functions of concentration.

To examine this in more detail,* irrespective of the slit used let the following terms be defined more closely than was done above:

n = conc. of iodine molecules (normal).
N = conc. of argon atoms.
A_r = number of molecules excited into one of the original states r per sec. (some 12 such green states with a hot arc).
$r_r n_r'$ = number of radiation acts from the state r per sec.
$b_r n n_r'$ = number of molecules in state r quenched by iodine per sec.
$a_r N n_r'$ = number of molecules in state r quenched by argon per sec.
$c_{rs} n n_r'$ = number of transfer acts from state r to the state s due to iodine per sec. (s also includes any of the other r states.)
$d_{rs} N n_r'$ = number of transfer acts, etc., due to argon per sec.

Then for the equilibrium of the state r

$$A_r+\sum_s c_{sr}n_s'n+\sum_s d_{sr}n_s'N = r_r n_r'+b_r n_r'n+a_r n_r'N+\sum_s c_{rs}n_r'n+\sum_s d_{rs}n_r'N.$$

This supposes that transfer can also act to bring excited molecules into any one of the r states, either from one of the original r states, or from an s state which has been occupied as the result of a previous transfer. For any other state t (not one of those originally excited) the equilibrium is expressed by

$$\sum_s c_{st}n_s'n+\sum_s d_{st}n_s'N = r_t n_t'+b_t n_t'n+a_t n_t'N+\sum_s c_{ts}n_t'n+\sum_s d_{ts}n_t'N,$$

where s is any state except t. These two equations are typical of the two varieties of excited states (r and t) present in the assembly. If q be used to indicate any excited state, without restriction, then on adding all equations similar to the above two:

$$\sum_r A_r+\sum_q\sum_s c_{sq}n_s'n+\sum_q\sum_s d_{sq}n_s'N = \sum_q r_q n_q'+\sum_q b_q n_q'n+\sum_q a_q n_q'n+\sum_q\sum_s c_{qs}n_q'n+\sum_q\sum_s d_{qs}n_q'N.$$

But

$$\sum_q\sum_s c_{sq}n_s'n=\sum_q\sum_s c_{qs}n_q'n$$

and similarly for the other double sum. So that

$$\sum_r A_r=\sum_q r_q n_q'+n\sum_q b_q n_q'+N\sum_q a_q n_q'. \quad (3)$$

If *no transfer of energy occurs*, $q=r$, and comparing Eqs. (1) and (3)

$$A=\sum_r A_r, \qquad an'=\sum_r a_r n_r',$$

$$rn'=\sum_r r_r n_r', \quad \text{where } n'=\sum_r n_r'.$$

$$bn'=\sum_r b_r n_r',$$

The coefficients r, b and a are seen to be average values over the r states. They do not, however, remain constants after the gas concentration is changed; for due to inherent inequalities between the actual values r_r (which are in themselves constants), the new n' may consist of a different distribution of the n_r' values and this may shift the center of gravity of the average. This may perhaps become more apparent upon comparing equations like Eq. (2) written for states r_1, r_2, etc. Since it is impossible in this experiment to say anything of the coefficients of a single state, it can only be assumed that for the several states excited by one line the individual r_r values (and b_r and a_r) are nearly alike, so that a constant r, b and a can be used as in Eq. (1). Within the

* I am indebted to Professor E. U. Condon for the more formal treatment of this matter.

limits of its accuracy, the present experiment justifies this assumption.

In the autoquenching of iodine very little transfer occurs. It is not even apparent at 0.2 mm on plates which had strong resonance series lines, and Wood's[17] pictures of it were twenty hour exposures. For pure iodine, then, r and b will be considered practically constant, although subscripts will be appended to indicate molecular concentration.

For argon quenching the transfer effect is marked. With a wide slit this transferred radiation is also measured, and the unknown dependence of the effective r, b and a values on argon pressure prevents the deduction of exact quantitative results.

Returning to Eqs. (2) and (3), since the fluorescence intensity (resonance series and background) is proportional to rn':

$$I = crn' = crA/(r+bn+aN). \tag{4}$$

If the previously defined A be now taken to represent the percent absorption of the iodine, then

$$A/I = (1/C)(1+(b/r)n+(a/r)N). \tag{5}$$

From this it appears that the ratio of the absorption to the fluorescence intensity of the iodine (n=constant) should increase linearly with the argon concentration (N): and the ratio of slope to intercept yields a/r in terms of $(1+(b/r)n)$.

Suppose that the concentration of the iodine is varied in the *absence of argon*. Eq. (5) freed of its last term shows that A/I varies linearly with n; and in this case the ratio of slope to intercept gives b/r, so that a determination of a/r should be possible. The quenching of iodine by iodine and the absorption values were therefore measured. Only later was it realized that rigorous evaluation of the argon quenching was still impossible because of the transfer effect.

Pure iodine

Actual measurements of the fluorescence gave values which were relative to the intensity for a fixed condition of the vapor (i.e., crystals in a 0°C bath). Indicating temperature by subscripts, any two states of the vapor are related by

$$\frac{I_0 \cdot A_t}{I_t \cdot A_0} = \frac{r_0}{r_0+b_0n_0}\left(1+\frac{b_t}{r_t}n_t\right). \tag{6}$$

By using the approximation that $A=KnL$, then for a constant path length L, this becomes

$$\frac{I_0 \cdot n_t}{I_t \cdot n_0} = \frac{r_0}{r_0+b_0n_0}\left(1+\frac{b_t}{r_t}n_t\right). \tag{7}$$

In Fig. 5 the left member of Eq. (7) is plotted against n_t. For densities greater than 6×10^{15} molecules per cc the approximation $A=KnL$ does not hold. But within this range the curve is linear, providing that r_t and b_t are constant which is practically the case in pure iodine. The slope to intercept ratio of this line, by Eq. (7) gives

	5462A	5771+5792A
b_t/r_t =	4.50×10^{-16}	6.28×10^{-16}

TABLE I.

Temp. (°C)	Press. (mm)	n_t ($\times10^{15}$)	$(b_t/r_t)n_t$ (green)	$(b_t/r_t)n_t$ (yellow)
−6	0.015	0.55	0.25	0.35
0	0.03	1.06	0.48	0.67
6	0.055	1.92	0.87	1.21
7.5	0.064	2.22	1.00	1.40
12	0.098	3.34	1.50	2.10
20	0.20	6.63	3.00	4.16

When it is recalled that b_t is only the probability of energy loss when but one normal molecule per cc is colliding, then for an actual condition of the iodine, such as n_t molecules at t°C:

$$\frac{b_t}{r_t}n_t = \frac{\text{Probability of energy loss per single excited molecule due to collisions with } n_t \text{ normal molecules}}{\text{Probability of energy loss per single excited molecule due to radiation}}$$

A few values of this quantity within the experimental range are given in Table I (the concentrations given are for both vapor and crystals at the one indicated temperature). In the usual iodine experiments around room temperature,

[17] R. W. Wood, Phil. Mag. [6] **35**, 236 (1918).

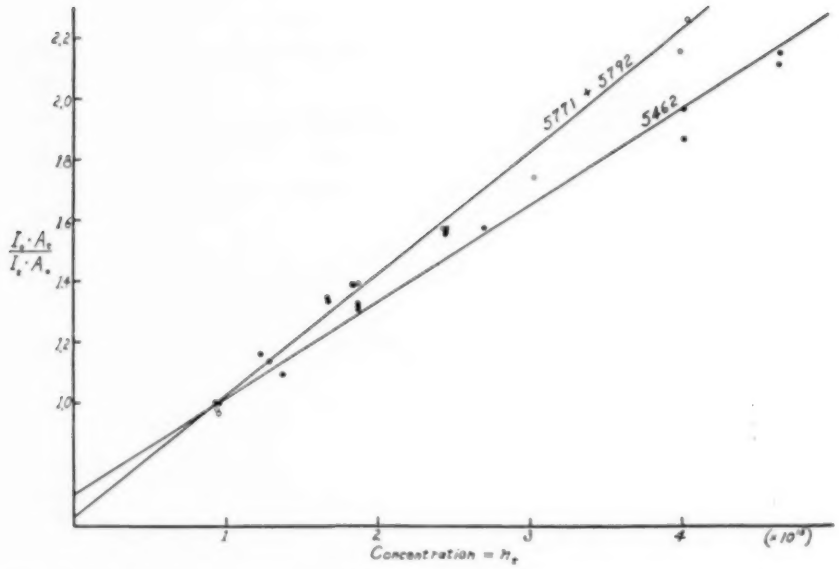

FIG. 5. Combined absorption and fluorescence in iodine: *points* green: *circles* yellow.

therefore, collision and radiation play rôles of the same order of magnitude in ridding excited molecules of their energy. Stern and Volmer were led to the same conclusion, but expressed it in a qualitative manner.

The fact that the pure iodine fluorescence is quenched in the yellow series more than it is in the green, is not in accord with any theory of collision enhancement of predissociation. For the work of Turner[3] on magnetic quenching shows that predissociation is most effective in the green series. The observed quenching is probably due to collisions of the second kind.

Iodine with argon

When argon was used the iodine concentration was held constant at t°C ($t=25.6$°C; $n_t=9.76\times10^{15}$ molecules per cc). If the subscript p indicates the argon pressure, the equation analogous to (7) is

$$\frac{I_0\cdot A_\rho}{I_\rho\cdot A_0}=\frac{r_0}{r_0+b_t n_t}\left\{\left(1+\frac{b_\rho}{r_\rho}n_t\right)+\frac{a_\rho}{r_\rho}N_\rho\right\}. \quad (8)$$

This equation is appropriate to the data plotted on Fig. 4. But the initial increase of green fluorescence shown by the experimental points is remarkable, in view of the result that argon did not increase the absorption ($A_\rho/A_0=1$). The failure of Eq. (8) to explain Fig. 4 may be due to the unknown dependence of the r, b and a values on argon pressure (because of transfer), or to other imaginable processes: such as a hindering of the autoquenching, or a change in the ratio of continuous to line absorption. Certainly no evaluation of the quenching efficiency of argon (a_ρ/r_ρ) is at present possible. While the yellow series is quenched more than the green, this cannot be taken as positive evidence against the enhancement of predissociation by argon; for with the possibility of variation in the b_ρ/r_ρ term, the actual values of a_ρ/r_ρ in both series would have to be known.

The opportunity is taken here to express my very warm gratitude to Professor Louis A. Turner, from whom came the idea of undertaking this investigation, and under whose counsel it has developed.

On the Cooling of a Radioactive Sphere

ARNOLD N. LOWAN, *Columbia University, New York City*

(Received December 20, 1932)

By means of the Laplace transformation, any physical problem characterized by a partial differential equation, the solution of which must satisfy prescribed initial and boundary conditions, can formally be transformed into a boundary problem for an ordinary differential equation. From the solution of the latter problem, that of the original problem may be obtained by the inversion of the Laplace transformation. The method is applied to the problem of the cooling of a radioactive sphere and the solution of this problem is applied to a discussion of the thermal history of the earth.

THE method based on the properties of the Laplace transformation, originally employed by G. Doetsch[1] in dealing with the temperature history of a homogeneous rod, is capable of considerable generalization. By making use of the properties of the Green functions of self-adjoint differential equations and, in particular, of the bilinear expansion formula, and also of the properties of the Laplace transformation, it is possible to obtain the solutions of a large number of problems in heat conduction, characterized by non-homogeneous partial differential equations of parabolic type, with constant or variable coefficients, the solutions of which must satisfy prescribed initial and boundary conditions, the latter being of a homogeneous or non-homogeneous type.

The method is presented in connection with the problem of the cooling of a heterogeneous radioactive sphere with spherical symmetry, both as regards its physical properties and its initial temperature distribution, the surface of which is either kept at, or radiates into a medium of variable temperature.

Let s = specific heat, d = density, K = thermal conductivity, $\phi(r, t)$ = heat generated per unit time per unit volume, σ = coefficient of heat transfer between the sphere and the medium, $f(r)$ = initial temperature, $F(t)$ = temperature of medium. The temperature T must then satisfy the following differential equation[2] initial and boundary conditions:

$$sd\frac{\partial T}{\partial t}-\left\{\left(\frac{\partial K}{\partial r}+\frac{2K}{r}\right)\frac{\partial T}{\partial r}+K\frac{\partial^2 T}{\partial r^2}\right\}=\phi(r,t)=sd\varphi(r,t) \quad \text{(say)} \quad \text{for } t>0, \tag{1}$$

$$\lim_{t\to 0} T(r,t)=f(r), \tag{2}$$

$$\partial T/\partial r=0 \quad \text{for } r=0, \tag{3}$$

$$\partial T/\partial r+\sigma T=\sigma F(t) \quad \text{for } r=R=\text{radius of sphere}, \tag{4}$$

where, for the sake of simplicity, we assume that s, d, K and the initial temperature distribution, are continuous functions of r (distance from the center) and $\varphi(r, t)$ is a continuous function of r and t.

By the application of Duhamel's theorem,[3] the general solution of the system of Eqs. (1) to (4), which system will be referred to as system (A), may be written in the form:

$$T(r,t)=u(r,t)+\int_0^t F(\tau)(\partial/\partial t)v(r,t-\tau)d\tau, \tag{5}$$

[1] G. Doetsch, Math. Zeits. **22**, 285 (1924).

[2] Weber-Riemann, *Differenzialgleichungen der Physik* **2**, 181 (1927).

[3] H. S. Carslaw, *Introd. Math. Theory of Conduction of Heat in Solids*, p. 18 (1921).

where $u(r, t)$ is a solution of the system (B) consisting of (1), (2), (3) and the new boundary condition:

$$\partial u/\partial r+\sigma u=0 \quad \text{for } r=R \tag{4'}$$

and $v(r, t)$ is a solution of the system (C) obtained from the system (A), by putting $f(r)=\varphi(r, t)=0$ and $F(t)=1$.

If, in the system (C) we make the substitution:

$$v(r, t)=[\sigma r^2/R(2+\sigma R)]+w(r, t) \tag{6}$$

it is readily seen that the function $w(r, t)$ must satisfy the system (D) obtained from (B) by putting $\varphi(r, t)=[2\sigma/R(2+\sigma R)](3K+r\partial K/\partial r)$ and $f(r)=-\sigma r^2/R(\sigma R+2)$. Thus, the problem reduces to the integration of the system (B).

Consider the Laplace transformation defined by:

$$L\{u(r, t)\}=\int_0^\infty e^{-\lambda t}u(r, t)dt=y(r, \lambda), \quad \text{(say)} \tag{7}$$

whence, symbolically, $u(r, t)=L^{-1}\{y(r, \lambda)\}$. It may be easily shown that the operators L and L^{-1} obey the distributive and associative laws of addition and that they can be commuted with the operations of differentiation and integration with respect to the variable r, which may be regarded as a parameter. If (7) is integrated by parts, we obtain the identity:

$$L\{(\partial/\partial t)u(r, t)\}=\int_0^\infty e^{-\lambda t}(\partial/\partial t)u(r, t)dt=\lambda L\{u(r, t)\}-u(r, 0). \tag{8}$$

A further important property of the Laplace transformation, which will be employed in the subsequent derivations, may be stated as follows:[1, 4, 5]

If
$$L^{-1}\{G_1(r, \lambda)\}=\Gamma_1(r, t) \quad \text{and} \quad L^{-1}\{G_2(r, \lambda)\}=\Gamma_2(r, t)$$
then
$$\begin{aligned} L^{-1}\{G_1(r, \lambda)\cdot G_2(r, \lambda)\} &= \int_0^t \Gamma_1(r, \tau)\cdot\Gamma_2(r, t-\tau)d\tau \\ &= \int_0^t \Gamma_2(r, \tau)\cdot\Gamma_1(r, t-\tau)d\tau. \end{aligned} \tag{9}$$

If the Eqs. (1), (3) and (4′) of the system (B) are acted upon by the operator L, then in view of the properties above mentioned, and with the use of (2), it is readily seen that the function $y(r, \lambda)$ must satisfy the self-adjoint differential equation:

$$(d/dr)(Kr^2dy/dr)-\lambda(sdr^2)y=-sdr^2\left\{f(r)+\int_0^\infty e^{-\lambda t}\varphi(r, t)dt\right\}=-r^2\psi(r, \lambda) \tag{10}$$

and the boundary conditions (3) and (4′). The solution of the latter system (E) may be written in the form[6]

$$y(r, \lambda)=\int_0^R G(r, \xi, \lambda)\cdot\xi^2\psi(\xi, \lambda)d\xi, \tag{11}$$

[4] J. R. Carson, *Operational Calculus and the Electric Circuit Theory*, Chapter IV (1926).

[5] B. van der Pol, Phil. Mag. **8**, 861 (1929).

[6] R. Courant and D. Hilbert, *Methoden der Math. Physik*, Vol. I, Chapter V (1924).

where $G(r, \xi, \lambda)$ is the "Green function" of our problem, defined as the solution of the homogeneous differential equation:

$$(d/dr)(Kr^2dy/dr) - \lambda(sdr^2)y = 0, \tag{12}$$

satisfying the given boundary conditions (3) and (4′) and the discontinuity condition:

$$\operatorname{Lim}_{\epsilon \to 0} \frac{\partial}{\partial r} G(r, \xi, \lambda) \Big|_{r=\xi-\epsilon}^{r=\xi+\epsilon} = -\frac{1}{\xi^2 K(\xi)}. \tag{13}$$

In the system (F), consisting of the Eqs. (12), (3) and (4′), we have a typical Sturm-Liouville boundary problem. As is well known,[6, 7, 8] the solutions of a problem of this type form a set of completely orthogonal functions which we shall consider as normalized, i.e., satisfying the condition:

$$\int_0^R s(\xi) \cdot d(\xi) \cdot \{y_n(\xi, \lambda_n)\}^2 \cdot \xi^2 d\xi = 1, \tag{14}$$

the y_n's being the characteristic functions corresponding to the characteristic values λ_n, which are known to form a sequence of simple, real and positive numbers. Furthermore, the Green function above defined may be expressed in the form:[9]

$$G(r, \xi, \lambda) = \sum_{n=1}^{\infty} \frac{y_n(r) \cdot y_n(\xi)}{\lambda_n + \lambda}, \tag{15}$$

where the second member is known to be uniformly convergent in the interval O–R. In view of (15) our solution (11) may be written in the form:

$$y(r, \lambda) = \sum_{n=1}^{\infty} \frac{y_n(r)}{\lambda_n + \lambda} \int_0^R \xi^2 \psi(\xi, \lambda) d\xi. \tag{16}$$

If (16) is subjected to the inverse Laplace transformation, L^{-1} then, in view of the significance of $\psi(r, \lambda)$ and by making use of (9), we ultimately get:

$$u(r, t) = \sum_{n=1}^{\infty} e^{-\lambda_n t} y_n(r) \left\{ \int_0^R s(\xi) \cdot d(\xi) \cdot \xi^2 f(\xi) y_n(\xi) d\xi + \int_0^R s(\xi) \cdot d(\xi) \cdot \xi^2 y_n(\xi) d\xi \cdot \int_0^t \varphi(\xi, \tau) e^{\lambda_n \tau} d\tau \right\}. \tag{17}$$

Since for any piecewise continuous and twice differentiable function $g(r)$, we have the identity:[10]

$$g(r) = \sum_{n=1}^{\infty} y_n(r) \int_0^R \xi^2 \cdot s(\xi) \cdot d(\xi) \cdot g(\xi) \cdot y_n(\xi) d\xi \tag{18}$$

it can be shown that (17) is convergent and may be differentiated once with respect to t and twice with respect to r, provided $f(r)$ and $\varphi(r, t)$ are bounded. If, in addition, these functions are piecewise continuous and twice differentiable, it can also be verified that (17) satisfies the differential Eq. (1) and the initial condition (2). Thus, (17) represents the complete solution of the system (B).

---

[7] Adolf Kneser, Die Integralgleichungen §§26–27–28.

[8] Weber-Riemann: Differenzialgleichungen der Physik, Vol. I, Chapter 7.

[9] A. Kneser, reference 7, p. 109; Weber-Riemann reference 8. Vol. 1, p. 292.

[10] A. Kneser, reference 7, p. 117; Courant-Hilbert, reference 6, p. 279.

In view of the definition of the system (D), its solution is obtained with the aid of (17), in the form:

$$w(r,t)=[\sigma/R(\sigma R+2)]\sum_{n=1}^{\infty}e^{-\lambda_n t}y_n(r)\left\{-\int_0^R \xi^4\cdot s(\xi)\cdot d(\xi)\cdot y_n(\xi)d\xi\right.$$

$$\left.+2\int_0^R \xi^2\cdot s(\xi)\cdot d(\xi)\cdot(3K+\xi\partial K/\partial\xi)y_n(\xi)d\xi\cdot\int_0^t e^{\lambda_n\tau}d\tau\right\}. \quad (19)$$

In view of (6), the solution (5) of the system (A) becomes:

$$T(r,t)=u(r,t)+\int_0^t F(\tau)(\partial/\partial t)w(r,t-\tau)d\tau, \quad (20)$$

where $u(r,t)$ and $w(r,t)$ are given by (17) and (19), respectively. If, in addition to the conditions imposed on $f(r)$ and $\varphi(r,t)$, we assume the convergence of the integral $\int_0^t F(\tau)\cdot e^{\lambda_n\tau}d\tau$, then (20) may be shown to satisfy the equations of the system (A) and, therefore, represents the complete solution of our problem.

In the particular case where $F(t)=0$, the second term in (20) vanishes and the complete thermal history of a heterogeneous radioactive sphere, cooling by radiation into a medium at 0°, is given by (17).

Since for $\sigma=\infty$ the boundary condition (4) reduces to $T(R,t)=F(t)$ it is clear that the solutions appropriate to the case where the surface of the sphere is kept at temperature $F(t)$ may be obtained from (20) by putting $\sigma=\infty$.

The solutions appropriate to a homogeneous sphere may be obtained from our general solution (20) by assuming that s, d and K are constant. Thus, in the case of a homogeneous sphere radiating into a medium at 0°, we ultimately get:

$$T(r,t)=\frac{2}{r}\sum_{n=1}^{\infty}\frac{(h^2+\lambda_n^2)\sin\lambda_n r}{R\lambda_n^2+h(Rh+1)}e^{-k\lambda_n^2 t}\left\{\int_0^R \xi f(\xi)\sin\lambda_n\xi d\xi+\int_0^R \xi\sin\lambda_n\xi d\xi\cdot\int_0^t \varphi(\xi,\tau)e^{k\lambda_n^2\tau}d\tau\right\}, \quad (21)$$

where $k=K/sd$; $h=\sigma-1/R$ and the summation is extended over the positive roots of the transcendental equation:

$$\lambda\cos\lambda R+h\sin\lambda R=0. \quad (22)$$

For $h=\infty$, (21) becomes:

$$T(r,t)=\frac{2}{Rr}\sum_{n=1}^{\infty}e^{-kn^2\pi^2t/R^2}\sin\frac{n\pi r}{R}\left\{\int_0^R \xi f(\xi)\sin\frac{n\pi\xi}{R}d\xi+\int_0^R \xi\sin\frac{n\pi\xi}{R}d\xi\int_0^t e^{kn^2\pi^2\tau/R^2}\cdot\varphi(\xi,\tau)d\tau\right\}, \quad (21')$$

this being the solution for the case where the surface of the sphere is kept at 0°.

Application to the Thermal History of the Earth

According to our present-day views, the earth was generated by tidal disruption from the sun and in the relatively short interval of 10,000–15,000 years had reached the stage of Leibnitz' "*consistentior status*" when the formation of the oceans became possible and when the viscosity and the temperature gradients were such as to prevent convective currents from playing any appreciable rôle.

From this point, which we may take as our $t=0$, the process of cooling is governed by conduction and if we assume, for the sake of simplicity, that the physical constants do not vary appreciably with depth, our solution (21′) is applicable.

The present-day temperature distribution, particularly at depths down to a few hundred miles, depends on the assumed (average) value of the thermal diffusivity, of the initial temperature distribution $f(r)$, of the radioactivity function $\phi(r, t)$ and of the age of the earth.

Most investigators[11, 12, 13] have treated the thermal history of the earth as that of a semi-infinite solid, hypothetically composed of diabase, for which the adopted thermal diffusivity varies between 0.005 and 0.007 c.g.s. units.

The initial temperature was taken in the form $S+mx$, where $S=1400°C=$ melting temperature of diabase at ordinary pressure, $x=$depth below the surface and $m=3\times10^{-5}°C$ per cm, the latter value being obtained experimentally by Barus.[14]

There are strong reasons for assuming that the initial temperature gradient was not constant down to the center of the earth but decreased considerably with depth. It is, therefore, reasonable to assume, for the initial temperature distribution, the function:

$$f(r)=S+m(R-r)-\beta(R-r)^2-\{(m-2\beta R)/3R^2\}(R-r)^3, \tag{23}$$

satisfying the following conditions: 1. The temperature and the temperature gradient diminishes with depth and becomes $=0$ at the center of the earth. 2. The temperature and the temperature gradient at the surface are those given by Barus.

Concerning the distribution of radioactive matter, there is considerable geological evidence to support the view that the concentration of radioactive constituents decreases with depth. Arthur Holmes has suggested the exponential law $Ae^{-\alpha x}$ for the radioactive heat per cc per sec., A corresponding to the average granitic rocks. While A is fairly well known, the actual value of α can only be computed by assuming a value for the percent of contribution of radioactivity to the known total loss of heat by the earth.

Concerning the age of the earth, it is fairly well known[15] that it is between 1460 and 3000 million years, the first estimate being the age of the oldest known rock as determined from the lead-uranium ratio, the latter estimate being an upper limit obtained by Holmes on the suggestion by H. N. Russell that all the lead in the igneous rocks is of radioactive origin.

In view of the uncertainty which thus attaches to the actual initial temperature distribution, to the distribution of radioactive matter, to the average thermal diffusivity and to the age of the earth, it becomes important to investigate the effect of fluctuations in the assumed data on the present-day temperature distribution, particularly at depths down to a few hundred miles.

For purposes of computation, our solution (21′), appropriate to a homogeneous earth, may be written in the form:

$$T=T_1+T_2, \tag{24}$$

where

$$T_1=(2R/r)\sum_{n=1}^{\infty} e^{-kn^2\pi^2t/R^2}\sin(n\pi r/R)\int_0^1 xf(Rx)\sin n\pi x\,dx, \tag{25}$$

$$T_2=(2R^3/\pi^2Kr)\sum_{n=1}^{\infty}(1-e^{-kn^2\pi^2t/R^2})\sin(n\pi r/R)\int_0^1 x\phi(Rx)\sin n\pi x\,dx. \tag{26}$$

If we assume $f(\rho)=f(Rx)=S+mR(1-x)$ we ultimately get:

$$T_1=\frac{2RS}{\pi r}\sum_{n=1}^{\infty}e^{-n^2c}\sin\frac{n\pi R}{R}\cdot\frac{(-1)^{n+1}}{n}+\frac{8mR}{\pi^3 r}\sum_{n=1}^{\infty}e^{-n^2c}\sin\frac{n\pi r}{R}\cdot\frac{1}{n^3}, \tag{27}$$

[11] H. Jeffreys, *The Earth*, Chapter V (1929).

[12] Arthur Holmes, Geol. Mag. **2**, 109 (1915); **62**, 507 (1925).

[13] L. H. Adams, J. Wash. Acad. Sci. **14**, 459 (1924).

[14] U. S. Geol. Survey, Bull. No. 103, p. 55 (1893).

[15] Arthur Holmes, *Physics of the Earth*, pp. 220, 454 (1931).

where $c=k\pi^2t/R^2$. If, on the other hand, we assume:

$$f(\rho)=f(Rx)=S+mR(1-x)-\beta(1-x)^2R^2-(R/3)(m-2\beta R)(1-x)^3,$$

we ultimately get:

$$T_1=\frac{2RS}{\pi r}\sum_{n=1}^{\infty}e^{-n^2c}\cdot\frac{(-1)^{n+1}}{n}\cdot\sin\frac{n\pi r}{R}+\frac{4R}{\pi^3}(m+\beta R)\sum_{n=1}^{\infty}e^{-n^2c}\sin\frac{n\pi r}{R}\cdot\frac{(-1)^{n+1}}{n^3}$$
$$+\frac{32R^2(m-2\beta R)}{\pi^5 r}\sum_{n=1,\,3,\,5\cdots}^{\infty}e^{-n^2c}\sin\frac{n\pi r}{R}\cdot\frac{1}{n^5}. \tag{27'}$$

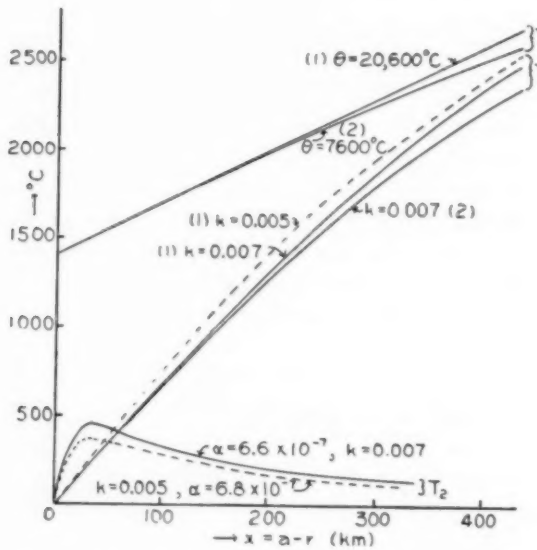

FIG. 1. k=thermal diffusivity; θ=initial temperature at center of earth; m=present-day superficial temperature gradient $=32\times10^{-5}$; λ_0=superficial thermal conductivity $=0.006$; λ=average thermal conductivity $=0.005$.

Present-day temperature distribution: $T=T_1+T_2$.
T_1=temperature arising from initial heat;
T_2=temperature arising from radioactivity;
T_0=initial temperature:
$\begin{cases}=S+m_0(a-r); \text{ curves (1)};\\ =S+m_0(a-r)-\beta(a-r)^2\\ \quad -(1/3a^2)(m-2a\beta)(a-r)^3; \text{ curves (2)}.\end{cases}$

Distribution of radioactive matter: $Ae^{-\alpha(-r)}$.
$A=10^{-12}$ cal. per cc per sec.;
$S=1400°C$, $m_0=3\times10^{-5}$;
Age of earth $=1.6\times10^9$ years;
$a\beta=m$.

With $\phi=Ae^{-\alpha(R-r)}$ (26) finally becomes:

$$T_2=\frac{2AR^2}{\pi K}\cdot\frac{R}{r}\sum_{n=1}^{\infty}(1-e^{-n^2c})\sin\frac{n\pi r}{R}\cdot\frac{(-1)^{n+1}}{n(R^2\alpha^2+\pi^2n^2)}. \tag{28}$$

Computations were carried out under the following assumptions pertaining to the physical constants: $S=1400°C$=initial temperature at the surface of the earth; m_0=initial temperature gradient at the surface$=3\times10^{-5}$; K_0=superficial thermal conductivity$=0.006$; k=average thermal diffusivity $=0.007$ or 0.005; m=present-day superficial temperature gradient$=32\times10^{-5}$; age of the earth$=1600$ million years; $A=10^{-12}$ calories=heat generated per cc per sec. by the average granitic rocks near the surface.

The value of α to be used in the computations follows from the previous data. Indeed, the sum of the slopes of the T_1 and T_2 curves must be $=32\times10^{-5}$ for $x=0$. The slope m_2 of T_2 can thus be found, and, therefore, also the contribution K_0m_2 to the heat lost by the earth due to radioactivity per cm per sec.

To a high degree of approximation, the latter quantity is $=A/\alpha$. Hence $A/\alpha=K_0m_2=K_0(32\times10^{-5}-m_1)$, where m_1 is the slope of the T_1 curve. From this equation we can calculate α.

The results of the computations shown on the graph, Fig. 1, bring out clearly the following facts:

The temperature distribution at depth of a few hundred km is inappreciably affected by fluctuations in the assumed initial temperature distribution, or in the assumed average value for the thermal diffusivity, the maximum deviation between the temperature curves corresponding to various sets of assumptions, being barely 100°C. It therefore appears very unlikely that the temperature of the basaltic layer (at depths of 10–30 km) can depart appreciably from that shown in Fig. 1; therefore, it cannot be present in the form of potential magma. If, then, the seat of the phenomena of vulcanism is at the depth of the basaltic layer, there must be some additional supply of heat, perhaps as Jeffreys suggests,[16] in the form of heat of reaction of certain active gases below the basaltic layer.

The method above described may be extended to the case where the boundary conditions involve the time derivative of the unknown function $T(x, t)$. A typical problem of this type is the heat conduction in a solid in contact with a stirred liquid. The method leads essentially to the same results as were obtained by Schumann[17] and Langer[18] by an extension of the Fourier analysis.

[16] H. Jeffreys, Phil. Mag. **1**, 923 (1926).

[17] Schumann, Phys. Rev. **37**, 1508 (1931).

[18] Langer, Tohoku Math. J. **35** (1932).

The Magnetic Susceptibility of MnO as a Function of the Temperature

RAYEN WELCH TYLER, *University of Illinois*

(Received June 10, 1933)

The magnetic susceptibility of manganous oxide for temperatures from 26 to −202°C.—There is a sharp discontinuity in the susceptibility-temperature curve at the same point, $t=-156$°C, as that in the specific heat temperature curve and a second one at a lower temperature, −188°C. The mass susceptibility at 26°C was found to be $\chi=68.6\times10^{-6}$ c.g.s. units. At −38.4°C, $\chi=73.6°\times10^{-6}$. At −154.7°C, $\chi=85.8\times10^{-6}$. At −188°C, $\chi=78.1\times10^{-6}$. At −202°C, $\chi=91.4$. The susceptibility-temperature curve follows Weiss' modification of Curie's law down to $t=-156$°C. The constants of this law were found to be $C=0.0575$ and $\theta=-548$°K. The number of Bohr magnetons in the compound calculated from experimental data is 5.7.

INTRODUCTION

THE specific heat of MnO as a function of the temperature at low temperatures has been studied by R. W. Millar[1] who found that at −157°C there is a very narrow peak in the specific heat curve which rises very abruptly, from a curve gradually falling with the temperature to over thirteen times the specific heats at neighboring temperatures.

The purpose of the present investigation was to learn whether there might not be a similar discontinuity in the magnetic susceptibility curve for MnO at the temperature −157°C. This was rendered the more probable by the recent discovery by C. H. Li[2] in this laboratory of marked changes in the magnetic properties of magnetite at −160°C, where there is a discontinuity in the specific heat of that substance.

METHOD OF INVESTIGATION

The Faraday method of measurement was used. The sample was placed at the point of maximum nonhomogeneity in the field of a large Dubois magnet with conical pole pieces. The force on it was measured with a Curie balance with an electrically controlled torsion head described by A. N. Guthrie.[3] The apparatus was calibrated by measuring the force on a sample of known susceptibility, neodymium oxide.

In the temperature range 0 to −182°C the temperatures were obtained by a copper cooling device, the ends of which were immersed in liquid air. Temperatures lower than −182°C were obtained by boiling fresh liquid air at reduced pressures. A special vacuum bottle of three chambers was designed for this purpose. The innermost chamber in which the sample swung was surrounded by a second which contained the liquid air and was evacuated through a side tube. The outer chamber was silvered and evacuated.

To prevent the condensation of oxygen upon the balance arm, the entire balance was encased in an atmosphere of hydrogen. Commercial hydrogen was used and was freed from possible traces of oxygen by passing over platinized asbestos heated to 500°C and dried by passing over ascarite and anhydrone. Temperatures were measured with a copper-constantan thermocouple. One junction was kept in ice water and the other was supported on a fine glass tube beside the balance arm at the level of the sample. The thermocouple was calibrated against the freezing points of mercury, −38.9°C, and carbon disulphide, −111.6°C and the boiling point of oxygen determined with an oxygen vapor pressure thermometer. The temperature corresponding to a given vapor pressure was computed from the equation $t=369.83/(6.98460-\log_{10}P)$.[4]

PROCEDURE AND RESULTS

Corrections for the susceptibility of the quartz container were made in the usual way. Several

[1] Russell W. Millar, J. Am. Chem. Soc. **50**, 1875 (1928).
[2] Ching Hsien Li, Phys. Rev. **40**, 1002 (1932).
[3] Guthrie and Bourland, Phys. Rev. **37**, 303 (1931).
[4] *Tables Annuelles de Constantes et Donnees Numerique*, Vol. LVI, p. 290.

samples of MnO weighing between 20 and 30 milligrams were used. The cooling chamber was cooled to the lowest possible temperature and readings taken every few degrees as it slowly warmed up. The observed deflections, corrected for the susceptibility of the quartz container, varied from 11 to 23 cm. From the observed deflections the susceptibilities were calculated and plotted against temperature. The result was a series of curves forming a band of points whose width varied from 1 to 3 percent of the susceptibility. The graphical average of these curves is plotted in Fig. 1.

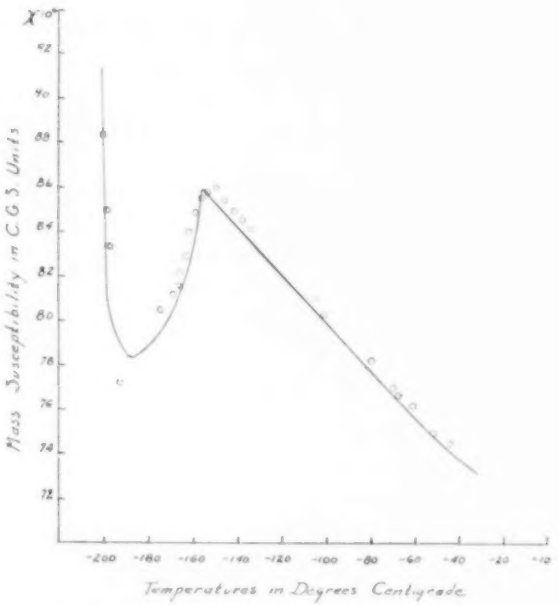

FIG. 1. Magnetic susceptibility of MnO. Average curve. Circles represent actual measurements taken in one run.

DISCUSSION OF RESULTS

The abrupt discontinuity in the magnetic susceptibility curve at -155°C is apparently to be correlated with the discontinuity in the specific heat curve, reported by Millar, at -156°C. The temperature difference is probably not significant because of a possible lag in the temperature of the sample behind that of the thermocouple. The susceptibility curve falls very rapidly at the discontinuity. The minimum at -188°C and the subsequent steep rise at lower temperatures is without parallel in the specific heat curve.

Measurements at still lower temperatures to determine the further course of this curve should be made because the substance must either become ferromagnetic or exhibit another discontinuity. Such measurements were not possible in the present experiment without liquid hydrogen.

The susceptibility obeys the Weiss law $\chi = C/(T-\theta)$ for temperatures above -155°C. The Curie constant C was 0.0575 erg dynes per gauss per gram and $\theta = -548$°K. The number of Weiss magnetons was found to be 28.4. The ion Mn^{++} has the ground state $^6S_{5/2}$, a single state. The number of Bohr magnetons then is $p = g[j(j+1)]^{1/2}$, where g is the Landé splitting factor and j the total angular momentum quantum number. For Mn^{++}, $g=2$, $j=5/2$, and $p=5.92$. The ion O^{--} has a closed outer shell and is therefore diamagnetic. The number of Bohr magnetons in the compound can be calculated from experimental data by the equation $p=(1/B)(3kC/N)^{1/2}$, where B is the Bohr magneton, k, Boltzmann's constant, C, the Curie constant and N, the number of molecules per gram. From the value of C here determined, p is found to be 5.7.

To Professor Jakob Kunz and Professor E. H. Williams the author wishes to express his gratitude for the suggestion of this problem and for assistance in the research.

LETTERS TO THE EDITOR

Prompt publication of brief reports of important discoveries in physics may be secured by addressing them to this department. Closing dates for this department are, for the first issue of the month, the twentieth of the preceding month; for the second issue, the fifth of the month. The Board of Editors does not hold itself responsible for the opinions expressed by the correspondents.

Ionization Potential of Be III

In a recent communication[1] Kruger and Cooper report new wave-length measurements in the series $1s^2\,{}^1S_0 - 1snp\,{}^1P_1$ of Be III and a calculation of the series limit differing from my earlier determination[2] beyond its limits of error. The present communication shows that new investigations have confirmed my earlier value.

On plates taken in 1931 the first line of the series was observed in all orders including the twentieth. Its wave-length (Table I) determined from the sixth to the fifteenth

TABLE I. *The series* $1s^2\,{}^1S_0 - 1snp\,{}^1P_1$ *of Be III.*

n	λ	ν	$1snp\,{}^1P_1$
2	100.254±0.002	997,466±20	243,714
3	88.308±0.005	1,132,400±60	108,780
4	84.75 ±0.01	1,179,941±140	61,739

order is in good agreement both with the old and with Kruger and Cooper's value. The second line was measured in the second order, where it appears quite distinct and near to the oxygen standard lines (Fig. 1).

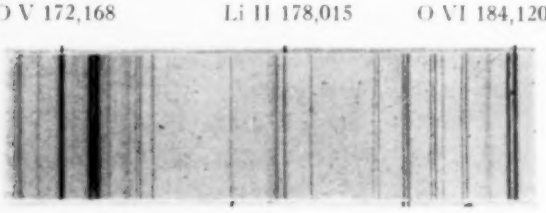

FIG. 1.

The measured wave-length 88.308A agrees with my earlier value 88.30A but differs from that of Kruger and Cooper by 0.13A in the second order, where they also measured it. For the third line the earlier wave-length was likewise confirmed in contradiction with Kruger and Cooper's results.

As the wave-lengths of the lines for which $n=2$ or 3 are decidedly more accurate than those corresponding to higher values of n, the most reliable limit is likely obtained if β in the Ritz formula: $n^*=n+\alpha+\beta/(n^*)^2$ is made equal to β in the same formula for Li II. In doing so the α for Li II and for Be III will also nearly coincide as shown in Table II.

TABLE II. *The effective quantum numbers,* n^*, *of* $1snp\,{}^1P_1$.

n	He I	Li II	Be III
2	2.0094	2.0135	2.0130±1
3	3.0111	3.0136	3.0131±8
4	4.0115	4.0136	4.0158±50

The series limit turns out to be: $1s^2\,{}^1S_0 = 1{,}241{,}180$ cm^{-1} in complete agreement with my previous value, which was implicitly given with the statement[2] that $n-n^*=-0.013$ for the $1snp\,{}^1P_1$-series. It is also in accordance with the quantum mechanical value as derived by Hylleraas:[3]

$$1s^2\,{}^1S_0 = R_M(Z^2-1.25Z+0.31488-0.01752/Z + 0.00548/Z^2)\ \text{cm}^{-1}.$$

This expression has proved to agree surprisingly well with the observed values for He I and Li II. In fact my last measurements in Li II have shown that the difference is only 0.002 percent (see Table III). According to this it

TABLE III.

	$1s^2\,{}^1S_{0\text{calc.}}$	$1s^2\,{}^1S_{0\text{obs.}}$
He I	198,322	198,298
Li II	610,054	610,064±15
Be III	1,241,148	1,241,180±100

would be rather strange that for Be III a deviation of more than 0.1 percent should appear as might be the consequence if the value 1,239,703 of Kruger and Cooper were accepted.

BENGT EDLÉN

Physics Laboratory,
University,
Upsala, Sweden,
September 25, 1933.

[1] P. G. Kruger and F. S. Cooper, Phys. Rev. **44**, 418 (1933).

[2] B. Edlén, Nature **127**, 405 (1931).

[3] E. A. Hylleraas, *Die Grundlagen der Quantenmechanik*, Oslo, 1932.

Distribution of Cosmic-Ray Nuclear Disintegration in Time

In connection with the investigations of W. F. G. Swann and the authors on nuclear disintegrations produced by cosmic rays,[1] the question arose as to whether these disintegrations occurred individually and collectively at random in time. To test this, observations were taken for a thirty-five hour period with the large ionization vessel and recording system previously described. The time intervals between the occurrence of bursts of ionization larger than four million ions in nitrogen at a pressure of 100 pounds per square inch were measured, and the number of intervals between certain limits were obtained. These data were compared with the numbers to be expected by the method used by Marsden and Barratt[2] for alpha-particles. If n is the number of intervals and τ is the average interval, then n is given by

$$n = N(e^{-t_1/\tau} - e^{-t_2/\tau}).$$

The agreement between these expected numbers and the observed ones can be seen from Table I. The fit between the observed and calculated values has been measured by Pearson's criterion and the value of χ^2 obtained is given in the last column. From distribution tables of χ^2 we find[3] that the probability of a divergence greater than this is between 0.7 and 0.5. Thus the data are in good accord with the hypothesis that the nuclear disintegrations observed are randomly distributed in time.

TABLE I.

t_1 (sec.)	t_2 (sec.)	n calculated	n observed	difference r	divergence $r^2/n_{calc.}$
0	50	19.38	22	+1.62	0.14
50	100	17.89	17	−0.89	0.04
100	200	30.46	26	−4.46	0.65
200	500	63.47	68	+4.53	0.32
500	1000	50.48	47	−3.48	0.24
1000	2000	26.62	31	+4.38	0.72
2000	5000	4.69	2	−2.69	1.54
5000	∞	0.01	0	0	
Totals		213.00	213	$\chi^2 = 3.65$ $\tau = 521.6$ sec.	

The authors wish to express their thanks to Dr. W. F. G. Swann for his enthusiastic support.

C. G. MONTGOMERY
D. D. MONTGOMERY

The Bartol Research Foundation
of the Franklin Institute,
October 5, 1933.

[1] W. F. G. Swann and C. G. Montgomery, Phys. Rev. **44**, 52–53 (1933).

[2] Marsden and Barratt, Proc. Phys. Soc. **23**, 367 (1911); **24**, 50 (1911); Rutherford, Chadwick and Ellis, *Radiations from Radioactive Substances*, p. 172, Cambridge, 1930.

[3] T. C. Fry, *Probability and its Engineering Uses*, p. 468, New York, 1928.

Neutrons from Cosmic-Ray Stösse

Some preliminary results of the cloud photography of cosmic-ray Stösse, or ionization bursts, in argon, seem sufficiently interesting to be described here. Numerous neutron-recoil atom tracks, two long nucleus tracks, and groups of simultaneous tracks that converged at different points, were found.

A cloud chamber 15 cm in diameter has been arranged to be set off immediately after the simultaneous discharge of 3 Geiger-Müller cosmic-ray counting tubes, placed with two above and one below the chamber, but as far *out of line* as possible. The principle of its operation is similar to that of the apparatus of Blackett and Occhialini,[1] except that the counters are not set off by single rays. Of the triple-coincidence counting rate, 1.26 hr.$^{-1}$, it is estimated from the photographs taken that about one-third of the discharges are from Stösse and two-thirds from branched tracks, double tracks, and so on. Surrounding the chamber are 1350 lb. of massive material, consisting of 750 lb. of lead, 400 lb. of copper and brass, and 200 lb. of iron. A cloud atmosphere of argon at 64.5 cm pressure is used. The specific ionization of tracks in argon is high; the relatively high viscosity makes the tracks persist better than tracks in air; the expansion ratio is small (1.18, as compared with 1.3 for air), and the probability of obtaining recoil atoms from any neutrons present is relatively high. Since the ionizing particles traverse the chamber about 0.01 sec. before the expansion, the tracks are somewhat diffused by thermal agitation and the expansion; equality of diffuseness of tracks of like densities serves to establish approximate simultaneity of their formation, and makes it easy to discriminate between pre- and post-expansion tracks.

Figs. 1, 2, and 3 are stereophotographs of interesting

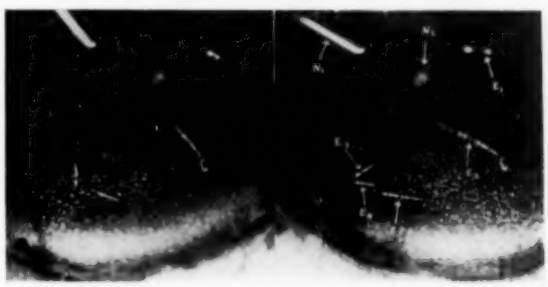

FIG. 1. Stoss with 2 nucleus tracks (N), and 5 electron tracks (E). E_1, E_2 and N_1 converge at a point in the lead, above and behind the chamber. E_3, E_4 and E_5 converge at another point. N_2 is believed to be an argon atom recoiling after elastic collision with a neutron. The heavy nucleus track, N_1, ends in the chamber with a sharp bend. (Mag. ×0.35)

[1] Blackett and Occhialini, Proc. Roy. Soc. (London) **A139**, 699 (1933).

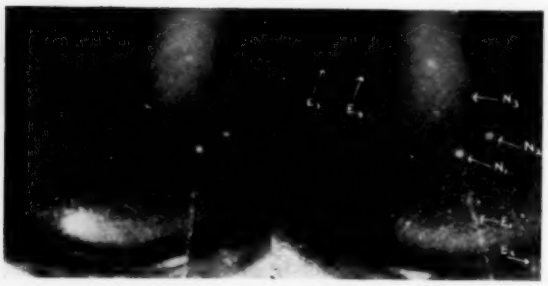

FIG. 2. Stoss with 4 electron tracks, 2 neutron-recoil tracks, N_1 and N_2, and a long, diffuse nucleus track, N_3, near the bottom of the chamber. (Mag. $\times 0.35$)

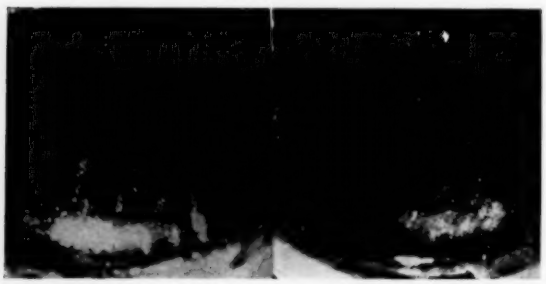

FIG. 3. Stoss with 13 tracks of the same "age." Eleven of these converge in a lead block about 40 cm above and in front of the cloud chamber; the other two appear to be secondary branches originating in the glass lid of the cloud chamber. (Mag. $\times 0.35$)

Stösse; Figs. 4, 5, and 6 are single photographs of three others. Conspicuous features found in nearly every burst photographed are the non-convergence to a single point of the (simultaneous) tracks of each burst, and the presence of very short nucleus-tracks in the gas, which closely

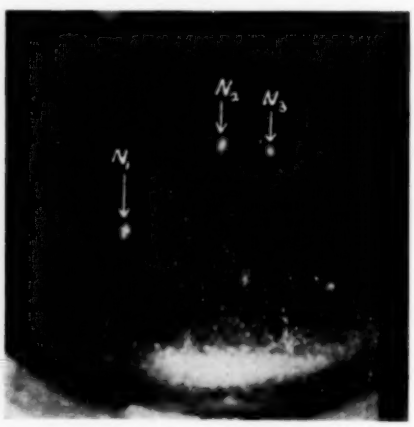

FIG. 4. Stoss with 15 tracks: 11 simultaneous pre-expansion electron tracks, 3 neutron-recoil argon atoms, N_1, N_2 and N_3, and a post-expansion electron track. Most of the electron tracks traverse the chamber in nearly vertical directions, but could not have come from less than 4 points of convergence. (Mag. $\times 0.53$)

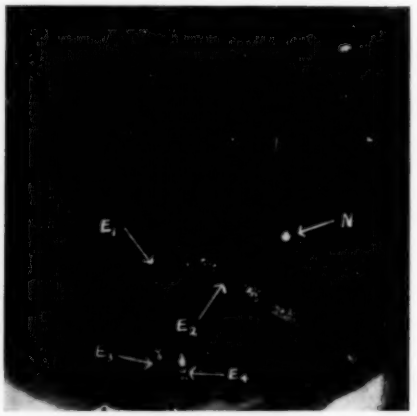

FIG. 5. Four electron tracks of the same age, and a neutron-recoil argon atom, N, E_1 and E_2 do not intersect; E_3 and E_4 seem to intersect in the iron of the arc used for illumination. (Mag. $\times 0.53$)

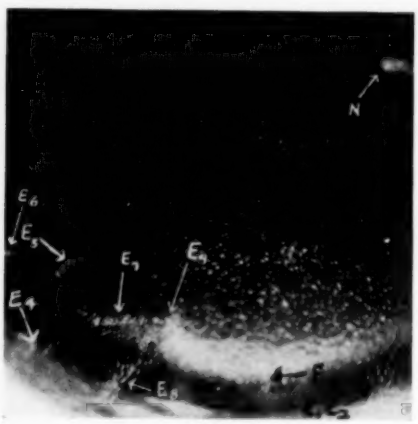

FIG. 6. Stoss with at least 9 electron tracks and one nucleus track, N. E_1 and E_2 are nearly horizontal and in line with the arc; E_3, E_4, and E_5 are nearly parallel and vertical; E_7, E_8 and E_9 diverge upward from a point near the bottom of the chamber. N is believed to be neutron-recoil nucleus; it is somewhat out of focus, and appears larger than it really is. (Mag. $\times 0.53$)

resemble the recoil-atom tracks formed by beryllium neutrons in argon. Blackett and Occhialini[1] mention cases of showers emanating from more than one point, and Anderson[2] has photographed a shower showing the same characteristic.

If we postulate that each burst derives its energy from a *single* primary entity, *we must suppose that the primary entity generates secondaries that are extremely efficacious in setting up tertiary centers of disruption,* since the tertiary track-foci are relatively close together. From the evidence so far available, it seems improbable to the writer that the secondary entities are photons. The necessarily high energies of such photons would be incompatible with the ob-

[2] Anderson, Phys. Rev. **43**, 368 (1933).

served facility of their absorption by matter near the cloud chamber, unless their numbers were so very great as to impose excessive requirements on the energy drawn from the primary entity. On the other hand, it seems reasonable to expect that some low-energy quanta, at least, are set free from Stösse. Against the possibility that the secondary agents are ionizing particles, is the fact that on no picture was there a track *observed* which linked two track-foci together. Photographs of additional bursts will doubtless help to clarify the question of the nature of these secondary entities that react with nearby matter by starting new disintegration points.

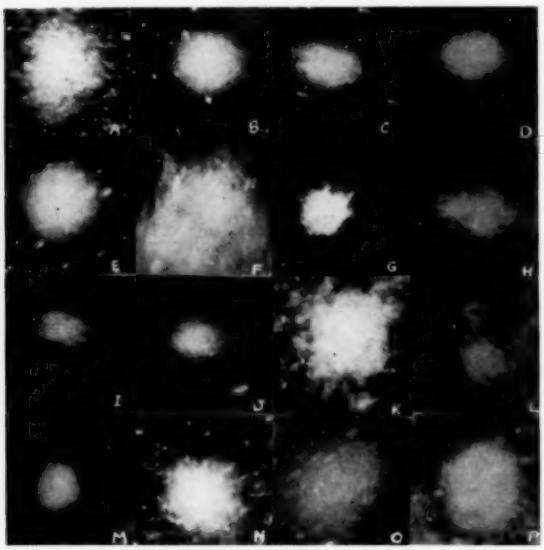

FIG. 7. *A* through *J*, short nucleus tracks from cosmic-ray Stösse photographs, attributed to argon atoms recoiling from elastic collisions with neutrons emitted from the Stösse. *K* through *P*, recoil-atom tracks formed in the same atmosphere, but with beryllium neutrons from a Po–Be source. The energies of the atoms of the two groups are of the same order of magnitude. (Mag. ×2.8)

Fig. 7 shows microphotographs of some of the short recoil-atom tracks from Stösse, also some recoil-atom tracks from Be neutrons, in the same cloud atmosphere, for comparison of ionization density and energy. The similarity is very evident. Tracks of this kind are recognizable with considerable certainty because of the enormous density of their ionization. The use of argon greatly facilitates the detection of neutrons; Bonner[3] has found from ionization measurements that the target area of the argon atom for Be neutrons is about 17 times that of hydrogen or 4.85 times that of nitrogen. Since the tracks of the Stösse do not converge to single points, it is impossible to tell from what material the neutrons arise, but the infrequency of appearance of recoil atoms on pictures other than those of Stösse indicates that the neutrons somehow arise from disintegration processes. The numbers of short recoil-atom tracks from Stösse is about the same as the number of Be neutron-recoil atom tracks from a Be–Po source of 0.05 millicurie radium equivalent, placed on top of the cloud chamber, or 1 to 10 millicuries at the Stoss track-foci. But the energy and ionization characteristics of the Stoss-neutrons are unknown, so that comparison of their number with those of Be neutrons is little more than speculation.

The secondary agents responsible for ejecting the convergent groups of tracks found in Stösse are still unidentified. If the low-energy recoil tracks observed are produced by high-energy neutrons, the latter *might* satisfy the difficult requirement of an agent having high energy and producing numerous subsidiary points of disintegration within a small region. But this hypothesis is based rather on our *lack* of knowledge of the energy-dissipation properties of such neutrons than on our knowledge of them.

These experiments are being continued with masses of aluminum about the chamber, in place of lead, in order to determine whether the heavier ionization produced by Al-Stösse[4] results from the generation of nucleus tracks or more numerous electron tracks.

The writer is indebted to Dr. W. F. G. Swann for suggesting the cloud-photography of Stösse, and for his discussion of the subject.

GORDON L. LOCHER*

Bartol Research Foundation
of the Franklin Institute,
October 7, 1933.

[3] Bonner, Phys. Rev. **43**, 871 (1933).
[4] Steinke, Gastell and Nie, Naturwiss. **21**, 560 (1933).
* National Research Fellow.

Neutrons from Deutons and the Mass of the Neutron

Last spring we directed 1.2 MV (million volt) deutons against many different targets and in every instance observed the production of 18 cm (3.6 MV) protons.[1] The most reasonable interpretation of the observations seemed to be that the deuton itself was disintegrated as a result of nuclear collisions with atoms of the various targets.

It was observed also (except in the case of gold where the observations were meager) that when the energy of the bombarding deutons was changed, the energy of the disintegration protons changed an equal amount, indicating that all of the kinetic energy of the deuton was acquired by the proton alone. Thus it appeared that the deuton has by far the greatest probability of disintegrating when it is nearest another nucleus and that the liberated proton gains in the process 2.4 MV in addition to the kinetic energy of the deuton. Assuming that the interaction of the liberated neutron with the heavier nucleus is negligible, it follows from the principle of conservation of momentum that the neutron acquires 2.4 MV of kinetic energy. Thus, 4.8 MV

[1] Lawrence, Livingston and Lewis, Phys. Rev. **44**, 56 (1933).

of energy is released in the disintegration process. From this it is accordingly calculated that the mass of the neutron is about 1.0006 rather than 1.0067 as estimated by Chadwick.[2]

Recognizing that our lower value for the mass of the neutron has profound theoretical implications, we have meanwhile continued our experiments with the express purpose of proving or disproving the hypothesis of the instability of the deuton. Obviously the strongest additional evidence we could obtain would be the observation of the neutrons presumably produced in the process.

This we have done. First we counted the number of disintegration protons with an ionization chamber and linear amplifier and then, with a 1/8 inch lead screen coated with paraffin in front of the ionization chamber, observed recoil protons due to neutrons from the target. From a brass target (with some wax also in view of the deuton beam) 18 cm protons entered the ionization chamber at the rate of 40,000 per minute while with the lead-paraffin screen we observed 12 recoil protons per minute. Now it has already been established by the observations of neutron-proton collision cross sections of previous workers that in a paraffin lined ionization chamber such as ours, one in several thousand of the neutrons passing through gives rise to a betectable recoil proton. Consequently, the number of recoil protons observed per minute corresponds exactly with expectations on the hypothesis that the deutons disintegrate with the production of equal numbers of neutrons and protons. In other words, the present experiments do more than support the deuton disintegration hypothesis in qualitative fashion by demonstrating the production of neutrons in the process. A quantitative check is afforded in that the yield of neutrons is as expected.

The brass-wax target (we have not as yet determined what constituent of the conglomerate target is most effective) yielded 2 disintegration protons per 10^7 deutons. Calcium fluoride and platinum gave about 4 protons per 10^8 deutons while Be gave only 1 proton per 10^8 deutons.

We raised the energy of the bombarding deutons from 1.2 MV to 3.0 MV* and were rather surprised to find that the observed proton yield did not increase a great deal. However, the range of the disintegration protons did increase quite according to expectations. From the considerations outlined above it was to be expected that they would have an energy of 2.4 MV more than the bombarding deutons, i.e., 5.4 MV. Our observations indicated a range of 33 cm corresponding to 5.2 MV which, for the present experimental accuracy, constitutes agreement.

All of these observations corroborate the view that the deuton disintegrates with the release of about 4.8 MV of energy and consequently that neutrons produced in the process have a mass of about 1.0006 mass units.

We are much indebted to Professor G. N. Lewis who collaborated with us last spring, not only for providing a generous supply of deuterium but also for his continued close association with the experiments. We acknowledge also with pleasure the assistance of Commander T. Lucci. We are especially grateful for grants from the Research Board with the approval of the President of the University and from the Research Corporation and the Chemical Foundation.

M. Stanley Livingston
Malcolm C. Henderson
Ernest O. Lawrence

Radiation Laboratory,
Department of Physics,
University of California,
October 7, 1933.

[2] Chadwick, Proc. Roy. Soc. **A136**, 692 (1932).

* These are the most energetic atomic projectiles that have ever been produced artificially in the laboratory. It is of some interest to record here also that we have recently increased the intensity of the beam of swiftly moving protons generated by our apparatus to 0.2 microampere.

Neutrons from Beryllium Bombarded by Deutons

In our recent experiments (preceding letter) we found, as a few days earlier had been observed by Lauritsen, Crane and Soltan (private communication), that Be yields many more neutrons than can be accounted for alone by deuton disintegration. With a current of 10^{-8} amp. of 1.3 MV deutons we observed 240 recoil protons per minute in an ionization chamber subtending at the Be target a solid angle of $\pi/10$. From this we estimate (assuming 3 recoil protons for every 10,000 neutrons, as indicated by the observations from the brass target) that about 500,000 neutrons were produced per sec., i.e., about 10 neutrons per 10^6 deutons. Since the proton yield is a thousand times smaller it must necessarily be concluded that the neutrons result from the disintegration of Be.

Last spring we not only observed protons from Be bombarded by deutons, but also one alpha-particle of 3.3 cm range per 10^7 deutons.[1] These we supposed resulted from the disintegration of Be^9 without capture of the deuton, resulting in the production of two alpha-particles and one neutron. But this process also does not account for the large number of neutrons observed in the present experiments.

So it appears that in this instance the neutrons result from the disintegration of Be^9 with capture of the deuton to form B^{10} and a neutron. By assuming that the mass of the neutron is 1.0006 and that no gamma-radiation is given off in the process, it is calculated that these neutrons have about 14 MV of kinetic energy. We are planning in the near future to observe the ranges of the recoil protons and thereby determine whether at least some of them have this much energy.

We found also that the yield of neutrons from Be increases linearly with the range of the deutons for deuton ranges extending from 1 cm to 9 cm. This means that the

[1] Lewis, Livingston and Lawrence, Phys. Rev. **44**, 55 (1933).

probability that a deuton will disintegrate the Be nucleus on collision is independent of deuton energy over the observed range and that the increase in yield of neutrons with deuton range is due only to the increase of the frequency with which deutons make nuclear collisions.

It is hardly necessary to emphasize the importance of this disintegration process as a source of neutrons for nuclear research. Though the rate of production of neutrons in the present experiments exceeds considerably that of any heretofore used radioactive source, we intend to increase our deuton current to 10^{-6} amp. and thereby increase this neutron yield a hundred-fold.

Again we acknowledge our indebtedness to Professor G. N. Lewis for furnishing deuterium, to Commander T. Lucci for his assistance, and to the University Research Board, the Research Corporation and the Chemical Foundation for their financial support.

M. Stanley Livingston
Malcolm C. Henderson
Ernest O. Lawrence

Radiation Laboratory,
Department of Physics,
University of California,
October 7, 1933.

An Unusual Nitrogen Tube

Further study of the unusual nitrogen discharge described last December,[1] has led to a great improvement of the tube. In the present tube, the first negative bands are much more intense in relation to the first positive bands than they were last year. At least twelve new members of the Lyman bands of nitrogen have been discovered in this tube showing that one of the properties of the tube is a remarkable enhancement of very high vibrational levels. The Lyman bands, it may be recalled, are the $a^1\pi \rightarrow X^1\Sigma$ bands of N_2. High vibrational levels of the $B^3\pi$ level are also enhanced, and the first positive bands arising on these are present in the spectrum with a far greater relative intensity than in ordinary tubes. One of the most striking characteristics of the tube is a strong nitrogen afterglow in which bands arising on the very high vibrational states of the $B^3\pi$ level have been visually observed. The heretofore reported afterglows in nitrogen consist of bands chiefly from the B_{10}, B_{11} and B_{12} levels. Visual observation indicates that in this new afterglow, strong bands appear which originate on levels around B_{18}. Since no photographs of the afterglow have been obtained so far, the actual origin of these new bands is not accurately known. It is certain, however, that the afterglow is considerably different from the heretofore reported afterglows of nitrogen. This tube also has characteristics which are of value in auroral studies, but these will be discussed in a more detailed communication.

Joseph Kaplan
University of California at Los Angeles,
October 9, 1933.

[1] Kaplan, Phys. Rev. **42**, 807 (1932).

On the Production of Neutrons from Lithium

It was mentioned in a previous letter to the *Physical Review*[1] that lithium, when bombarded with protons gave a measurable intensity of neutrons. The effect has since been investigated further, and a curve plotted of the yield of neutrons as a function of voltage from 400,000 to 800,000 volts, with an ion current of 20 microamperes. As in the previous measurements of neutrons, an electroscope, the inner walls of which were coated with paraffin, was used as a detecting device. The electroscope was enclosed in a lead cylinder with 5 cm walls, through which the neutrons were obliged to pass. To determine whether the effect observed was due to neutrons or to γ-rays, a measurement was made with the paraffin removed from the electroscope. The deflection without the paraffin was less than half the deflection with the paraffin, indicating that the greater part of the effect was due to recoil hydrogen particles ejected from the paraffin by neutrons. The effect observed without the paraffin is not to be attributed entirely to γ-rays, because the neutrons are capable of producing some ionization by means of recoil oxygen and nitrogen atoms produced in the air in the chamber.

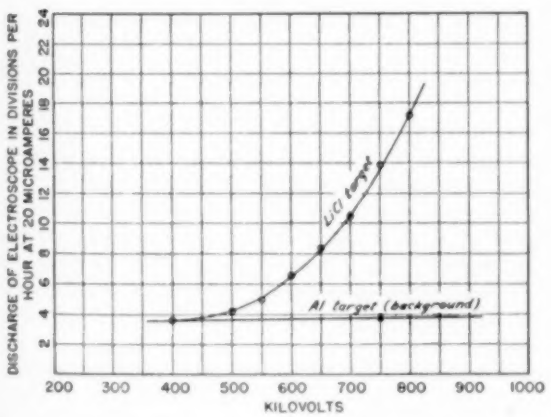

Fig. 1. Yield of neutrons from the disintegration of lithium by protons as a function of voltage

No simple and plausible reaction, which gives a neutron from lithium and a proton, suggests itself, so we have considered a double reaction in which the α-particles produced by protons and Li^7 in turn bombard Li^7 with the production of neutrons.

$$Li^7 + H^1 \rightarrow 2He^4 (+17\times10^6 \text{ e.v.}) \quad (1)$$

$$Li^7 + He^4 \rightarrow B^{10} + n^1 (-3\times10^6 \text{ e.v.}). \quad (2)$$

The first of these reactions is well known from the work of

[1] Crane, Lauritsen and Soltan, *Production of Neutrons by High Speed Deutons*, Phys. Rev. **44**, 692 (1933).

Cockroft and Walton and others,[2] and the second has recently been reported by Curie and Joliot.[3] Taking, for the purpose of calculation, the mass of the neutron to be 1.0065, and the other atomic masses

Li^6	6.0145	He^4	4.0022
Li^7	7.0147	H^1	1.0078
B^{10}	10.0137	H^2	2.0136

we find that the second reaction requires 3×10^6 electron-volts energy. However, each of the α-particles produced by the first reaction has an energy of about 8.5×10^6 electron-volts, so it is to be expected that the second reaction takes place with a rather high efficiency. The efficiency of the first reaction at 800,000 volts can be obtained from the results of Henderson,[2] and is about 5×10^{-8}. The overall efficiency of the double process at the same voltage is about 10^{-11}, assuming that the factor between neutrons and recoil particles is 10^{-3}. This gives an efficiency of 2×10^{-4} for the second reaction.

A reaction suggested by Oliphant and Rutherford[2] in which lithium could give neutrons when bombarded with protons is

$$Li^7+H^1\rightarrow He^4+He^3+n^1 \qquad (3)$$

although there has so far been no evidence of He^3. Since this is a three particle disintegration, the energy could be distributed at random, and each of the three products would have a continuous range of velocities. The process might therefore be used to account for some of the low energy α-particles which have been reported by several investigators, and for which there seems to be as yet no explanation except the assumption that a γ-ray sometimes accompanies the two α-particles.

In the production of neutrons from lithium by deutons, where the heavy hydrogen used to produce the deutons is very much diluted with ordinary hydrogen, the intensity of neutrons contributed by the above double process cannot in all cases be neglected. Also, in addition to the reaction

$$Li^7+H^2\rightarrow 2He^4+n^1(+16\times10^6 \text{ e.v.}) \qquad (4)$$

there must be a double process involving deutons

$$Li^6+H^2\rightarrow 2He^4(+22\times10^6 \text{ e.v.}) \qquad (5)$$

$$Li^7+He^4\rightarrow B^{10}+n^1(-3\times10^6 \text{ e.v.}). \qquad (2)$$

Finally, for the sake of completeness, it must be mentioned that the α-particles produced in reaction (4) are effective in contributing some neutrons by means of reaction (2).

The experimental data available at the present time on the disintegration of lithium seem entirely too meager to allow anything definite to be concluded about the various ways in which neutrons might be produced from it. An experiment which would shed considerable light on the subject would be a study of the disintegration of targets of the individual isotopes, Li^6 and Li^7.

H. R. Crane
C. C. Lauritsen

Kellogg Radiation Laboratory,
California Institute of Technology,
October 14, 1933.

[2] Cockroft and Walton, Proc. Roy. Soc. **A137**, 229 (1932). Lawrence, Livingston and White, Phys. Rev. **42**, 150 (1932). Oliphant and Rutherford, Proc. Roy. Soc. **A141**, 259 (1933). Henderson, Phys. Rev. **43**, (1933).

[3] Curie and Joliot, J. de Physique 4, 278 (1933).

The Production of High Velocity Ions and Electrons

Previous methods of producing high velocity electrons and ions may roughly be divided into two general classes, one in which the electron or ion is given its acceleration by falling through a single potential drop applied to the terminals of a discharge tube, and the second in which ions are accelerated by sending them by various means through several fields so arranged as to be in the correct direction at the proper time. In this note we wish briefly to describe a method that belongs to another class[1] in which the electron or ion is accelerated by a field which is so adjusted as to move with the same velocity as the ion or electron.

In the first method referred to above in which the ion receives its acceleration in a single electric field the upper limit to the velocity of the ion is usually set not only by the trouble of producing sufficiently high voltage but also by the difficulty of maintaining this voltage across a single discharge tube. The second class of methods avoids this difficulty as has been so beautifully shown by Lawrence and his collaborators. Up to the present time, however, these latter methods have been highly successful only in the case of ions and not in the case of electrons. The method to be described here also avoids this difficulty with the first class of methods and may be used to accelerate electrons as well as ions.

It is well known that an electrical surge will travel along an artificial transmission line with a virtual velocity that depends upon the constants of the line and may be made to vary over large ranges. For a straight parallel wire transmission line the velocity approaches to approximately that of light. If the artificial transmission line is connected to a series of electrodes in a long vacuum tube in such a way that the travelling potential fall is applied successively to the electrodes an ion or electron moving with the approximate speed of the surge or potential fall on the line will be continuously accelerated and thus may reach very high velocities.

Our preliminary apparatus consisted of a discharge tube of about 3 cm diameter and 160 cm length containing 15 ring electrodes spaced at intervals of 10 cm. The tube was terminated by a bulb partially coated with willemite on the inside for detecting the electron beam. A pair of Helmholz coils was used to measure the electron velocities by the magnetic deflection method. The electron beam was produced by applying a negative empulsive potential of approximately 28 kv between the first and second electrodes from a condenser sparkgap circuit, the second electrode remaining at ground potential. The next nine electrodes were connected to the elements of the artificial transmission

[1] A method somewhat similar to that here to be described was discussed by one of the authors (L. B. S.) with Dr. K. H. Kingdon about two years ago.

line, the last four electrodes were grounded. A negative impulse of 15 kv was applied to this line from an auxiliary condenser sparkgap circuit. This impulse was timed to occur after the glow discharge between the first and second electrodes had started. This insured the presence of an electron beam inside of the line electrodes.

The artificial line was of the low pass filter type having inductance as the series impedance and capacitance as the shunt impedance. This type of line has a virtual velocity of current propagation of $1/(LC)^{\frac{1}{2}}$ sections per second where L and C are respectively the lump values of inductance and capacitance. The constants were chosen to give approximately the correct velocity of voltage propagation per electrode. The line was terminated by a resistance of such a value that reflections from the end of the line were negligible. It would obviously produce better results to vary the line constants in such a way that the time between sections is decreased as the wave passes down the line, but for this preliminary work the constants were approximately the same although the inductance was progressively decreased to some extent.

With this arrangement we have obtained electrons with a maximum velocity of between 80 and 90 kv. Assuming that the electrons entered the first line electrode with a velocity corresponding to 28 kv this represents a threefold multiplication. Since the glow discharge current was limited by a high resistance it is very probable that the electron beam velocity was much lower than the maximum potential appearing between the first and second electrodes, and that consequently the line was producing an even greater multiplication.

These rough preliminary experiments lead us to believe that there is no inherent difficulty in obtaining a multiplication factor of 10 or more. Since it is not very hard to construct a tube capable of withstanding surge potentials of several hundred kilovolts this method should be capable of easily producing electrons having velocities corresponding to several millions of volts. We hope to continue these experiments using voltage sources of much higher potential. It would obviously be much easier to work with positive ions rather than with electrons due to the lower velocities and correspondingly longer time intervals between sections. We have not as yet performed an experiment of this kind.

J. W. Beams
L. B. Snoddy

Rouss Physical Laboratory,
University, Virginia,
October 18, 1933.

The Faraday Effect at High Frequencies

In view of the general interest in the work of F. Allison,[1] in which the results obtained were attributed to differential time lags in the Faraday effect for isotopes of certain elements, it seemed worth while to see if such effects could be detected using continuous oscillations. The work here reported is the result of some preliminary experiments with apparatus already on hand in the laboratory. A 210 tube was used as an oscillator, followed by an 852 as an amplifier. This fed two more 852 amplifiers in parallel which were made as symmetrical as possible. The plate inductances of these surrounded cells of carbon disulphide which were placed in the optical path in the manner described by Allison. The relative phase of the magnetic fields in the two coils was adjustable over a small range near 180° by varying the coupling arrangement between the first amplifier and one of the final amplifiers. The optical arrangement was similar to Allison's except that a continuous source of light, generally Hg 5461, was used.

Since the time lags reported by Allison are small compared to the period of any feasible oscillatory circuit, conditions would appear to be more favorable at high frequencies. For this reason a frequency of 7.5 megacycles was used at first. This is about five times the resonant frequency of Allison's apparatus as computed from his published data. If we assume that the eye integrates light received over an interval as long as 1/60 of a second, and that the light transmitted by a nicol is proportional to the square of the angle of rotation from the position of extinction, we should have observed, when only one cell was in position, a brightening of the field of about the same order as that found by Allison. However no brightening could be observed. This was probably due to a departure from the square law for transmission by the nicol at small angles. The circuit constants were then changed making the frequency about 1.7 megacycles and increasing the peak rotation to be expected to about 10°. Under these conditions a definite brightening of the field was observed with either cell singly. With both cells in, the field was dark. Within the amount of phase shift available, which corresponded to a motion of the trolleys of Allison's apparatus of about 5 meters, no sudden variations in intensity were observed. This result is not considered conclusive since the rotation produced by the individual coils may have been too small.

It is considered, however, that the feasibility of the general method of investigating the effect with continuous oscillations has been established. It has the advantages of steadiness of operation and greater flexibility, for the currents in the coils may be varied independently to allow for differences in the Verdet constant, and the phase of the currents may be varied without changing their magnitude. The work is being continued by the construction of more powerful amplifier tubes which should be capable of giving greater rotation. With these we hope to investigate further the Faraday effect at high frequencies, and also the possibility that the phenomenon may be due to some type of Kerr effect as suggested by Webb and Morey[2] or to the presence of a longitudinal electric field.

G. P. Harnwell
W. Bleakney
S. N. Van Voorhis
J. B. H. Kuper

Palmer Physical Laboratory,
Princeton, New Jersey,
October 19, 1933.

---

[1] F. Allison, J. Chem. Ed. **10**, 71 (1933) and references there cited.

[2] Webb and Morey, Phys. Rev. **44**, 589 (1933).